3-D MULTIFUNCTIONAL SENSORS FABRICATED ON FIBER TIPS USING A TWO-PHOTON POLYMERIZATION PROCESS

THESIS

Jonathan W. Smith, Captain, USAF

AFIT-ENG-MS-19-M-056

DEPARTMENT OF THE AIR FORCE
AIR UNIVERSITY

AIR FORCE INSTITUTE OF TECHNOLOGY

Wright-Patterson Air Force Base, Ohio

AFIT-ENG-MS-19-M-056

3-D MULTIFUNCTIONAL SENSORS FABRICATED ON FIBER TIPS USING A TWO-PHOTON POLYMERIZATION PROCESS

THESIS

Presented to the Faculty

Department of Aeronautics and Astronautics

Graduate School of Engineering and Management

Air Force Institute of Technology

Air University

Air Education and Training Command

In Partial Fulfillment of the Requirements for the

Degree of Master of Science in Electrical Engineering

Jonathan W. Smith, BS

Captain, USAF

March 2019

AFIT-ENG-MS-19-M-056

3-D MULTIFUNCTIONAL SENSORS FABRICATED ON FIBER TIPS USING A TWO-PHOTON POLYMERIZATION PROCESS

Jonathan W. Smith, BS

Captain, USAF

Committee Membership:

Dr. Hengky Chandrahalim
Chair

Maj. Tod V. Laurvick
Member

Maj Nicholas C. Herr
Member

Dr. Nicholas G. Usechak
Member

Dr. Joseph S. Suelzer
Member

AFIT-ENG-MS-19-M-056

Abstract

This thesis conducts research involving designing, fabricating, and testing optical fiber tip refractive index sensors. The fabrication process used for these sensors is a two-photon polymerization process utilizing a photo sensitive polymer. Unlike planar lithography, this fabrication process allows the creation of arbitrary shapes with a great degree of freedom. Three different fiber tip sensors were fabricated and tested. The first is a flat surfaced single cavity Fabry-Pérot interferometer (FPI) device, the second is a flat surfaced double cavity FPI device, and the final is a confocal surfaced double cavity FPI device. These sensors are tested for thermal radiation and volatile organic compounds (VOC) sensing. Thermal radiation sensing involves exposing the fiber tip device to temperatures ranging from room temperature up to 120^{o}C. As the temperature increases, the fiber tip structure expands which changes its reflection spectrum. For VOC sensing each device was also exposed to isopropanol in gaseous form which results in a refractive index change. This change is also observed in the reflection spectrum. Lastly, research was conducted on thin dielectric reflective coatings for the purpose of increasing the reflectivity of the device surfaces resulting in a higher quality factor.

Acknowledgments

I would like to express my sincere appreciation to my faculty advisor, Dr. Hengky Chandrahalim, for his guidance and support throughout the course of this thesis effort. Thank you to Dr. Vincent Tondiglia for providing the Nanoscribe and all the training and expertise on how to use it. I would also like to thank Dr. Joseph Suelzer and Dr. Nicholas Usechak for providing access to the lab necessary for all testing and the expertise they provided. Lastly I would like to thank Maj Tod Laurvick and Maj Nicholas Herr for being a part of my committee. The insight and experience from all of you was certainly appreciated. Thank you.

Jonathan W. Smith

Table of Contents

Page

List of Figures

Page

3-D MULTIFUNCTIONAL SENSORS FABRICATED ON FIBER TIPS USING A TWO-PHOTON POLYMERIZATION PROCESS

I. Introduction

General Issue

As technology continues to advance devices become more powerful and shrink in overall size. Almost all devices used, no matter the application, rely on some sort of input. That input can be provided by the user, other devices, or a variety of sensors. To keep up with the technological advancement, input sensors also need to become smaller in size and more efficient. Two of these input sensors that will be focused on in this thesis research is a thermal radiation sensor, and a volatile organic compound (VOC) sensor. Thermal radiation sensors can detect changes in temperature, and VOC sensors can detect the presence of a VOC which is a gas made of various chemicals.

These sensors have been created by utilizing complimentary metal-oxide semiconductor (CMOS) technology. A variety of CMOS thermal radiation sensors have been fabricated [7, 8, 60] and are able to detect a temperature change due to a change in leakage current. Generally in electronics, the higher the ambient temperature the more leakage current is present. This approach to measuring thermal radiation consists of a microchip scaled integrated thermal sensor that is able to achieve accurate temperature measurements at a high resolution. However using this method to measure temperature creates more heat as an amplifier is required to operate the thermal radiation sensor which

demands more space and power consumption. With many Air Force systems it is desirable to have a plug-n-play design meaning if a thermal sensor is needed, one can be procured and installed. With CMOS thermal radiation technology the thermal sensor must be included in the design of the technology. The thermal radiation sensor cannot be inserted into existing technology and function correctly.

There have been VOC sensors created using CMOS technology [18, 19, 66]. These sensors rely on a sensitive polymer layer that can absorb components of a surrounding VOC which will change that layers dielectric properties. This change can then be detected with the use of amplified CMOS technology. Similarly to that of the thermal radiation CMOS sensors, this can result in a power hungry sensor. A disadvantage to these sensors is ample time is needed for the sensitive layer's dielectric properties to change due to the presence of a VOC. This results in a delay of VOC detection.

Another approach to detecting thermal radiation or VOC's is with the use of a Fabry-Pérot (FP) system. A Fabry-Pérot Interferometer (FPI) is very sensitive to both cavity lengths and the refractive indices of all the material involved. In the case of thermal radiation, depending on a materials coefficient of thermal expansion, a material will expand as temperature increases, known as the thermo-elastic effect, which will change the cavity length of the FPI. Heat also has an impact on a materials refractive index which is known as the thermo-optic effect which will also influences the reflection spectrum. Similarly, if the FPI is exposed to a VOC the refractive index will change which will impact how an FPI operates. The sensors designed in this thesis are microscopic FPI's that are fabricated onto the tip of a fiber optic strand which will be

utilized as both a thermal radiation and VOC sensor. Implementing this sensor onto an optical fiber gives the sensor great flexibility, low operating power, and is able to plug-n-play with other subsystems with non-invasive instillation.

Problem Statement

Next-generation warfighter systems demand the development of multifunctional smart sensors to enable game-changing technologies and maintain battlespace supremacy. Recent advancements bring new capabilities like three-dimensional nanostructuring and miniaturization of highly sensitive multifunctional sensors on unconventional substrates closer to realization. The ability to accurately sense thermal radiation and the presence of VOC's in real time is crucial for the operation and maintenance of weapon systems. Having the ability to sense thermal radiation in of any current subsystem will give immediate insight on the overall health of that system. The ability to detect an abnormal heat change of a known operating system can immediately notify the user that something is potentially wrong. The ability to detect any airborne VOC's is crucial as they can be extremely harmful when inhaled by the operator. The development of sensors that give real time feedback of the presence of VOC's can prevent catastrophic failures due to the user's exposure. to said VOC's. This is extremely relevant in a situation of a pilot flying a multimillion-dollar weapon system.

Research Objectives & Hypotheses

The objective is to create a single fiber optic sensor that can detect different gases, liquids, temperatures, or other environmental conditions instantaneously. This objective will be explored and accomplished with the research and experimentation completed in

this thesis. The two main goals for this research is to fabricate a microscopic fiber optic sensor that can detect both thermal radiation and a refractive index change due to the presence of a VOC. The detection will be observed by a shift in the sensor's reflection spectrum due to a change in temperature and/or refractive index.

The hypothesis for the thermal radiation optical fiber tip sensor is that expansion will occur as temperature increases. This expansion will increase the cavity length(s) of the device which will alter the device's reflection spectrum. The thermal expansion will influence the reflection spectrum more so than the change in refractive index due to temperature showing the thermo-elastic effect will dominate over the thermo-optic effect. The reflection spectrum will experience a linear shift to the right (resonant wavelengths will increase) as temperature increases. The flat surfaced single and double cavity FPI sensors will be tested and it is expected that the double cavity FPI sensor will achieve a greater sensitivity due to multiple cavities and smaller anchor area allowing more expansion.

The hypothesis for a VOC optical fiber tip sensor is much simpler. The exposure of a VOC will increase the refractive index of the area surrounding the fiber tip sensor. This will shift the reflection spectrum of the fiber tip sensor to the right because an increase in refractive index (due to the VOC) will result in a resonant dip occurring at a larger wavelength. Again, the flat surfaced single and double cavity FPI sensors will be tested and it is expected that the double cavity FPI sensor will be drastically more sensitive as it is the only sensor with a cavity open to the atmosphere. This open cavity will be exposed to a VOC dramatically changing the sensors reflection spectrum.

Research Focus

This research utilizes information from a variety of fields to construct an optical fiber tip sensor. Material properties of a thermoset polymer was utilized to fabricate a microstructure. Mechanical properties were utilized in the design of this microstructure to ensure its strength and durability. Optics has a large part in this research as a fiber optic strand was used as the microstructure's substrate, and optical properties are utilized in this sensors detection system. The fabrication method utilized in this research is another point of interest. It involves a micro 3-D fabrication process which utilizes a two-photon polymerization process with a photo sensitive polymer. Combining these areas of research with this state-of-the-art micro fabrication process will yield an efficient, robust, multifunctional fiber optic sensor.

Investigative Questions

One of the big questions that needed to be answered in this research was how to fabricate the fiber tip sensors. Two main methods were considered. The first was selectively etching into the optical fiber leaving behind the desired fiber tip structure. This can be done with the use of a femtosecond laser [5] selectively exposing the areas of the fiber tip to be etched away followed by developing in hydrofluoric acid. The other approach to creating these sensors is to use specialized equipment that will fabricate the 3-D sensor structure onto the tip of the optical fiber. It was determined that there are more benefits to the 3-D fabrication process so this process was used for the sensor fabrication throughout this thesis. The characterization results in chapter four go into greater detail on why this decision was made.

Assumptions/Limitations

There were a few assumptions made for the research conducted in this thesis. First, it was assumed that there was negligible humidity and consistent environmental conditions in the lab where all experimentation was done. This same assumption was made for the lab utilized to fabricate the optical fiber tip sensors. An experiment was completed that measured the transmittance of light through a coated glass slide and the amount of absorption was assumed to be negligible so that the reflectance could be obtained. During temperature sensing experimentation a thermocouple was used to monitor the temperature of the fiber tip sensor. It was assumed that the thermocouple and fiber tip sensor were exposed to the same temperatures. Lastly, for the VOC sensing experiment it was assumed that the area surrounding the fiber tip sensor was 100% isopropanol.

Throughout this research there were a few limitations encountered. First, the adhesive used to mount the fiber tip sensor to the thermocouple started to burn at temperatures greater than 140^{o}C. To test at any higher temperatures new adhesive would need to be utilized. The 3-D printing process used to fabricate the fiber tip sensors has a small limitation. The sensors are constructed layer by layer starting from the bottom. If any portion of the sensor is fabricated without being anchored then the probability of a successful fabrication significantly reduces. The last limitation observed is the sensors ability to withstand environmental conditions. When the sensor is exposed to humidity the reflection spectrum is significantly impacted. All the fabricated sensors were stored in dry boxes to ensure consistent data in between runs.

Implications

If these assumptions are incorrect or cannot hold true for certain situations, then there could be some differences in the resultant data. First, if these experiments were conducted in an environment with different conditions (such as humidity) than the reflection spectrum of each sensor would be significantly different. When testing the reflective coatings, the reflectivity increase would be reduced if there is some absorption experienced by the input light. Lastly, it is understood that the assumption of the area around the VOC sensor being 100% isopropanol is an assumption that may not true. If this is the case, then the actual sensitivities of the various sensors will be less than the sensitivities stated in this thesis. The limitations experienced did not have a significant impact on the research conducted as the temperature range tested did not exceed 130^{o}C, the structures 3-D fabricated on fiber tips were always anchored, and all samples were stored in air tight containers.

Thesis Outline

This thesis is organized into five main chapters. The first chapter is the introduction to the research completed in this thesis. The research topic, problem statement, and hypothesis are covered in this section. The bulk of the material in this research is covered in chapters two through four. Chapter two is a review of relevant literature which spans from the basics of optical properties to fiber optic sensors that have been fabricated by other individuals which are used for comparison to the research conducted in this thesis. Chapter three discusses the methodology of all conducted research. There is a detailed explanation of each experimental set up, each process for

testing and fabrication, and a detailed list of the equipment utilized. Chapter four shows all results obtained from experimentation and analysis of the data determining if each hypothesis was correct and the potential impact of the data. Lastly, chapter five is a conclusion of the conducted research and discussion on potential follow on research that could be conducted to add more value to this specific area of research.

II. Literature Review

Chapter Overview

The purpose of this chapter is to document all of the applicable research that was necessary for completion of the work described in this thesis. This literature review starts at a very basic level to ensure complete understanding of how fiber optic sensors operate. Understanding this material is crucial for understanding the concepts tested throughout this thesis.

The motivation for the fiber optics field of study is covered followed by a brief history showing the origin of utilizing light to transfer information. Then the basics of fiber optics and how light propagates is covered. Lastly, relevant journal papers and articles will be reviewed and pertinent information to the work completed in this thesis will be discussed.

Motivation

The desire to shrink all electronic devices is abundantly clear. More capabilities, features, and better performance are being demanded from current technologies and the big push for smaller electronics allows for more computing power in a smaller package. Many, if not all, of these technologies require input devices or sensors that pass some sort of necessary information to the functioning device. Because of this there is also a need for developing smaller, more efficient sensors to be integrated with these new technologies. One of the new areas of study for these smaller, more efficient sensors is fiber optics.

There are some fiber optic sensors already being researched and used today. There are fiber optic sensors used to detect pressure, air flow, vibrations, viscosity, and other environmental conditions. The optical fiber sensors created in this thesis are all Fabry-Pérot single mode sensors which can sense temperature change and index of refraction change.

Using fiber optics for sensors comes with many strengths. All fiber optic material is passive, meaning it is dielectric and can be manipulated using polarization. Fiber optics come in very small sizes and is made of light weight material. Electromagnetic effects have no impact on fiber optics which results in less interference. Due to the material that optics are made of they can perform well in high temperature environments, withstand shock, and resist environmental corrosion. Fiber optics operate with a relatively large bandwidth of wavelengths typically ranging from 850 to 1550 nanometers. It is easy for electrical and optical multiplexing meaning fiber optics can be used to send multiple signals or bits of information over the same link at the same time. Lastly, fiber optic material is inexpensive as the cost is driven by the large commercial telecommunication and optoelectronic market [65].

History

The basics of how fiber optics work is simply the ability to transfer light energy over a large distance. Using light as a means of communication or transfer of information is something that has been done for years. One of the first examples of this was Alexander Graham Bell and his work with the photophone in 1877. This device is

illustrated in Figure 1 and was used to communicate over hundreds of meters using a beam of light.

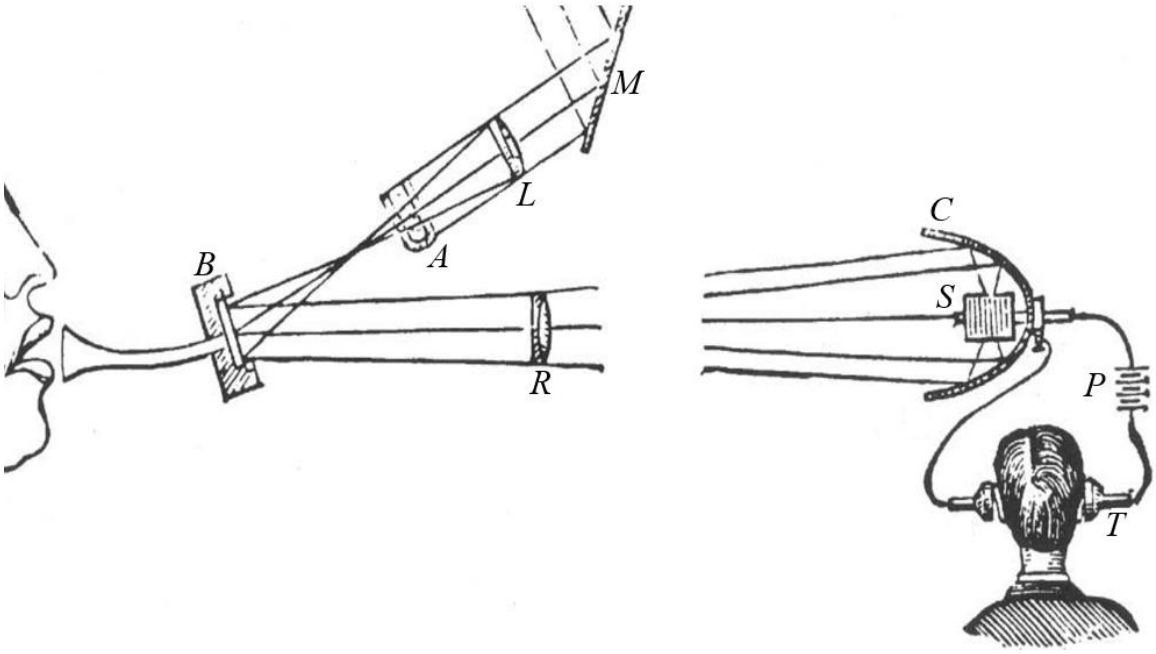

Figure 1. Alexander Graham Bell's Photophone Operation [23]

Mirror *M* reflects a beam of light (provided by the sun) into lens *L* which focuses the light onto cell *A*. This cell is designed to absorb heat from the incoming light to prevent any damage to the transmitter *B*. The transmitter is made of a thin glass disc mirrored on one side to reflect the incoming light. This thin glass disc will modulate from slightly concave to convex as a response to the speaker's voice which will modulate the reflected beam. This modulated beam is reflected into lens *R* which collimates the light in the direction of the receiver. The receiver is comprised of a parabolic mirror *C* which directs the incoming light to a selenium cell *S*. The resistance of the selenium cell changes with different light intensities which can be converted back to an audio signal using a battery *P* and speaker *T* [23].

For years, the use of light to transmit data was very limited for two main reasons; lack of a good light source, and the absence of a reliable transmission medium. The invention of the dye laser with continuous tunability over a broad spectrum by Peter Pitirimovich Sorokin in 1966 provided the perfect light source for fiber optics [2]. Laser is an acronym that stands for light amplification by stimulated emission of radiation. Lasers operate by energizing an electron which will then emit a light photon. A laser can do this over a large distance which results in a large production of photons of the same wavelength and direction [39]. This focused light is ideal for transmitting any kind of information with the use of light.

A short while later F. P. Kapron discovered a way to transmit light over long distances with extremely low losses with the use of glass optics in 1970. Kapron was able to construct optical waveguides with a loss of 60 to 70 dB/km. He discovered a circular waveguide will have a lower bending loss (loss due to the waveguide changing direction) than a square waveguide [27]. The birth of the laser light source and low loss light waveguides gave way to a large optical fiber area of study.

Optic Principals

Similarly to the photophone, the optical fiber tip sensors created in this thesis will use light to transmit information. Understanding how light is transmitted and the different types of fibers that are used is crucial for understanding fiber optic sensor operation. There are many different types of optical fibers which all treat light in different ways. All basic fibers are constructed of a core, cladding, and protective sheathing which can be seen in Figure 2. The fiber core is the medium in which the input light waves travel

through. The cladding is what surrounds the core and has a different refractive index which is why the input light is able to continually reflect within the core and propagate through the fiber. The refractive index of the fiber core is always greater than that of the fiber cladding. The sheathing is normally a polymer jacket that acts as a protective coating to the entire fiber.

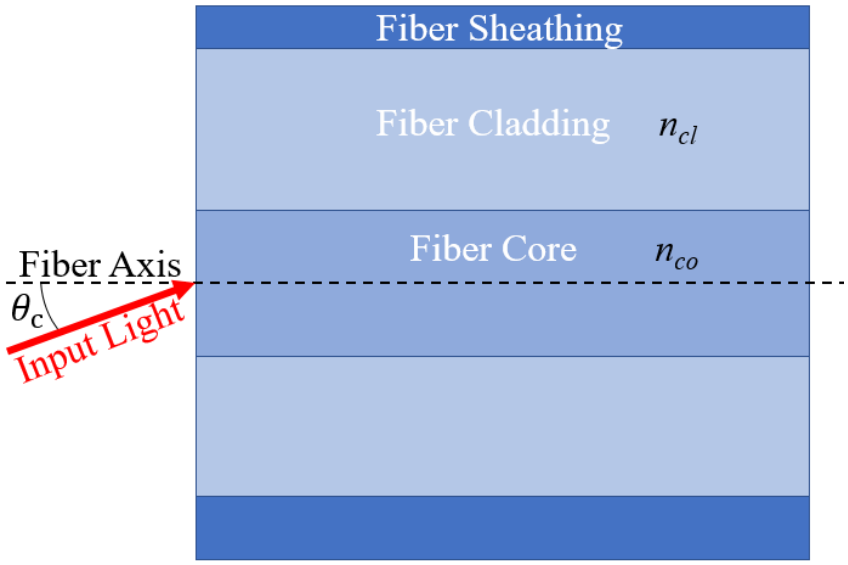

Figure 2. Basic Optical Fiber Construction

A multi-mode (MM) fiber is a fiber which has a core diameter that is a large multiple of the wavelength of the incoming light [65]. There is a maximum acceptable input angle allowable for incoming light to be transmitted through the fiber. This maximum allowable angle is called the numerical aperture (NA) and is described by the equation below.

$$NA = sin\,\theta_C = \sqrt{n_{co}^2 - n_{cl}^2} \tag{1}$$

θ_c is the angle of the input light from the fiber axis, n_{co} is the refractive index of the fiber core and n_{cl} is the refractive index of the fiber cladding. Any input light with an angle equal to or less than θ_c will propagate through the fiber. It is important to note as the angle of input light approaches θ_c more time it will be taken for that light to propagate along the fiber. The greater the input angle the more reflections take place inside the fiber core. When reflections are increased, the overall distance light travels is increased which results in a longer travel time. The "Multi-Mode" in MM fibers refers to the different modes of light propagating through the fiber. The more reflections that take place in the fiber core, the higher the mode for that light. Figure 3 illustrates this.

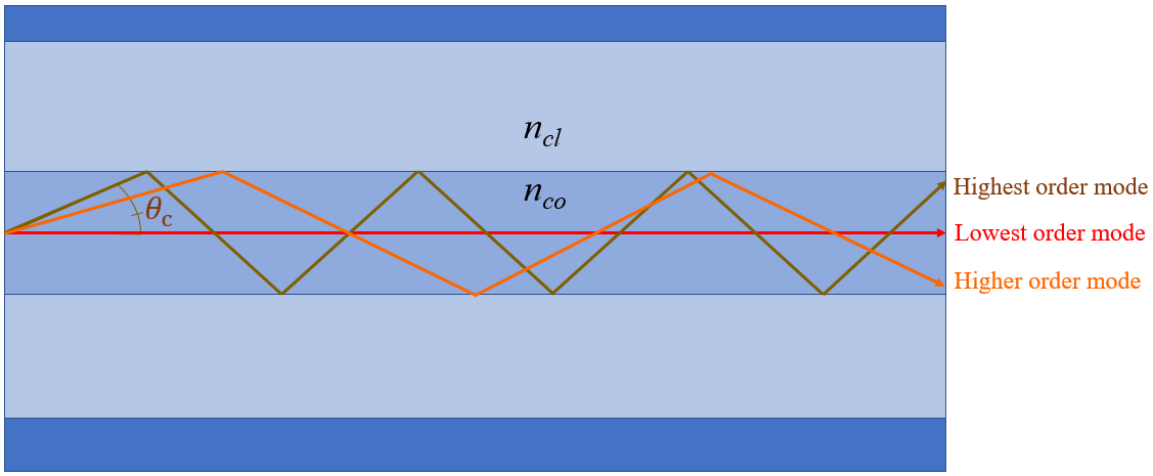

Figure 3. Illustration of Multiple Modes in a MM Fiber

In a MM fiber, the core diameter is a large multiple of the input wavelength. As the fiber core diameter is decreased it starts to approach the wavelength of input light. Eventually the diameter of the fiber core will be so small that light can only propagate along the fiber axis in the lowest possible order. This is how a single-mode (SM) fiber works, and SM fibers will only work for light with a wavelength less than or equal to its

cut off wavelength. Understanding the normalized frequency parameter (or V number) is essential to understanding the cutoff wavelength of a SM fiber [65].

$$V = 2\pi(NA)\frac{a}{\lambda} \tag{2}$$

V is the normalized frequency parameter, NA is the numerical aperture, a is the fiber core radius and λ is the wavelength of input light. The cutoff V number is a known value and equals 2.405. The above equation can be rearranged to find the cutoff wavelength of input light λ_c for a SM fiber.

$$\lambda_C = 2\pi(NA)\frac{a}{V_C} \tag{3}$$

Any input light with a wavelength greater than λ_c will only allow the lowest order of propagation through the fiber. Any input light with a wavelength less than λ_c will allow higher order modes of propagation through the fiber. With this information it is easy to see that the fiber chosen for a certain experiment or task is highly dependent on the wavelength of the light that it will be used with.

The two types of fibers discussed this far are both randomly polarized fibers meaning there is nothing in the fiber itself that maintains the polarization of the input light. With fibers like these, anytime the fiber is moved, twisted or bent the polarization of the light inside the fiber can be affected. There are optical fibers that have the ability to maintain the polarization of the light traveling through them. These are called polarization maintaining (PM) fibers [65].

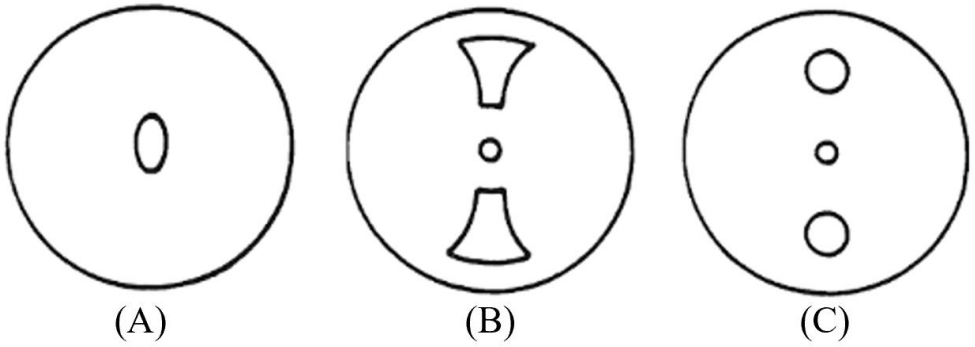

Figure 4. Types of PM SM Optical Fibers [65]

Figure 4 shows three different types of PM optical fibers. There are fibers with elliptical cores (A) and when light is coupled into them with polarization lined up with the major axis of the ellipse the polarization of the light will be maintained. Another form of PM fiber is a stress induced birefringent fiber seen in Figure 4 (B) and (C). There are cores of a different material aligned along one axis of the fiber core. These cores induce internal stresses which result in a slight change in refractive index of the cladding which results in a slight difference in refractive index along the major and minor axis of the fiber core. When input light polarization is aligned to the major axis of the fiber core the polarization of the input light will be maintained [65].

Last optical fiber concept to cover is a Fabry-Pérot Interferometer (FPI). This is a device that is constructed of two reflective surfaces which can trap reflected light between them. Figure 5 shows a diagram of an FPI and how it operates.

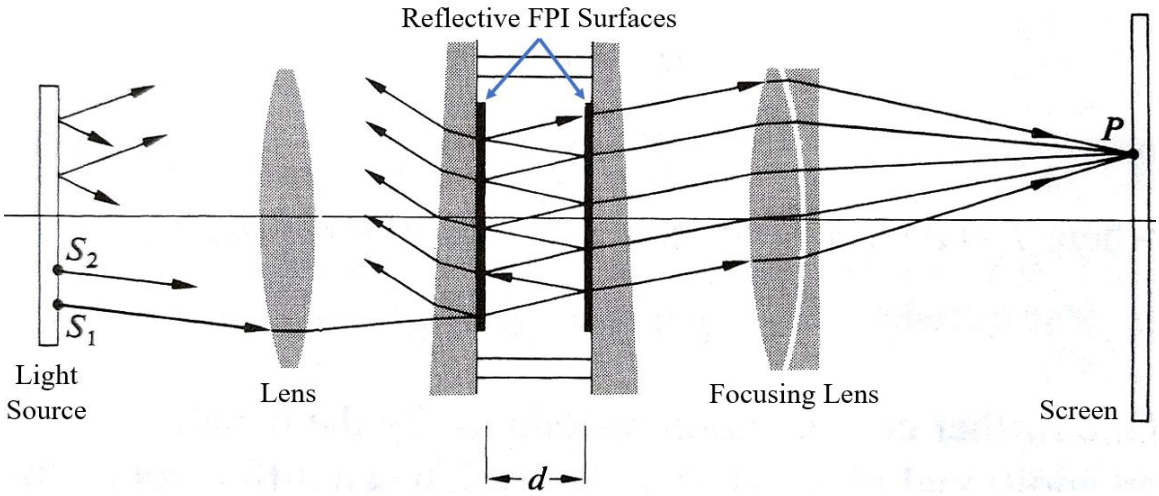

Figure 5. Diagram of an FPI [21]

Light S_1 is transmitted through one of the reflective surfaces to enter the FPI. The remaining light then is partially reflected back and forth between the two surfaces. Every time the light collides with one of the reflective surfaces, a portion of that light transmits through the surface and escapes the FPI (assuming negligible absorption). This escaped light is then refocused using a lens onto point *P*. As the diagram shows, a single input light wave is split into multiple waveforms by the FPI. This is what an interferometer does. The input light is divided up into many transmitted beams which have all traveled a different length and when reunited through a focal lens they will interfere with one another (either constructively or destructively). Every transmitted beam having traveled a different path length results in light at many different phases. The interference experienced by these light beams appears as a pattern of light and dark bands known as fringes. Figure 6 shows one of these projections from and FPI.

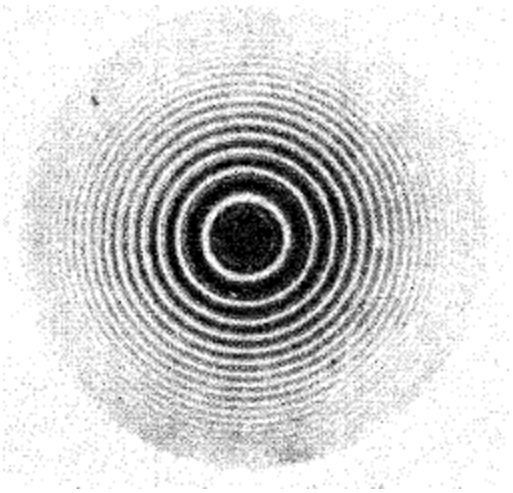

Figure 6. Centric Interference Fringes of a FPI with Plane Mirrors [67]

The bright fringes are where multiple light waves constructively interfere to where the dark bands are created due to destructive interference. Information that can be gathered from these fringes include precise wavelength determinations, measurements of small distances, and determination of refractive indices. The thinner the light fringes the higher the quality factor of the FPI which is due to a higher reflectivity of the two FPI reflective surfaces [21, 67].

Related Work in Fabry-Pérot Interferometry

Once the basic concepts of light and how it is transmitted is understood it is time to dive into other research. The first area of research that will be investigated is other work with FP sensors created using fiber optics. There are many examples of these [6, 10, 20, 35, 36, 38, 63, 64, 70, 76] and a few of them will be covered in greater detail.

All these sensors create an FP cavity(s) with the core of a certain type of optical fiber(s). These sensors are made to detect a variety of things such as temperature,

humidity, and/or airborne chemicals. L. H. Chen fabricated a humidity sensor by splicing a short segment of hollow optical fiber (HOF) onto the tip of a single mode fiber and coated the very tip (of the HOF) with a thin sensing film that reacts to atmospheric humidity [6]. Figure 7 shows the diagram of this humidity sensor.

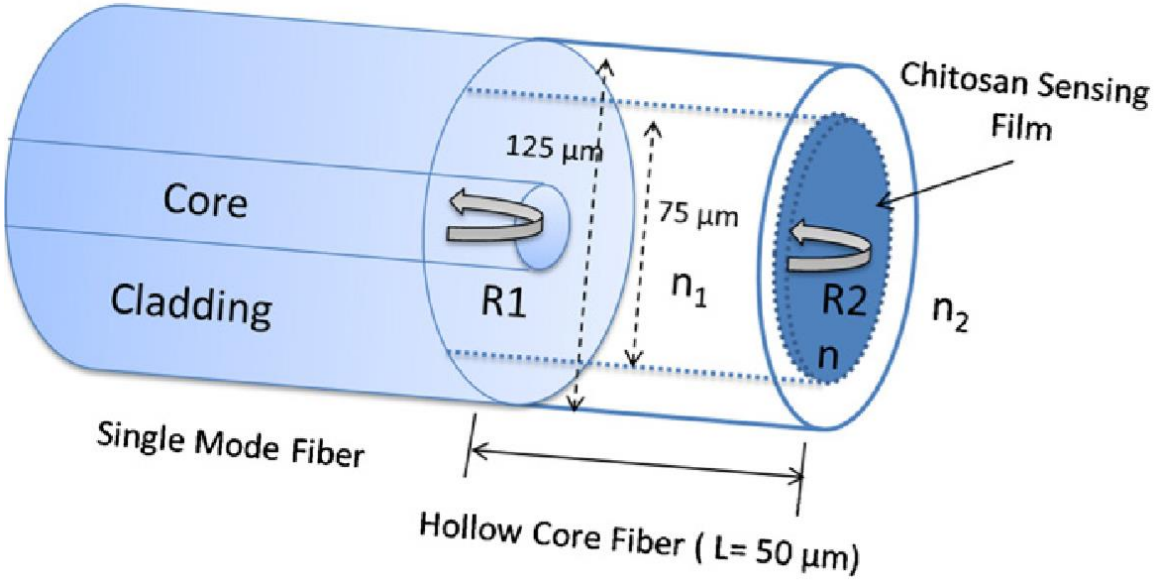

Figure 7. Schematic Diagram of Fabry-Pérot Fiber Humidity Sensor [6]

The cavity of the FPI is the hollow core of the HOF with the two reflective surfaces being the end face of the SM fiber and the humidity sensing film. As this film is affected by the atmospheric humidity it expands which changes the length of the HOF cavity. This expansion results in an altered reflection spectrum of this HOF FPI. This relationship can be seen by the equation below.

$$\lambda_m = \frac{2n_1 L}{m} \tag{4}$$

Where λ_m is the wavelength at which a resonance dip occurs. The refractive index of the medium the light is traveling through is n_1 and the length of that medium is L. The order of the spectral dip is m. A wavelength resonant dip occurs when light being reflected from the first reflective surface destructively interferes with light reflecting off of the second reflective surface which results in no (or very little) light transmitting back to the detector. If the refractive index of the medium or the length of the cavity increases, then the wavelength the resonant dip will occur at also increases. The change in this resonance dip is how a change in temperature is sensed. This formula is useful for theoretically calculating how much a certain resonant dip should shift. Another very useful formula is the relationship that determines the free spectral range (FSR). The FSR is the change in wavelength between two adjacent wavelength resonance dips. The formula for FSR is shown below [21]. $\Delta\lambda$ is the change in wavelength between two adjacent resonance dips, and λ_0 is the wavelength at the first resonance dip.

$$\Delta\lambda = \frac{\lambda_0^2}{2n_1 L} \tag{5}$$

This fiber tip FPI sensor, like many others, has a simple fabrication process of splicing two different types of fibers together. It comes in a small and flexible overall package allowing for easy application. L. H. Chen has shown that this sensor is very sensitive, achieving a sensitivity of 0.13nm wavelength shift per one percent change in humidity, and is able to respond in almost real time.

There are two other cases where different types of optical fibers are spliced together to create an FPI specifically for temperature sensing [10, 64]. Woo-Hu Tsai

constructed a fiber tip temperature sensor similar to the humidity sensor created by L. H. Chen. It consists of a short segment of SM fiber with core diameter size of four micrometers spliced onto another SM fiber with a larger core diameter of eight micrometers. The short segment of four-micron diameter core acts as an FPI and when exposed to thermal radiation this cavity can expand and/or the refractive index of the cavity can change. These changes cause a phase shift in the reflected light which is detected. Woo-Hu Tsai was able to achieve a sensitivity of 0.2333 radian phase shift per degree Celsius [64]. A slightly more complicated FPI fiber tip sensor was created by Hae Young Choi having two separate FPI cavities created by splicing together two different segments of optical fiber onto the tip of a third fiber. This is displayed in Figure 8.

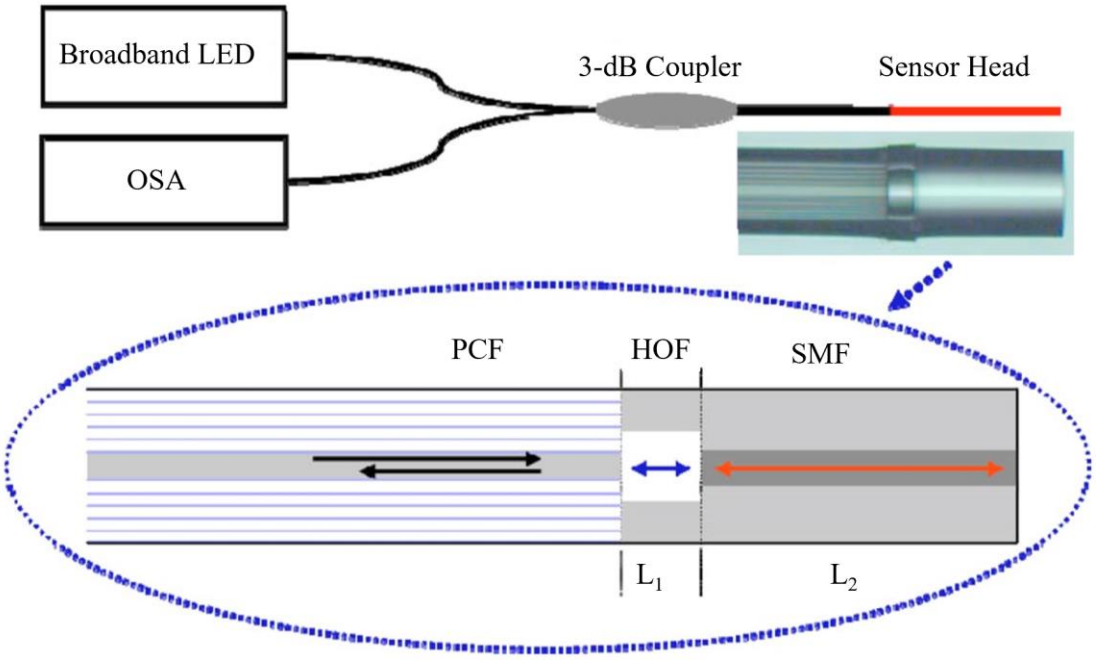

Figure 8. Schematic of the Sensor System and Sensor Head [10]

The fiber that guides the input light to the sensor head is photonic-crystal fiber (PCF). This type of fiber comes with advantages such as the ability to carry more power,

larger contrast available for effective index guidance, and less significant attenuation effects [30]. The middle section of the sensor is a short segment of HOF, and the last segment of the sensor is a simple SM fiber. This sensor has two FPI cavities each created by the HOF and SM fiber of length L_1 and L_2 respectively.

Equation (4) already explained above shows the relationship of how altering the refractive index or cavity length will alter the wavelength at which the resonant dip occurs. L can increase as thermal expansion takes place resulting in an increase in wavelength which is a shift to the right in a reflection spectrum. This is known as the thermo-elastic effect. Temperature also influences the refractive index of materials [29, 37, 45, 58, 71] which is known as the thermo-optic effect. Generally, as temperature of a material increases the refractive index will decrease [15, 79]. This results in a smaller wavelength which will shift the reflection spectrum to the left.

The sensitivity achieved by this sensor is a frequency shift of 1.2 oscillations (over a 100 nm wavelength change) over a 1000^{o}C change. This comes to a 0.0012 frequency shift per degree Celsius. The thermo-optic effect in the SM fiber portion of the sensor dominated meaning that these frequency peaks shifted to the left as temperature increased. This is not surprising since fused silica fiber does not expand a lot with heat as its coefficient of thermal expansion (CTE) is roughly $10^{-6}K^{-1}$. These temperature sensors could achieve a higher sensitivity if a material with a larger CTE was utilized. Another complication with these fiber tip designs is the splicing between different fiber types needs to be done carefully and be properly aligned. It is difficult to control the exact lengths of the fibers spliced onto the tip. If the fibers are not correctly aligned or lengths aren't correctly manufactured tremendous losses can occur.

Related Work in Bragg Gratings

There have been many optical fiber sensors created using a different technique called Bragg gratings. A Bragg grating is simply a periodic FPI which acts as a filter for certain wavelengths of light. This is accomplished by having periodic variation in the refractive index of the medium that the light is traveling through. This period of changed refractive index is in phase with a certain wavelength which is the only wavelength that will be reflected. The wavelength that is reflected, λ_B, due to a Bragg grating is shown by the equation below [22].

$$\lambda_B = 2n_e\Lambda \tag{6}$$

Where n_e is the effective refractive index and Λ is the grating period. Some examples of fiber optic Bragg grating sensors are shown here [3, 11, 17, 25, 26, 28, 42, 43, 46, 52, 54, 57, 59, 75, 77] and a few of these will be covered in greater detail. Some of these fiber optic Bragg grating sensors were used for measuring temperature [26, 75, 77] and they were all constructed with the same technique. Each of these sensors utilizes a SM fiber that has been selectively exposed by a femtosecond laser to create the periodic change in refractive index in the core of the fiber. This creates a Bragg grating sensor inside the fiber. This grating acts as a sensor the same way a FP sensor operates. When the Bragg grating is exposed to thermal radiation, or any material that may change refractive indices then the reflection spectrum of the Bragg sensor will change. A diagram of an optical fiber Bragg grating sensor is shown in Figure 9.

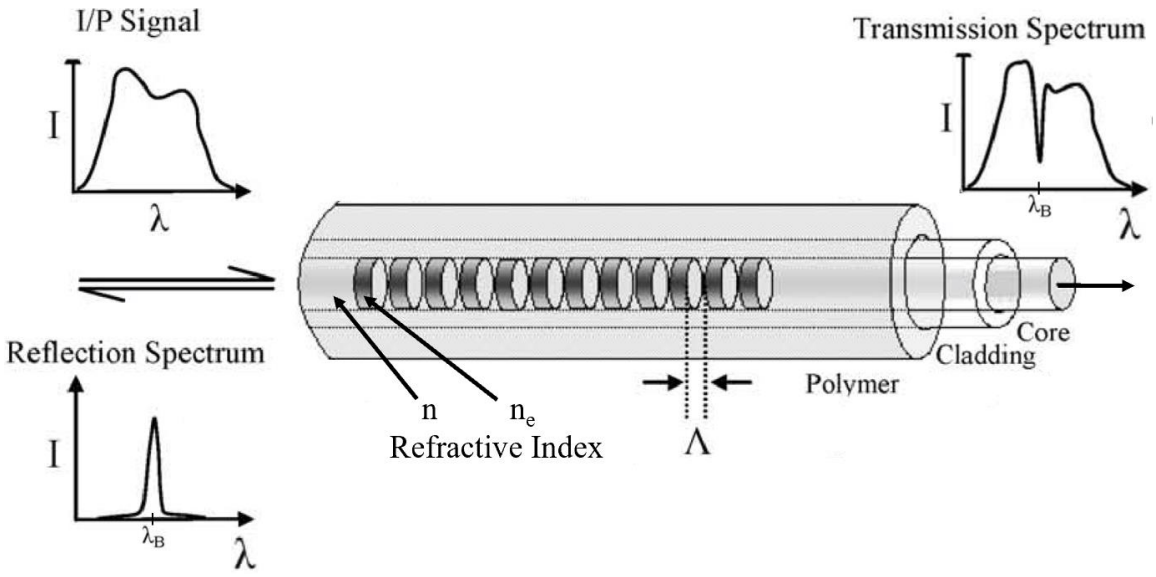

Figure 9. Diagram of Optical Fiber Bragg Grating Sensor [75]

These sensors come with the many benefits of utilizing fiber optics, but have an advantage over the FP sensors discussed before as the fabrication process does not rely on proper alignment or properly fused fibers. Instead the fabrication process is slightly more complicated with the use of a femtosecond laser, but the resultant sensor device is more robust and has no fiber to fiber interfaces that can result in loss of power. These sensors are able to obtain sensitivities ranging from 11 to 32 picometer shift in wavelength per degree Celsius. This is even more sensitive then the FP sensors discussed earlier. The one large disadvantage that both FP and Bragg grading sensors share is still the material in which they are made of. The sensitivity of these devices thermal radiation sensing is limited to the low CTE of the material used.

Bragg grating sensors are also used to detect VOC's or any other airborne material that has a different refractive index [3, 11, 59]. This is accomplished by taking the same Bragg grating sensor illustrated in Figure 9 and exposing the core of the fiber to

the atmosphere. This is accomplished by stripping away the protective polymer sheathing and etching away a portion of the cladding. The closer the cladding diameter gets to the core diameter the more sensitive the sensor will be. The maximum sensitivity achieved by these sensors is a 1394 nanometer shift in wavelength per refractive index unit (RIU) [11]. Though this sensitivity is appealing it comes at a cost. Constructing a sensor in this way, exposing the core of the fiber to the environment severely reduces the durability and robustness of the sensor. This sensor structure is also much longer in comparison to fiber tip sensors which makes specific placement more difficult. These drawbacks limit its real-world application.

Related Work on 3-D Fiber Tip Sensors

A third style of fiber optic sensors consists of 3-D structures that are fabricated onto or near the tip of an optical fiber. These structures provide cavities and surfaces for input light to travel through and reflect off. Here is a list of many related works who have accomplished things like this [13, 24, 31, 32, 33, 40, 41, 56, 61, 62, 72, 74, 78]. The majority of these sensors are fabricated by etching a very precise notch(s) in the side of an optical fiber. This notch is cut deep enough into the fiber to reach the entire fiber core. This creates an FPI with the two reflective surfaces being the sidewalls of the micro notch. Both an optical image and diagram of one of these sensors is shown below.

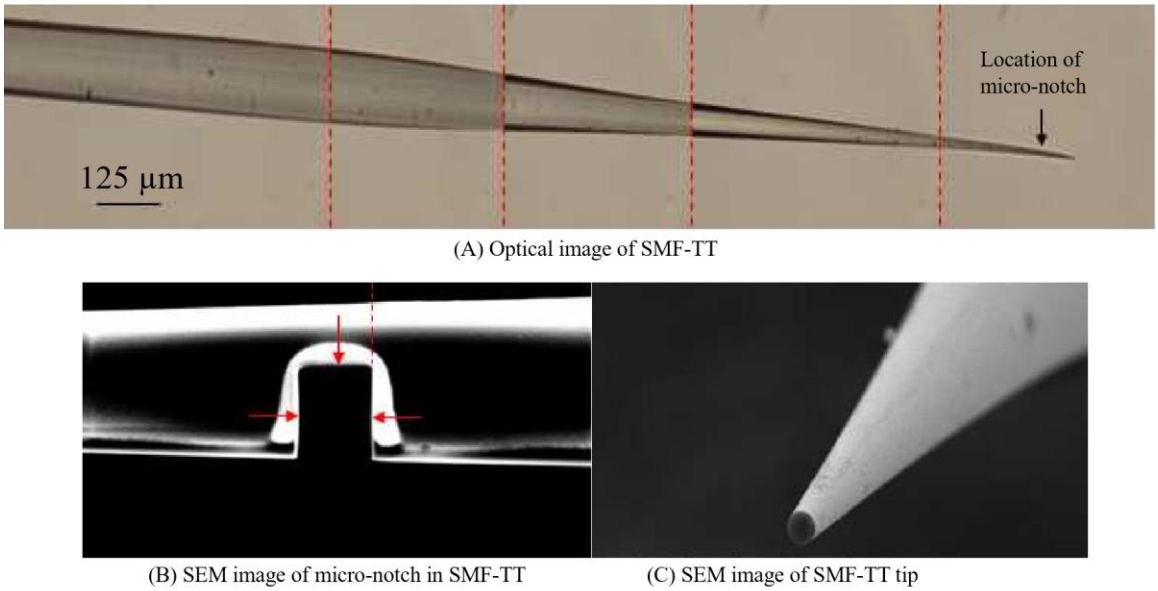

Figure 10. Images of SMF-TT and Micro-Notch FPI [31]

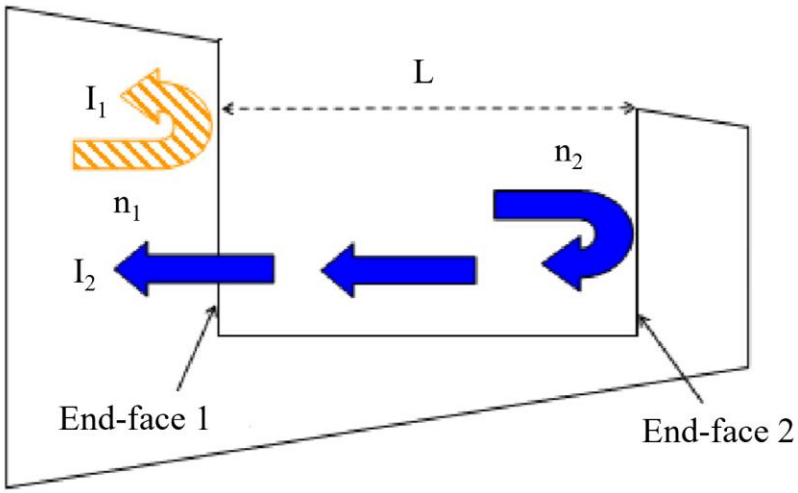

Figure 11. Diagram of SMF-TT and Micro-Notch FPI [31]

In this specific case a SM fiber with tapered tip (SMF-TT) was used which granted greater sensitivity to temperatures. The cavity of this FPI is open to the atmosphere which will yield much greater sensitivity when measuring the presence of

any VOC's. This can even be accomplished when creating a Bragg grating sensor by etching multiple periodic micro notches as shown in Figure 12.

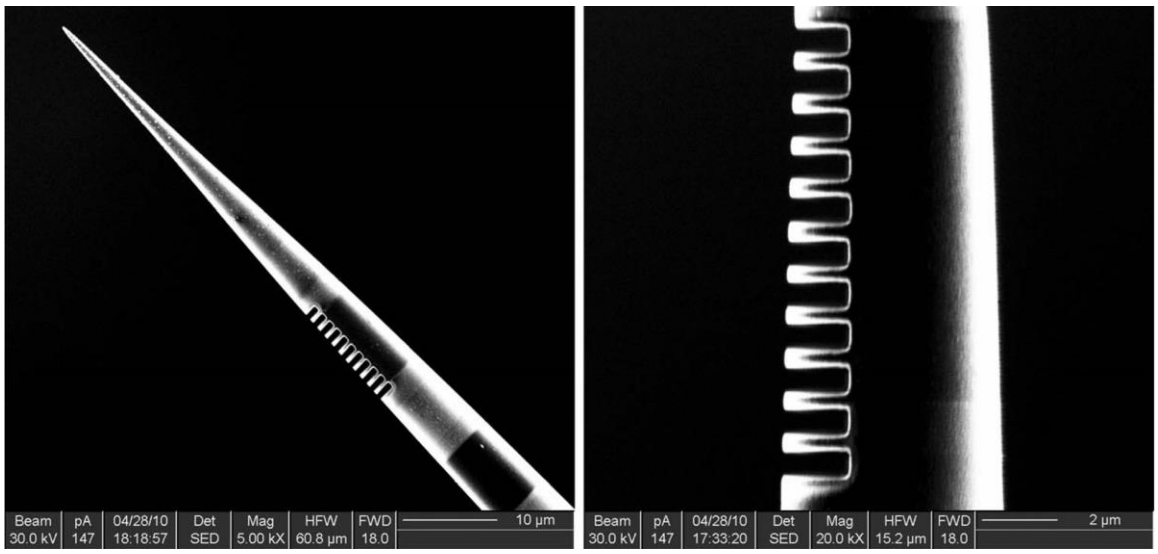

Figure 12. Bragg Grating Structure Fabricated with Micro Notches [13]

Creating fiber optic sensors in this way adds yet another complicated fabrication process that requires specialized equipment with the capability and resolution to etch these micro notches. Fiber sensors with these micro notches also lose robustness as the structural integrity is degraded by performing these cuts. That being said, some of these sensors are able to achieve sensitivities of around 43 picometers per degree Celsius [24] and 1,163 nanometers per RIU [72].

In all the literature reviewed the closest example to the research completed in this thesis is an optical fiber-tip sensor created by Mian Yao [74]. A polymer structure made of SU-8 is 3-D micro-printed onto the tip of a fiber. This structure covers the core of the fiber and acts as a reflective surface. The surface of the fiber face and the surface of the

structure together act as an FPI. Figure 13 shows the different structures printed by Mian Yao and their reflection spectrum.

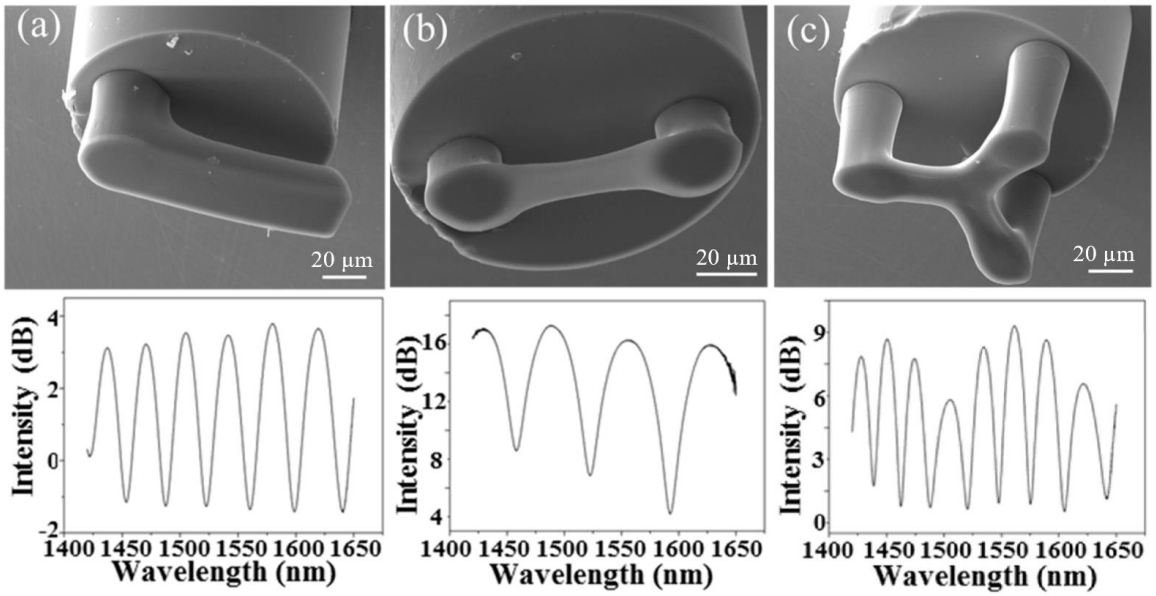

Figure 13. SEM Images of Optical Fiber-Tip Sensors [74]

The fabrication process used by Mian Yao is similar to a semiconductor device fabrication. Once the fiber tip is properly cleaned a thin layer of SU-8 is accurately deposited onto the fiber tip using an ultrasonic nozzle and xy-axis motorized stage. This SU-8 film was then soft baked to remove leftover solvent. Then the SU-8 is exposed with a digital camera-based machine vision metrology according to a CAD file specifying the design of the device. Following exposure was a post bake. This process was repeated layer by layer until the entire structure was complete. Once all layers were completed the SU-8 was developed using propylene glycol methyl ether acetate (PGMEA) which would only leave behind the exposed SU-8 resulting in the designed structure on the tip of the fiber. This fabrication process is precise but takes a long time as the device must be made layer by layer [74]. The minimum feature size of this fabrication process was not

included in this paper, but it is dependent on the minimum thickness of a SU-8 layer and the resolution of the exposure technology.

The sensor operation is simple, the polymer structure has a certain refractive index. The dimensions of the structure and the distance from the bottom of the structure to the face of the fiber are all known. Light traveling through the fiber will travel through the airgap between the fiber face and structure, and then collide with the bottom of the structure. A portion of that light will be reflected back into the core of the optical fiber and a portion will be transmitted through the polymer structure. When air (with a refractive index of 1) fills the gap between the fiber face and structure there is a certain reflection spectrum with resonant dips at certain wavelengths. These resonant dips occur when the light reflecting off of the fiber tip face and the light reflecting off of the structure bottom destructively interfere. When a substance in gas or liquid form (with a different refractive index) fills the gap under the structure the reflection spectrum changes and this change is what is detected. This is the same relationship described in equation (4).

If the refractive index of the medium increases, then the wavelength of the resonance dip will increase. The change in this resonance dip is how a change in refractive index is sensed. Figure 14 shows the change in reflection spectrum due to a change in refractive index in the gap underneath the structure.

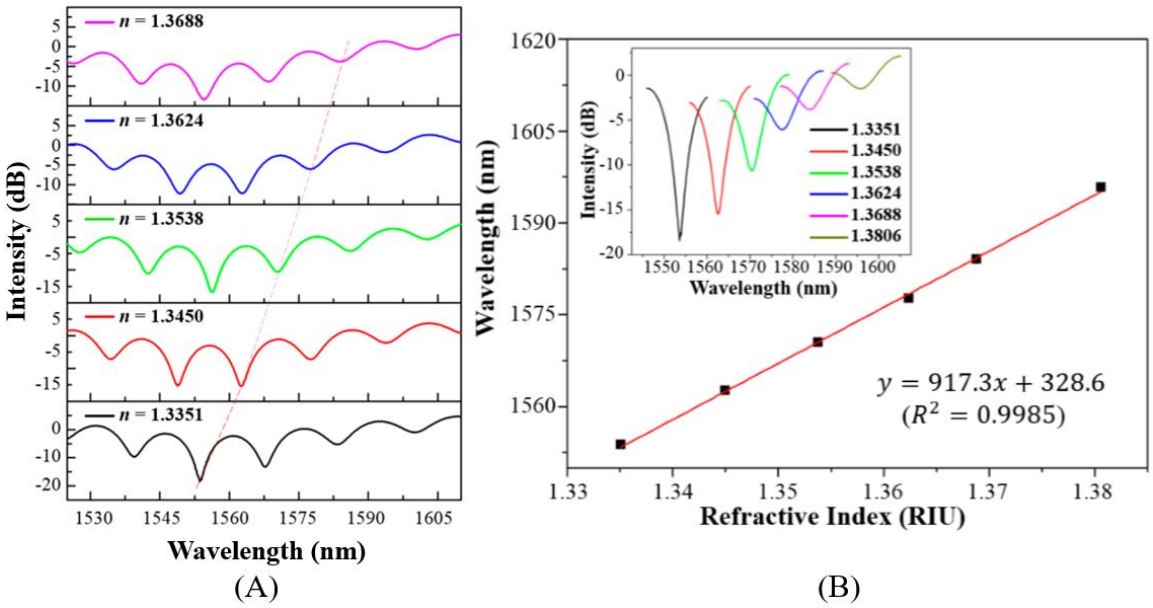

Figure 14. Measured Reflection Spectrum of an Optical Fiber Tip Sensor Immersed into Liquid with Different Refractive Indices (A). Change in Wavelength due to Change in Refractive Index (B) [74]

The liquid used in this experiment is calcium dichloride ($CaCl_2$) with varying concentrations. The dashed red line seen in (A) tracks the same resonance dip as the concentration of $CaCl_2$ was changed to increase the refractive index. The sensitivity, or change in wavelength due to refractive index, of the fiber tip sensor is shown in (B). The sensitivity Mian Yao was able to achieve was 917.3nm/RIU.

Quality Factor

Now that some fiber tip sensors have been explored and various reflection spectra's have been observed it is useful to understand more about reflectivity and how increasing it can possibly improve a sensor. Once a device is created and tested it is important to determine the resolution of the device, or the minimum detectable change in whatever is being sensed. In the case of the temperature sensor the resolution would be

the minimum temperature change that can be detected. To improve the resolution of a sensor the quality factor needs to be increased. For optics the quality factor is closely related to the finesse which is the ratio between the adjacent maxima (or minima) and its half-width [21]. The higher the quality factor the narrower the peak (or dip). Smaller shifts can be detected with higher quality factor sensors. Obtaining a higher quality factor can be done by increasing the reflectivity of the surfaces in the FPI.

$$Q = \frac{nL}{\lambda} f \tag{7}$$

$$f = \frac{\pi\sqrt{F}}{2} \tag{8}$$

$$F = \left(\frac{2\sqrt{R}}{1-R}\right)^2 \tag{9}$$

Where Q is the quality factor, n & L is the refractive index and length of the cavity respectively, λ is the input wavelength and f is the finesse. Breaking down finesse, F is the coefficient of finesse which is determined by R, the reflectance of the surface. The value for reflectance always lies between zero and one as the sum of total transmission, reflectance and absorption equals one. As the reflectivity approaches one the finesse increases which will result in a higher quality factor [21].

Applying a thin reflective film is a method that can be used to increase the reflectivity of the FPI devices created on optical fiber tips. There are many materials that can be deposited in thin films which increase the reflectivity of a surface [50]. Most of these materials are metallic. Before a material is chosen for a thin reflective coating it is important to know how the thin layer will be deposited onto the fiber sensor.

Sputtering and evaporation are the two most common methods for applying metallic coatings, but both of these processes only deposit on a line-of-sight basis. This is a problem for a device with an airgap underneath it as not all of the surfaces will be coated. The same issue is present when plasma-enhanced chemical vapor deposition (PECVD). The only deposition process that applies a uniform layer on all surfaces of a device is the atomic layer deposition (ALD) process [16]. The ALD is able to deposit many different materials [4, 9, 47, 48] some of which will be tested for reflectivity in this thesis.

Increasing the reflectivity will increase the amount of light reflected back into the core, and as previously discussed we know this increases the quality factor. Another method for increasing the amount of light reflected is to use confocal surfaces to guide the reflected light back to the fiber core. A confocal surface can be designed by a curved surface with a radius two times the distance to the focal point [21].

Summary

How light propagates, and how it interacts with various surfaces was cover in detail to provide a basis of understanding how light can be utilized for sensor applications. Many related articles were covered showing examples of how fiber optics can be used to create both refractive index sensors and temperature sensors. The three main types of fiber optic sensors covered were FP sensors created through splicing fibers, Bragg grating sensors, and 3-D fabricated fiber tip sensors through etching and other processes. For temperature sensing the best sensitivity achieved was a 43 pm/^{o}C shift in wavelength. For refractive index sensing the best sensitivity achieved was 1394 nm/RIU.

These results will be used for comparison later in chapter 4. Lastly, the reflectivity was discussed and how it is related to the performance of certain optical fiber tip sensors.

III. Methodology

Chapter Overview

The purpose of this chapter is to outline the entire process for designing, fabricating, and testing the optical fiber tip sensors created in this thesis. As mentioned before, the fabrication process utilizes a photosensitive polymer 3-D micromachining process to fabricate the sensors. A total of three different sensor designs were fabricated and tested, and each of these designs will be covered in great detail.

Sensor Design

There will be a total of three different device designs that will be 3-D micromachined out of polymer onto an optical fiber tip. The first device will be a simple layer of polymer which will act as a single cavity FPI. The second will be a suspended structure with three interfaces acting as a two cavity FPI. Figure 15 shows these devices and the surfaces that will reflect/transmit light.

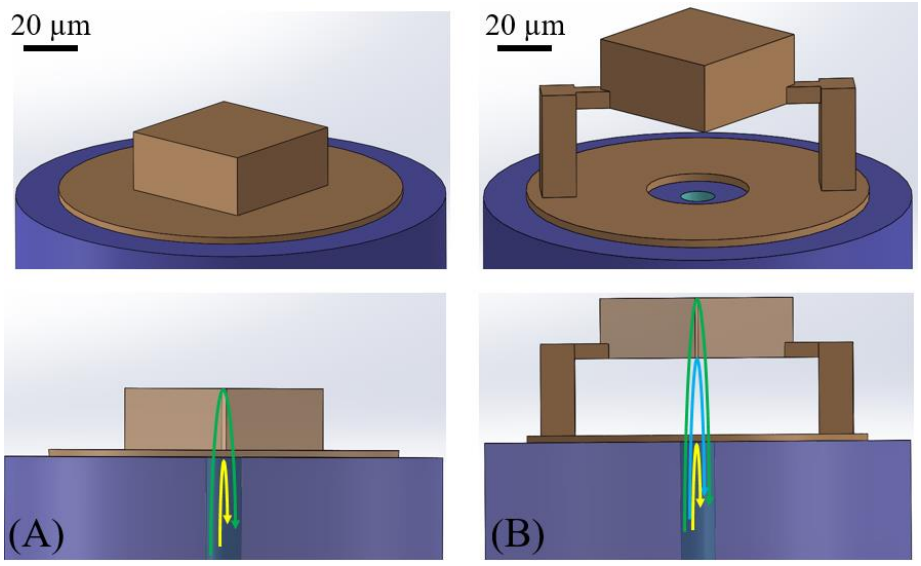

Figure 15. Single Cavity FPI (A) and Double Cavity FPI (B) Fiber Tip Sensors

For the single cavity device (A) there is the interface between the fiber core and the polymer structure (represented by the yellow arrow) followed by an interface between the polymer structure and air (represented by the green arrow). For the double cavity device (B) there are three interfaces. One between the fiber core and air (yellow arrow), another between air and the polymer structure (blue arrow), and the last one between the polymer structure and air (green arrow).

Both these devices are 40 μm wide by 40 μm long and 17.58 μm tall. The air gap under the suspended structure is 22.5 μm tall. The width and length dimensions of the structure are not significantly important as they just need to be large enough to cover the entire NA of the light coming out of the fiber core. NA of SMF 28 fiber (the fiber used for these sensors) is 0.14 and with an air gap of 22.5 μm the light coming out of the fiber core can cover a circular area on the bottom of the structure of radius less than 8 μm. The height of the air gap was specifically designed to achieve a theoretical FSR of 53.4 nm in air at a 1550 nm wavelength. The same theoretical FSR for the IP-Dip Polymer structure is 35.5 nm. With FSR's of this size multiple peaks can fit within the 1463 nm to 1643 nm sweep range yet the FSR is large enough to observe the entire intensity change.

The last device designed is a suspended confocal surface structure which will also have two FPI cavities with the theoretical ability to focus more reflected light back into the core of the fiber. Figure 16 shows this confocal surfaced structure.

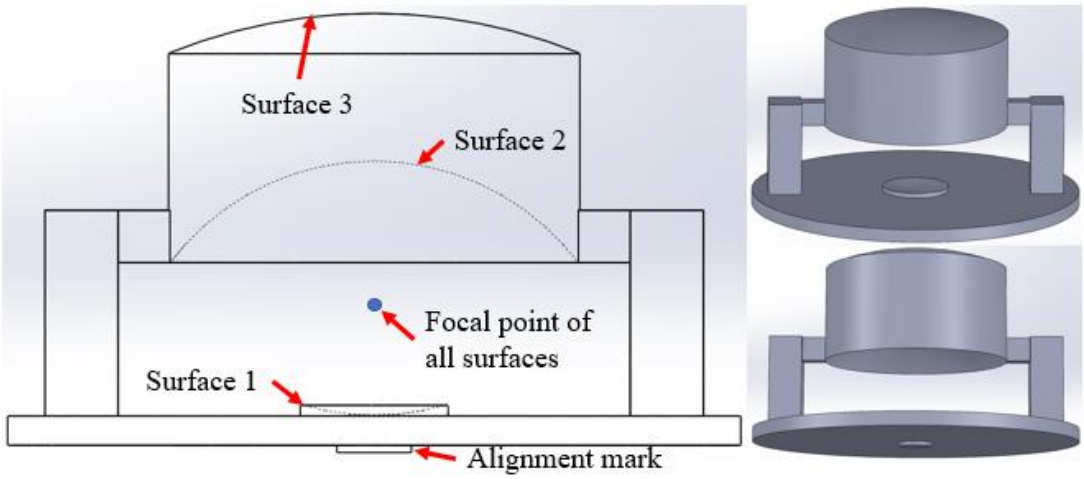

Figure 16. Confocal Surfaced Double Cavity FPI Fiber Tip Sensor

All three surfaces have a focal point in the center of the first air gap cavity for reflected light. This device will be tested to see if more light is reflected back to the fiber core leading to the detector. An alignment mark is utilized to enable proper alignment to the core of the fiber during the 3-D fabrication process. The large circle base on all three device designs are there to maximize the surface area between the fiber tip face and 3-D microfabricated polymer structure. This results in a stronger bond between the two surfaces which yields a more robust sensor. Full sensor design specifications can be found in Appendix A.

Now that the sensor designs have been covered, the functionality of the sensors must be explored. When light of varying wavelengths traveling through the fiber core collides with the surfaces of the 3-D fabricated structure some of that light will reflect back into the fiber core (and be detected) and some light will be transmitted through. When the input light wavelength is an integer multiple of double the cavity distance (round trip distance) then the light will destructively interfere with the light reflecting off

of the surface before the cavity [21]. This interference will result in little to no light reflected back into the detector which will result in a resonant dip in intensity. These dips will be observed in the reflection spectra recorded from experimentation. When the cavity lengths or refractive indices are altered then the wavelength at which these resonant dips occur will change. This change is resonant dip is what is detected and how these devices act as sensors.

Sensor Fabrication

The first step of the fiber tip sensor fabrication process is to properly prepare the fiber for the 3-D two-photon polymerization process. The fiber used for this thesis is F-SM1500-9/125-P which supports single mode light propagation for a 1550 to 1650 nm wavelength range. This fiber also has a polyimide sheathing which can withstand temperatures up to 300^{o}C. To prepare the fiber tip for anything it first needs to be cleaned and cleaved properly. Instructions on how to do this are given in Appendix B.

Once the fiber is properly cleaved it is ready for the 3-D two-photon polymerization process. The equipment used to do this is a Nanoscribe with IP-Dip polymer resin. Vincent Tondiglia from AFRL/RXAP was the expert utilized for training and usage of this equipment. The Nanoscribe and IP-Dip are proprietary equipment manufactured by Nanoscribe GmbH headquartered out of Hermann-von-Helmholtz-Platz 1, 76344 Eggenstein-Leopolds-hafen Germany. The Nanoscribe 3-D fabrication process is displayed in Figure 17.

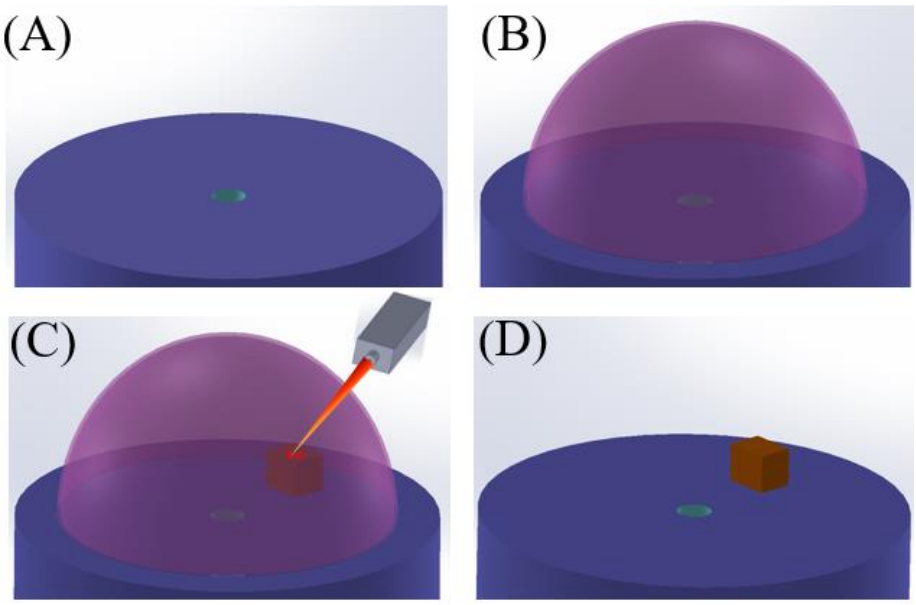

Figure 17. Nanoscribe 3-D Two-Photon Polymerization Process

Simply put, a flat clean surface is prepared for fabrication (A). IP-Dip resin, which is a photosensitive polymer resin is deposited onto the fabrication surface (B). A laser is then focused in the resin on the areas in which the fabrication takes place (C). Once the laser has hardened all the desired resin the surface is developed which will remove all the unhardened IP-Dip resin (D).

In greater detail the Nanoscribe's 3-D microfabrication process is based on the non-linear optical process of two-photon polymerization (2PP) [44]. This 2PP technology uses a laser that is focused in the IP-Dip resin. The IP-Dip is only exposed within the tight focal point of the laser that can vary in size depending on the structure design. The minimum laser focal point is 150nm wide by 150 nm long by 200 nm tall. The focal point is then scanned along according to an input CAD design resulting in a hardened polymer structure. The scan speed is constant for the entire fabrication process, but it can be set differently depending on the desired fabrication time and resolution. Specific instructions

on how to operate the Nanoscribe to fabricate 3-D fiber tip sensors are shown in Appendix C.

Sensor Testing

Before fabricating sensors onto fiber tips was conducted, sample sensors were fabricated onto a flat substrate for characterization purposes. A Bruker Dimension Icon Atomic Force Microscope (AFM) was used with scanasyst-air AFM tips to measure the surface roughness of the IP-Dip polymer structures. Once all characterization of the IP-Dip structures was completed, the fiber tip sensors were tested.

Nicholas Usechak and Joseph Suelzer from AFRL/RYDI were the experts who provided the lab, equipment, and expertise needed to test these fiber tip devices. The specific equipment used to test these devices was a D509254A digital storage oscilloscope, 8164B lightwave measurement system (laser source), Newport universal fiber optic detector (photo detector), Newport optical power meter model 1830-C, PM optical circulator, 28 SMF FC/APC optical fiber, and a Fujikura FSM-100P ARC Master fiber splicer. The first step is to splice the optical fiber strand with the 3-D microfabricated structure to another fiber of matching size with an FC/APC connector so that the device can be hooked up to the experimental setup for testing. The fiber splicer was set to a SM auto 1 splice mode with a tip length of nine millimeters and fiber diameter of 250 micrometers (including the sheathing). The heater mode was set to FP-03 60 millimeters. A reinforced shrink wrap was used to protect the spliced connection. Figure 18 shows how the testing experimental setup is done.

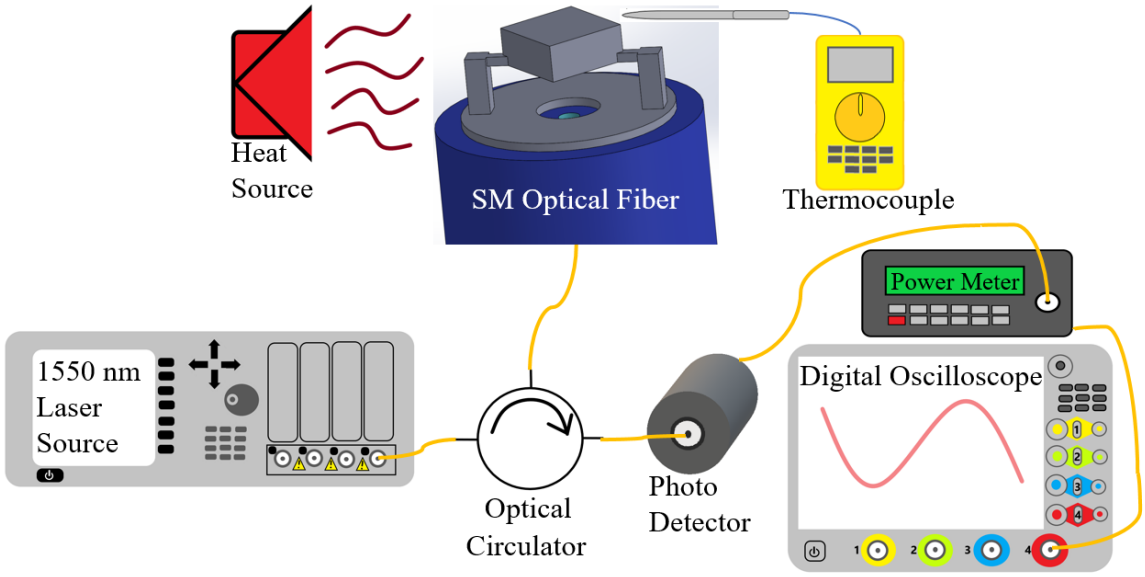

Figure 18. Optical Fiber Thermal Radiation Sensing Experimental Setup

The laser source was used to provide light to the fiber device at different wavelengths. The total wave lengths covered in the sweep is 1463 nm to 1634 nm (all in the infrared range). Specifically, the laser was ran at 1 mW cycling through the wavelengths at 2 nm per second with a 2 pm step size resulting in a total of 85,500 data points per sweep. This laser light is first sent to the optical circulator which then sends the input light through the fiber and into the device. Some of the light is reflected off one of the device surfaces and travels back through the fiber core to the optical circulator. The light reflected back is then sent to a photodetector which converts the amount of light detected to a voltage. This is then displayed by both the power meter and digital oscilloscope. The end of one complete data collection run yields a wavelength vs intensity dataset which can be compared to similar datasets obtained under different conditions. Before each experiment was conducted the fiber spliced to the fiber tip sensor was calibrated to maximize polarization therefore maximizing the amount of light

reaching the detector. This needed to be completed because the fiber tip sensor was fabricated on a non-polarization maintaining fiber. A trigger signal was also recorded which denoted the exact start and stop data locations of the wavelength sweep which is essential for comparing datasets to one another.

This experimental setup is specific to testing the fiber device for thermal radiation sensing. The heat source used is a hot plate with the thermocouple and fiber device suspended in air one centimeter above the hotplate surface. Data was collected from the device at room temperature through 120^{o}C at 20^{o}C increasing increments. Because of the airgap between the device and heat source, it was challenging to regulate the temperature of the device exactly. The temperatures usually ranged $\pm$ three degrees Celsius from the target temperature. Matlab 2017a was used to interpret the data gathered from each experiment. To mitigate any noise all the data was filtered in Matlab by using the smoothdata function which takes a moving average with a fixed window length. In addition to filtering each data set multiple experiments at each temperature was conducted to gather replicate data so they could be averaged together. This made the data more consistent as individual experiments can yield varying data due to the imprecise heat source.

A similar experimental setup was used for testing the optical fiber tip devices ability to sense VOC's, which can be seen in Figure 19.

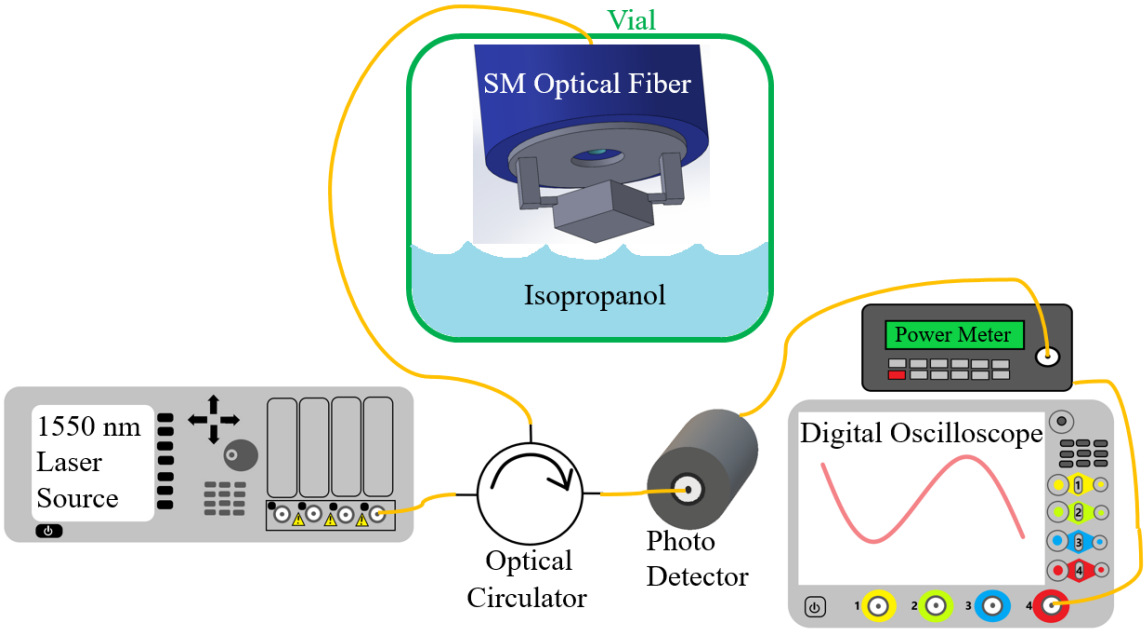

Figure 19. Optical Fiber Refractive Index Sensing Experimental Setup

As shown, the only VOC used in testing was IPA. This was used due to its low evaporation temperature which will fill the vial with a gaseous form which will be exposed to the fiber tip sensor. The vial used was sealed with a crimped aluminum cap and silicone seal. A hypodermic needle was used to house the fiber optic sensor and penetrate the silicone seal. A three axis micromanipulator was used to carefully insert the fiber tip sensor into the hypodermic needle. During experimentation the vial was placed on a hotplate at 50^{o}C which ensures a significant portion of IPA evaporates.

Each experimental run yielded a reflection spectrum of wavelength (in nm) versus intensity (in volts) which is the same output of the thermal radiation experimentation. Since the fiber tip sensor was not exposed to increased temperatures in this experiment there is minimal noise in the data. Because of this the raw data was used for analysis. The main difference between the thermal radiation experimental data and this data is that the

reflection spectrum shifts due to a change in refractive index caused by the presence of a VOC rather than a change in physical dimension due to thermal expansion.

The last experimental setup utilized is for measuring the reflectivity of a coated glass slide. Figure 20 is a diagram of this setup.

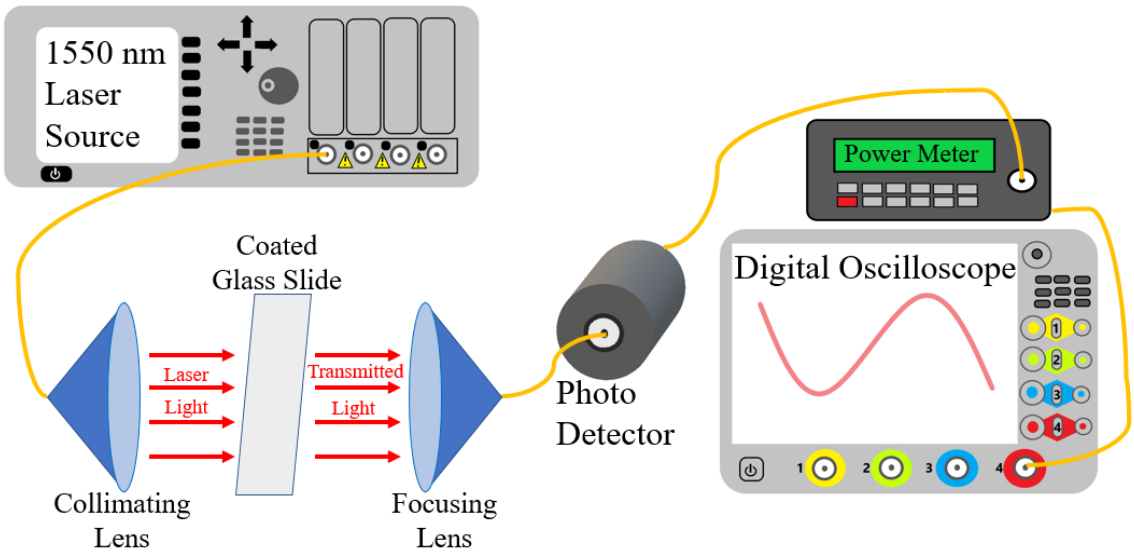

Figure 20. Transmission of Reflective Coating Experimental Setup

This experimental set up measures the light transmitted through the glass slide that is placed between the two lenses. It is assumed that the absorption of light is negligible so the reflectivity of the glass slide is simply one minus the transmission. Every time a glass slide is mounted in this setup it is properly aligned to maximize the intensity of the transmitted light. This setup is used to compare different thicknesses of reflective coatings.

Summary

This chapter covered how to prepare an optical fiber for sensor fabrication, how to utilize the Nanoscribe to fabricate the sensor, and how to test the sensors. A diagram for

each experimental setup was included and explained. Two of these setups are for testing fabricated fiber tip sensors and the third setup is strictly for testing the transmission and reflection of a coated glass slide. This chapter will be essential for anyone that is interested in follow on or verification work related to this thesis.

IV. Analysis and Results

Chapter Overview

The actual measured results of each fiber tip sensor will be displayed and analyzed. These results consist of different reflection spectra at different temperatures and refractive indices which are compared to one another. There is also discussion of some characterization data of the IP-Dip polymer used for 3-D fabrication of the sensors. All of the actual experimental results are also compared to theoretical values to demonstrate proper functionality.

Characterization Results

As mentioned earlier in chapter one the method of fabricating these optical fiber tip sensors needed to be chosen. There are four main factors in making this decision; ease of fabrication process, freedom in device design, device robustness, and surface roughness of the resultant structure. The two different fabrication processes evaluated is using a femtosecond laser to selectively expose areas of the fiber tip to be etched away and performing the etch with hydrofluoric (HF) acid [5]. The second fiber tip sensor fabrication process, which is what was chosen, is using the Nanoscribe to 3-D micro-fabricate a structure utilizing a photosensitive polymer.

The process for etching into the fiber tip must be done by a third-party company because the equipment for this process is not available to AFIT students. The Nanoscribe fabrication process was done in house as all the equipment and expertise was accessible. The Nanoscribe fabrication process was difficult to adapt for fabrication onto a fiber tip, but once adaptations were made the process was simple, and a single device could be

fabricated in roughly twenty minutes (followed by a forty-minute development). Both processes had a great deal of freedom in design as the femtosecond laser and Nanoscribe have the ability to focus in different areas allowing the fabrication of more complicated devices such as a confocal surfaced device. The device robustness for each method is comparable. Etching into the fiber tip does yield a very robust structure because the entire sensor is made of the same material. Creating a robust sensor with the Nanoscribe was accomplished, but some changes to the device design needed to be made. The anchor points of any 3-D fabricated structure needed to be enlarged to the size of the entire 125 micrometer diameter fiber face. This maximized the surface area for the fabricated device to adhere to the fiber tip. This had no impact on device functionality and improved the robustness greatly allowing fiber motion and exposure to various conditions without any sensor damage.

The last criteria for selecting a fabrication process is comparing the surface roughness of each resultant device. The first measurement taken was an AFM image of the surface of a 3-D micromachined structure fabricated using the Nanoscribe with IP-Dip. It is important to know the surface roughness of a material that will be used to reflect light because if the material surface has any change in elevation equal to a half of the input light wavelength then interference can occur. Figure 21 shows the surface roughness of a Nanoscribe fabricated clamped-clamped beam.

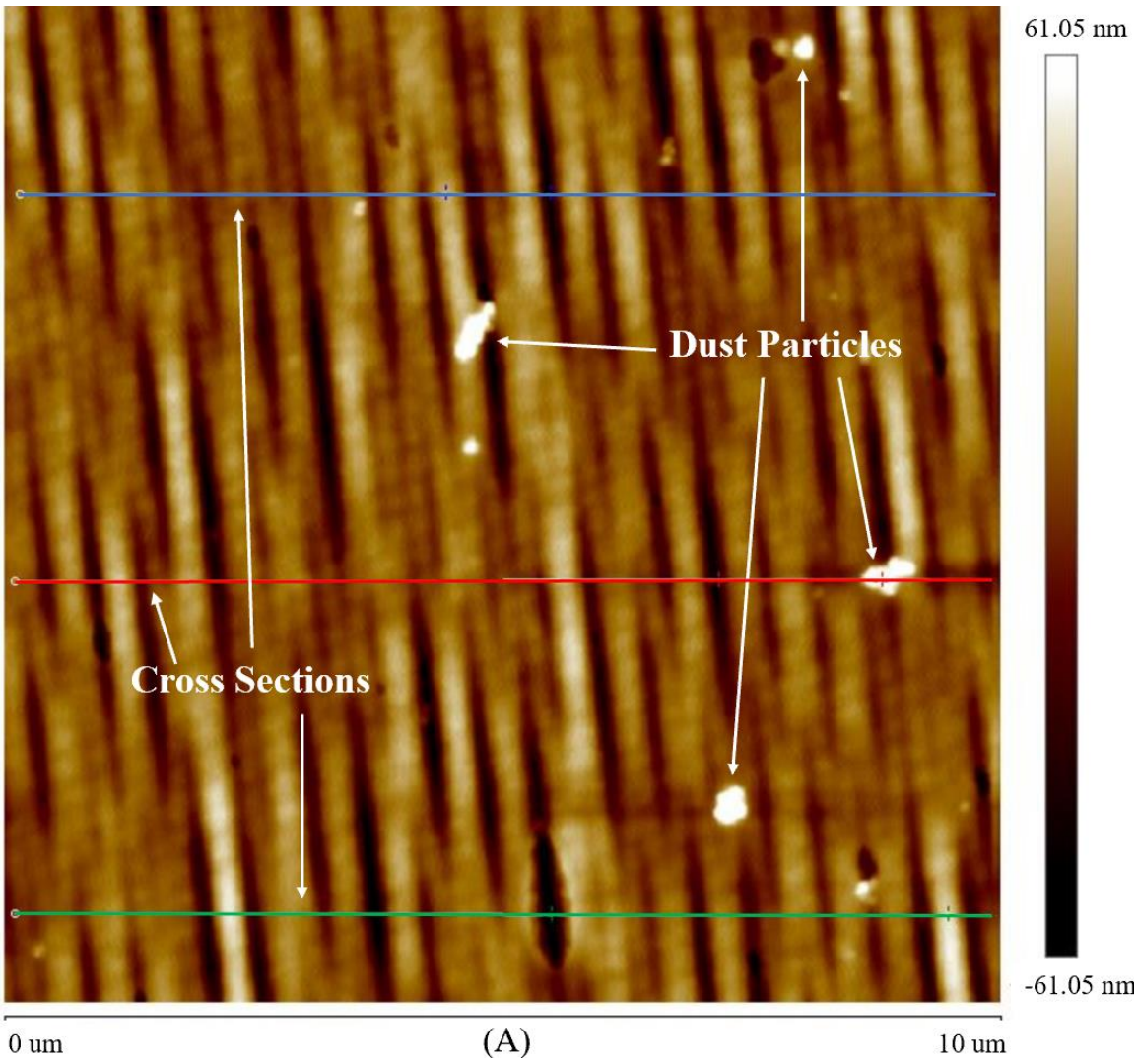
61.05 nm
Dust Particles
Cross Sections
-61.05 nm
0 um
(A)
10 um

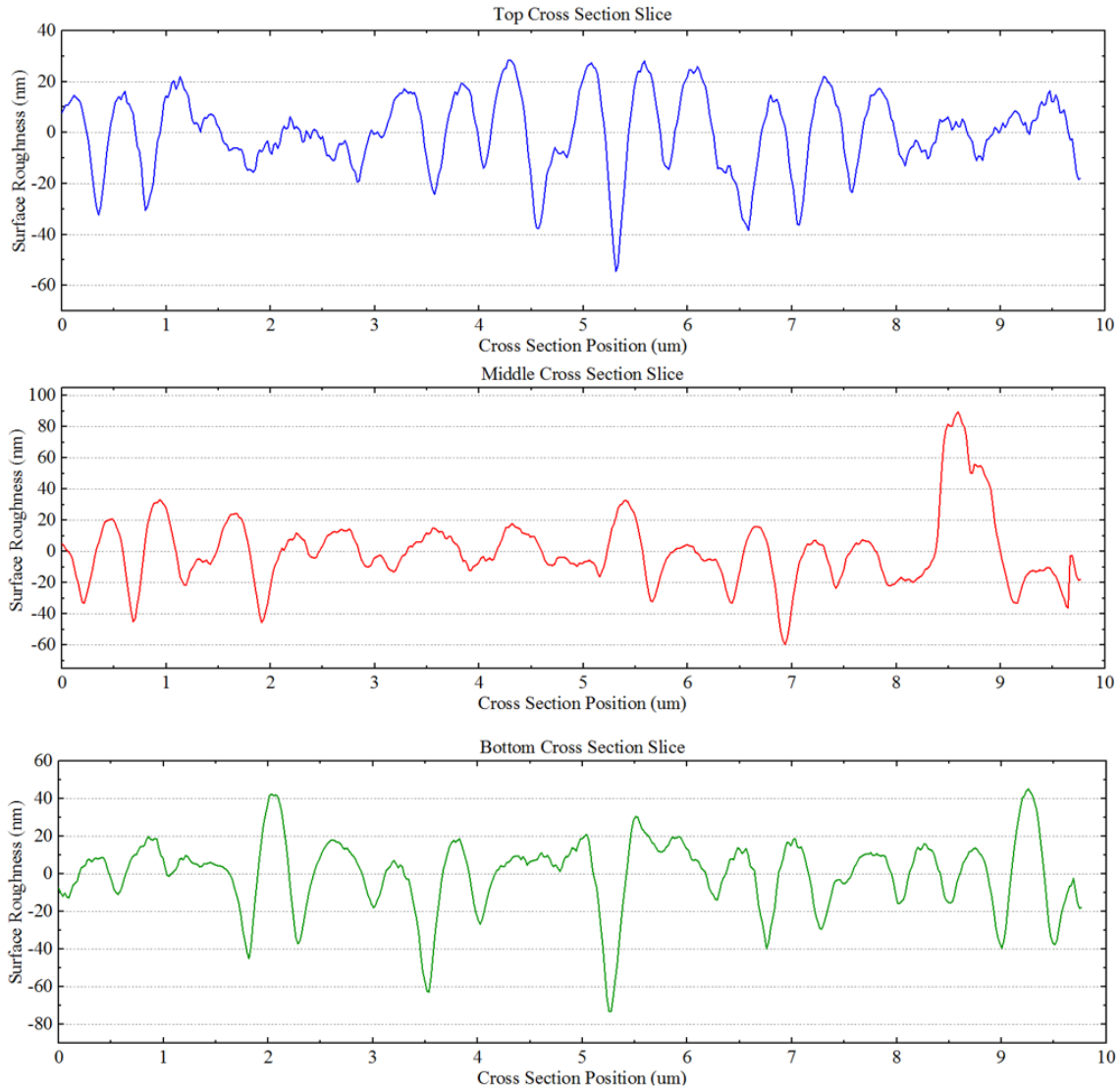

(B)

Figure 21. AFM Image of the Surface of a Nanoscribe Fabricated Structure Using IP-Dip (A) and Individual Cross Sections Showing Elevation Change (B)

As seen in Figure 21 the largest peak to peak difference in the surface of the polymer structure is roughly 120 nm. The smallest wavelength of light that is used in experimentation is 1460nm and a half of that is 730 nm which is still well above the 120 nm surface roughness. The light used in this thesis experimentation will reflect and

transmit off of the 3-D fabricated structure surfaces with negligible destructive interference. Figure 22 is a three-dimensional rendering of Figure 21 (A) which gives a better representation of the surface.

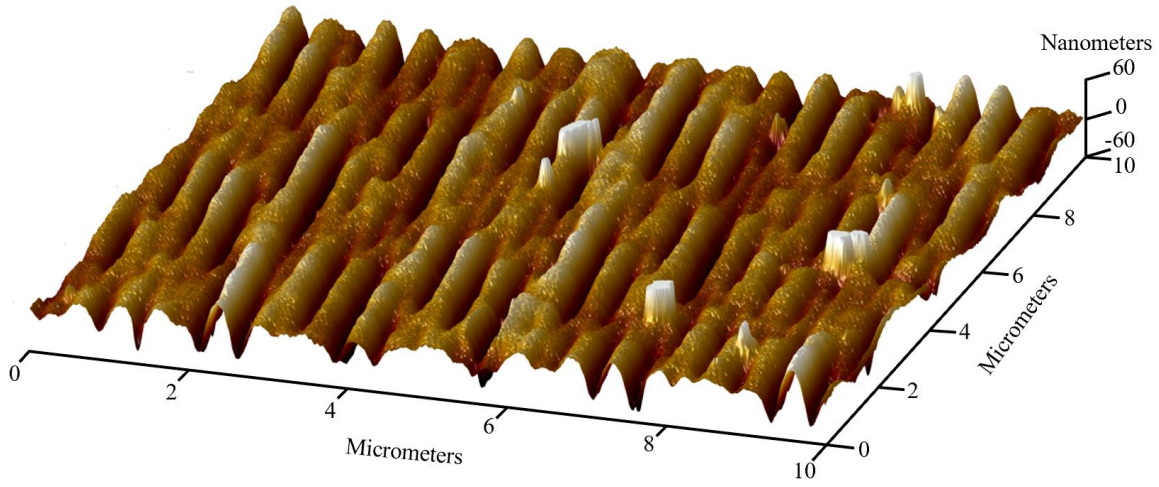

Figure 22. 3-D Rendered AFM Image of the Surface of a Nanoscribe Fabriced Structure Using IP-Dip

To measure the surface roughness of a fiber selectively etched with HF a 500 micrometer thick fused silica glass slide that was selectively exposed using a femtosecond laser and etched with HF for approximately three hours. The surfaced etched by the HF due to the femtosecond laser exposure was then measured using an AFM. These results are shown in Figure 23.

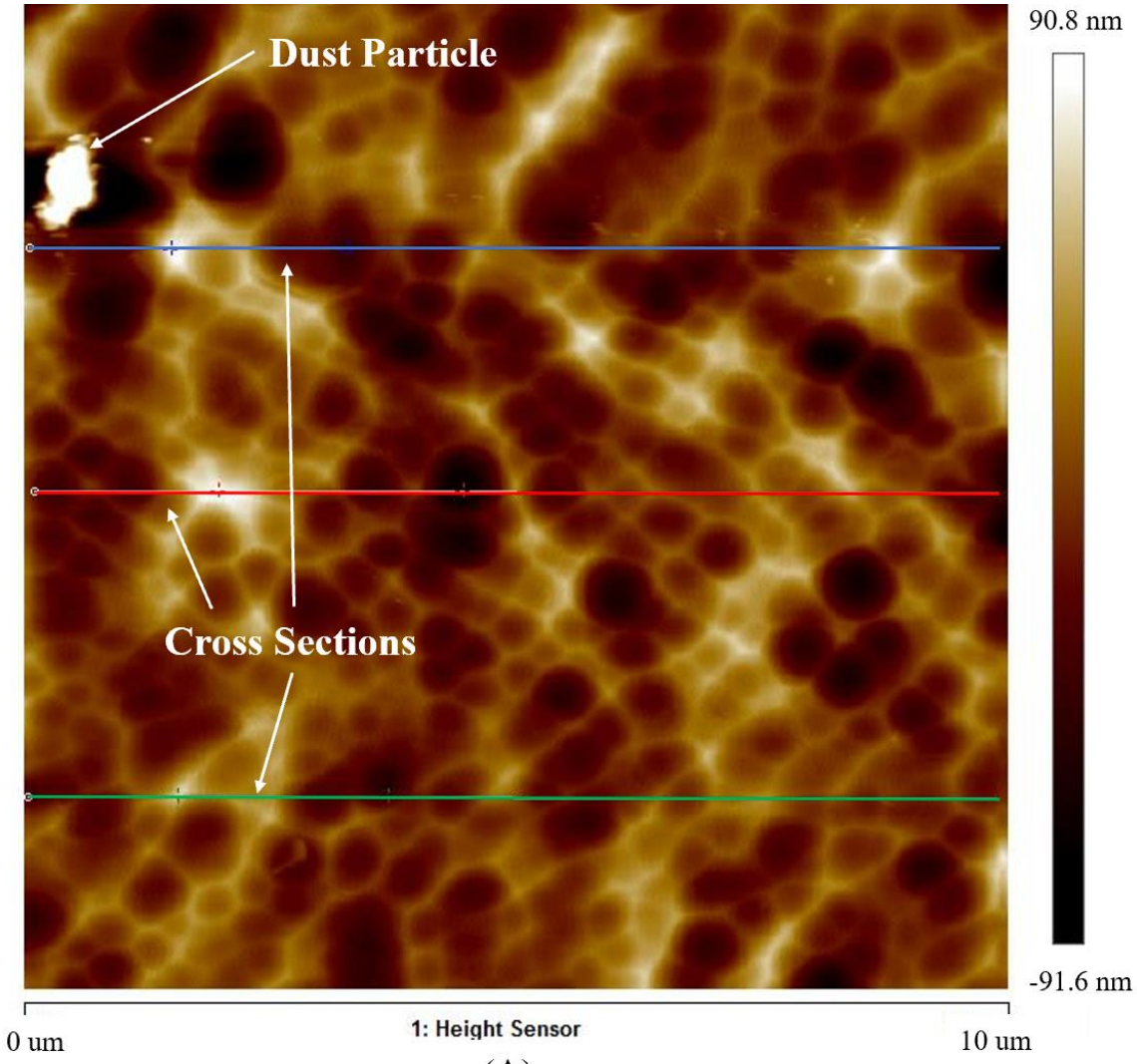
Dust Particle
Cross Sections
90.8 nm
-91.6 nm
0 um
1: Height Sensor
10 um

(A)

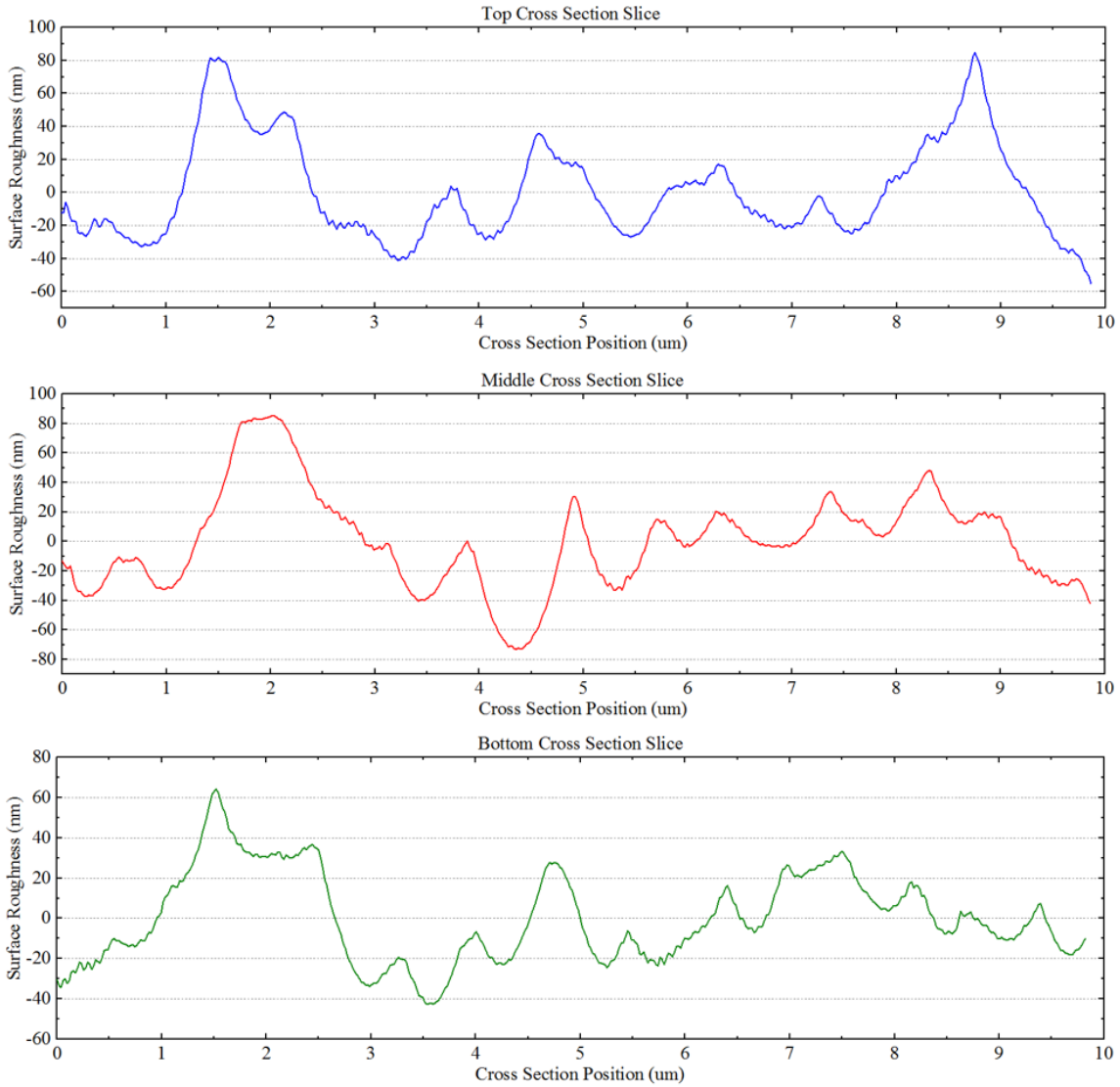

(B)

Figure 23. AFM Image of the Surface of an HF Etched Fused Silica Slide (A) and Individual Cross Sections Showing Elevation Change (B)

As seen in Figure 23 the largest peak to peak difference in the surface of the polymer structure is roughly 150 nm. This is still a smooth enough surface to prevent destructive interference, but it is rougher than the surface fabricated using the Nanoscribe. It is possible to anneal this surface to make it even smoother, but this would

add another step to the fabrication process further complicating it. Figure 24 is a three-dimensional rendering of Figure 23 (A) which gives a better representation of the surface.

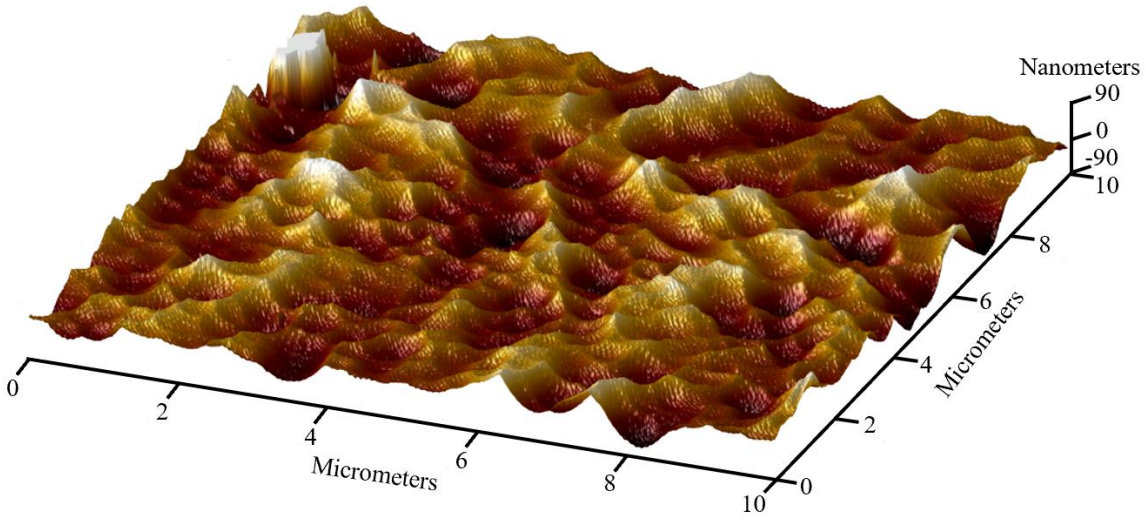

Figure 24. 3-D Rendered AFM Image of the Surface of an HF Etched Fused Silica Slide

Due to the in-house fabrication process and smoother surface the Nanoscribe fabrication process was chosen to fabricate all optical fiber tip sensors. The two main sensor structures tested for thermal radiation and VOC detection was a flat surfaced single and double cavity FPI structure. SEM images of the two devices are shown in below in Figure 25.

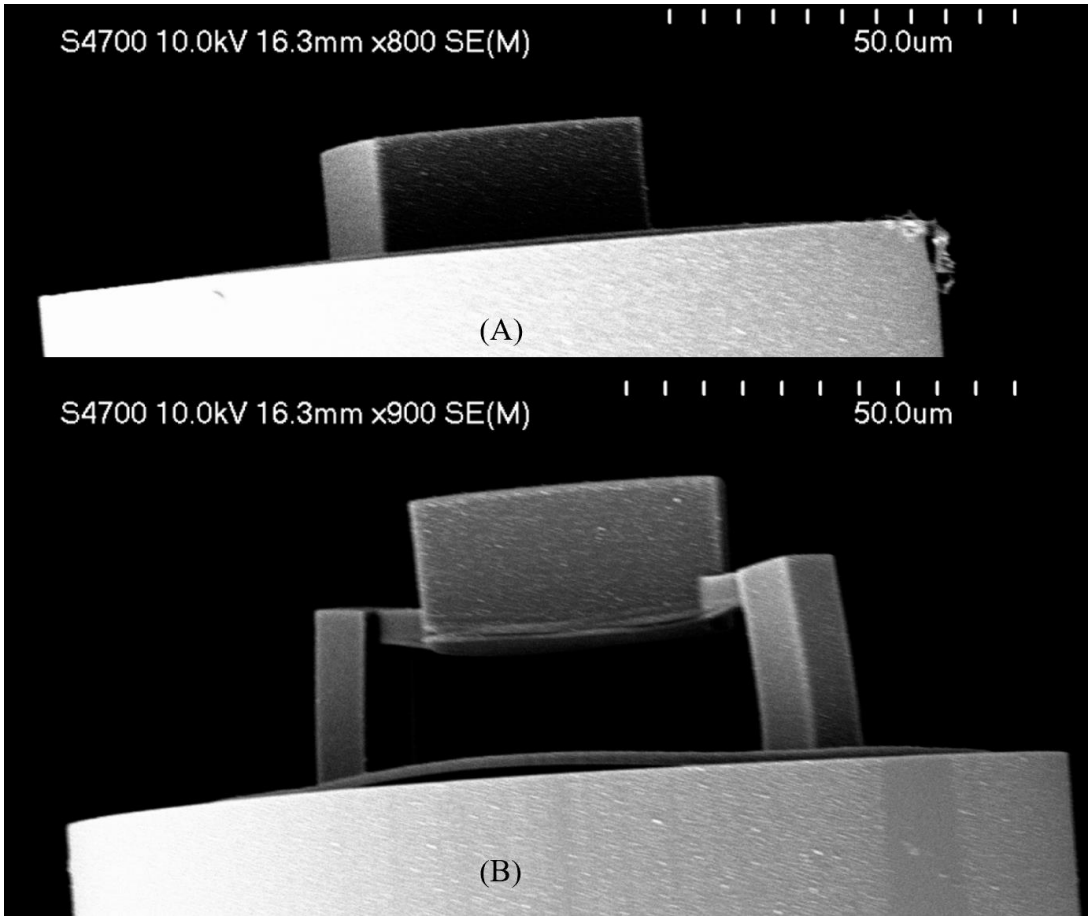

Figure 25. SEM Images of a Single (A) and Double (B) Cavity FPI Fiber Tip Sensor

Thermal Radiation Sensing Results

The hypotheses stated earlier said there will be a linear shift to the right in the reflection spectrum due to an increase in wavelength at the resonant dips. This is due to the change in overall dimension due to thermal expansion (thermo-elastic effect) which would be the dominating factor in the change in wavelength at resonant dips. The two cavity FPI device will have more room for expansion as there is less anchor area, and has two FPI cavities expanding resulting in a more sensitive temperature sensor. Initial results for the single and double cavity FPI sensors are listed in Figure 26 below.

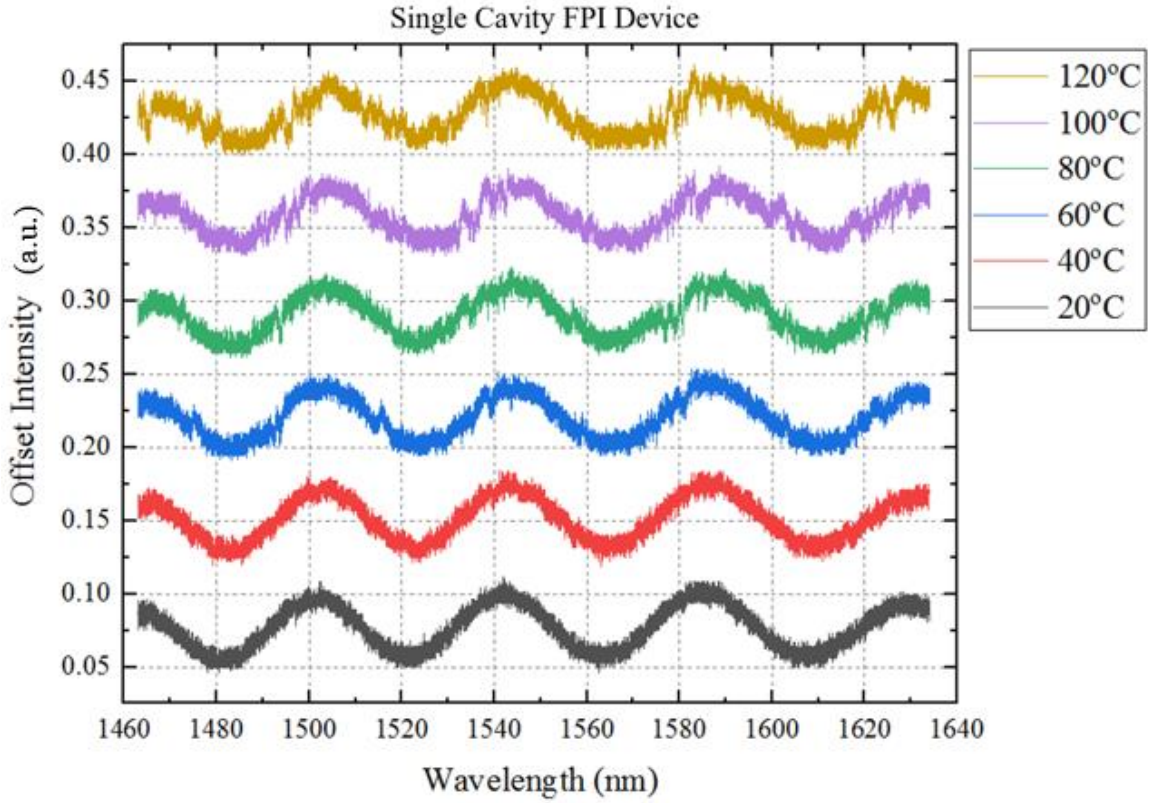
Single Cavity FPI Device
Offset Intensity (a.u.)
0.45
0.40
0.35
0.30
0.25
0.20
0.15
0.10
0.05
1460
1480
1500
1520
1540
1560
1580
1600
1620
1640
Wavelength (nm)
120°C
100°C
80°C
60°C
40°C
20°C

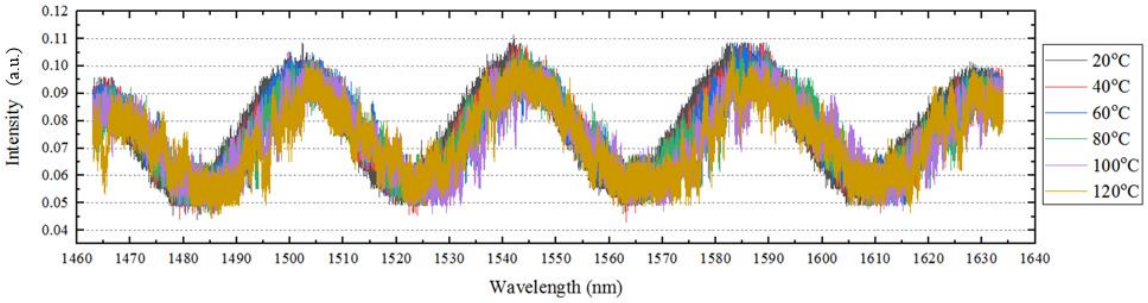
Intensity (a.u.)
0.12
0.11
0.10
0.09
0.08
0.07
0.06
0.05
0.04
1460
1470
1480
1490
1500
1510
1520
1530
1540
1550
1560
1570
1580
1590
1600
1610
1620
1630
1640
Wavelength (nm)
20°C
40°C
60°C
80°C
100°C
120°C

(A)

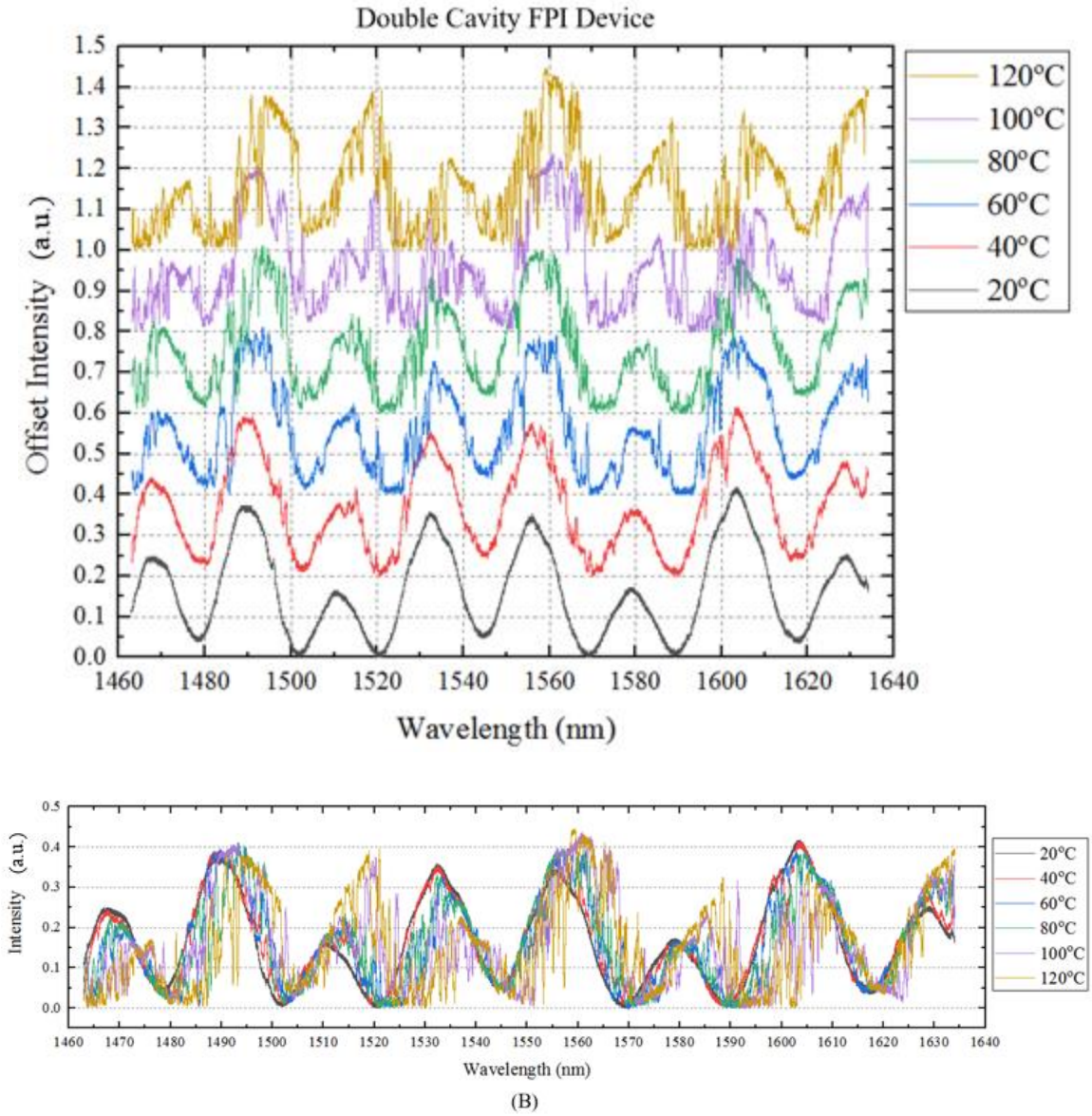

Figure 26. Reflection Spectrum from a Single (A) and Double (B) Cavity FPI Sensor Ranging from Room Temp. to 120°C

The data for both devices is displayed with an offset and overlaid one another for clarity. First thing to note is the extinction ratio for the double cavity FPI fiber device is better than that of the single cavity device. The highest and lowest recorded voltage (intensity) at room temperature of the single cavity device is 108.43 mV at a power of

15.78 µW and 43.73 mV at a power of 6.36 µW respectively. This yields an extinction ratio of 2.4811. The double cavity FPI fiber device recorded a high of 418.63 mV at 60.91 µW and a low of 0.16 mV at 0.023 µW yielding an extinction ratio of 2648.26.

Observing the entire temperature range, as the temperature increases so does the noise. This is especially evident in the double cavity FPI device. This noise is due to the imprecise heat application and the air rising from the heat source through the sensor itself. This makes the data hard to interpret and compare to one another at higher temperatures. It is nearly impossible to see a shift due to temperature with this unfiltered data. A rolling average was applied to the data to filter out the noise in the signal. Multiple duplicate runs were averaged together as discussed in chapter 3 to obtain more consistent data. Figure 27 shows the averaged filtered reflection spectrum data of the single (A) and double (B) cavity FPI sensor.

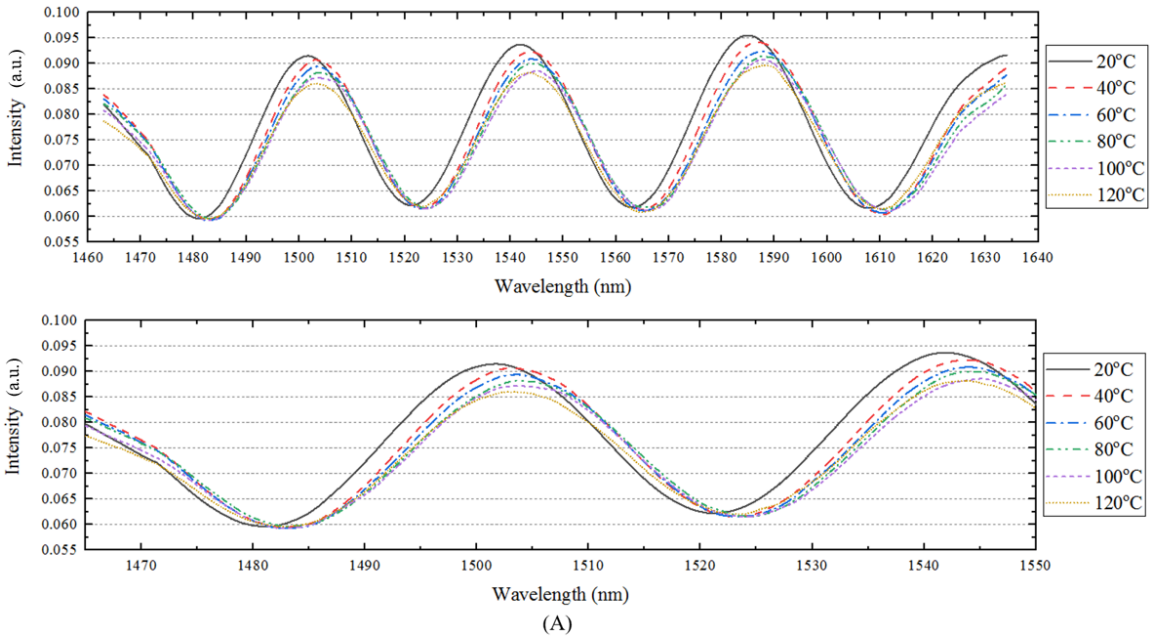

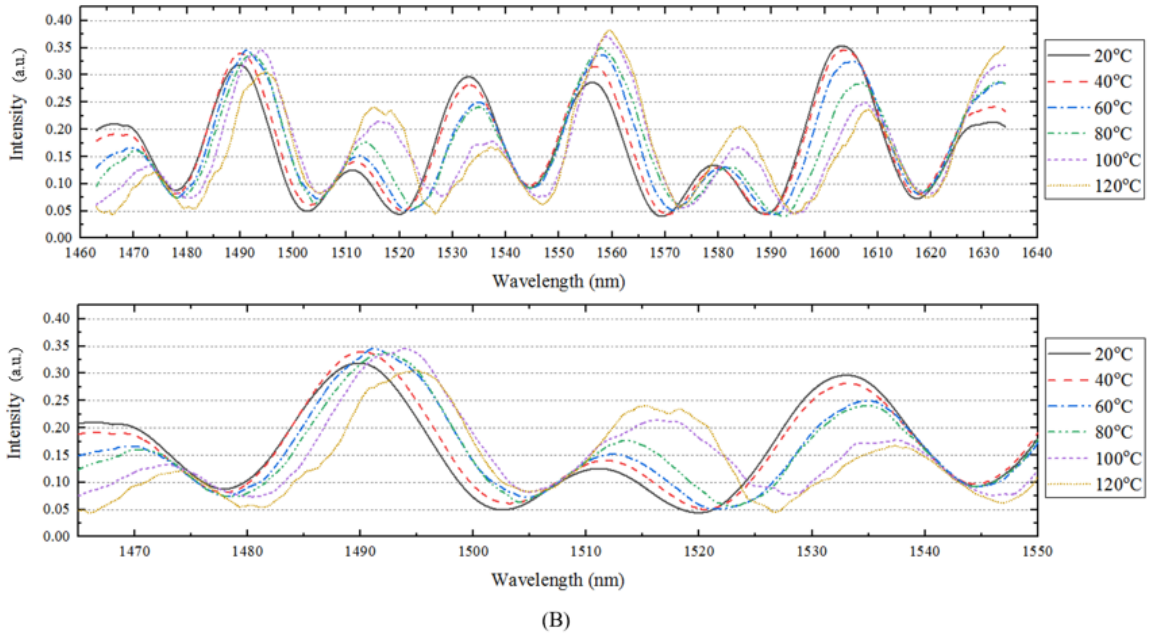

Figure 27. Averaged Filtered Reflection Spectrum from a Single (A) and Double (B) Cavity FPI Sensor Ranging from Room Temp. to 120ºC

With the filter applied and the data of each temperature overlaid on one another it is clear that there is a shift in the reflection spectrum due to the temperature change. The approximate wavelength shift is measured at a given peak or dip clearly showing the shift. Figure 28 shows the approximate shift due to temperature.

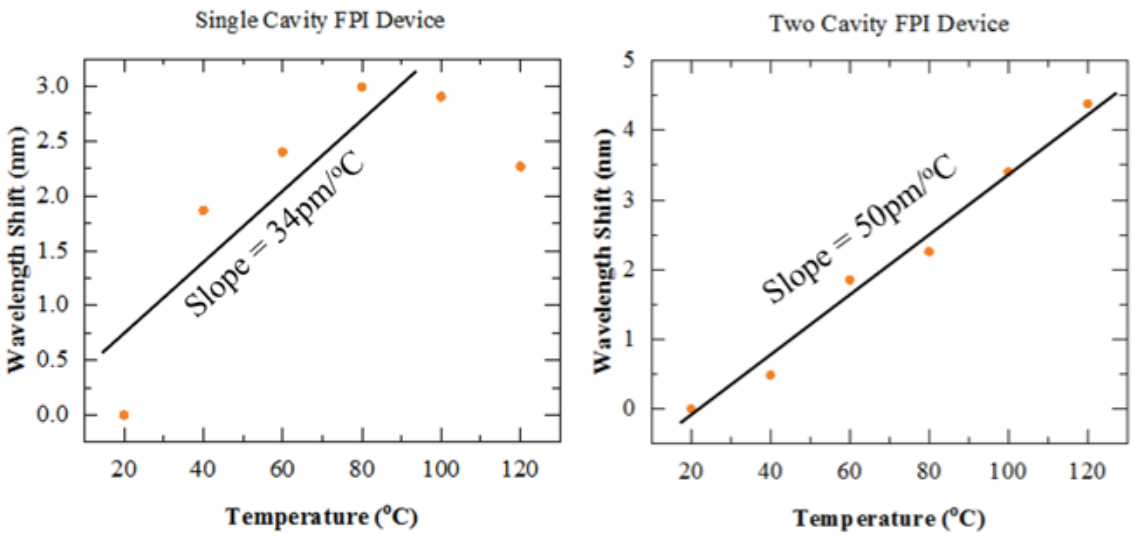

Figure 28. Temperature Vs Wavelength Shift for a Single (A) and Double (B) Cavity FPI Device

A best fit line was used to estimate the sensitivity of both the single a double cavity FPI sensor. The sensitivities achieved ranged from 34 to 50 pm per degree Celsius. This aligns with the initial hypothesis which states the resonant dips will occur at larger wavelengths at higher temperatures showing a shift to the right in the reflection spectrum. This confirms that the thermo-elastic effect is the dominating factor in these sensors when heat is applied. The surprising portion of this data is the non-linear change in sensitivity at higher temperatures (80°C to 120°C) for the single cavity FPI device. This is unusual as the initial hypotheses expected a linear shift which is observed with the two cavity FPI sensor.

The single cavity FPI fiber tip sensor not having a linear shift due to temperature needed to be verified. It was unexpected to see the shift reduce significantly at higher temperatures. A duplicate sensor was made with the same design on a new fiber tip. This sensor was fabricated using the same process as before and utilizing the same type of

fiber. Once the new duplicate sensor was created the same exact testing setup was utilized to test the device. Figure 29 shows the results of the duplicate single cavity FPI sensor.

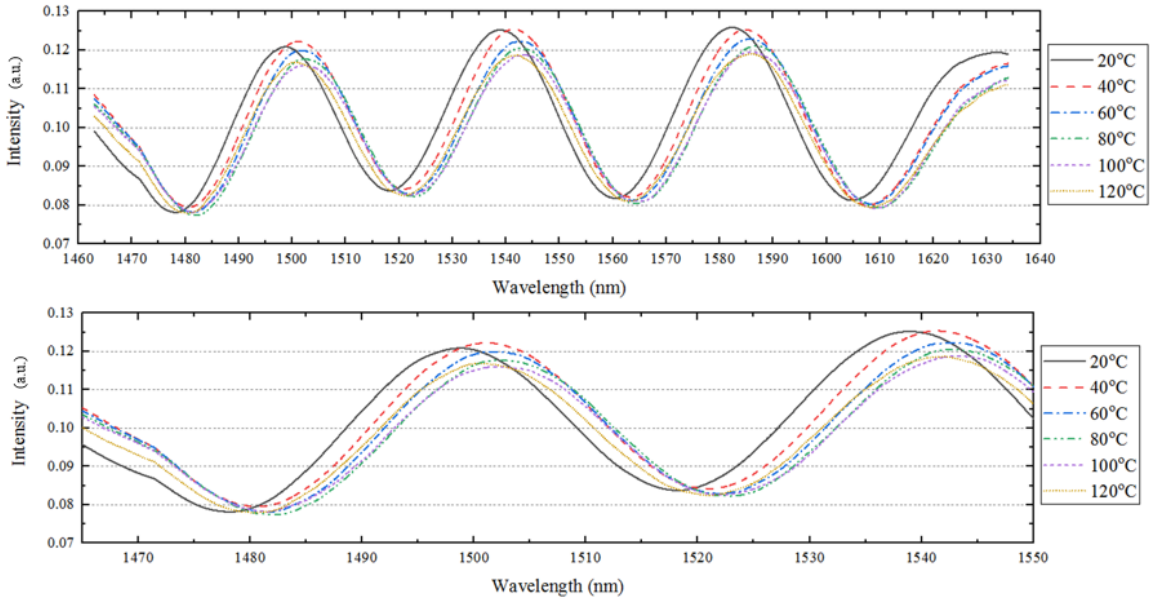

Figure 29. Averaged Filtered Reflection Spectrum from a Duplicate Single Cavity FPI Sensor Ranging from Room Temp. to 120°C

This data looks very similar to the first single cavity FPI sensor displayed in Figure 27 (A). The shift due to temperature change of this duplicate sensor is shown in Figure 30.

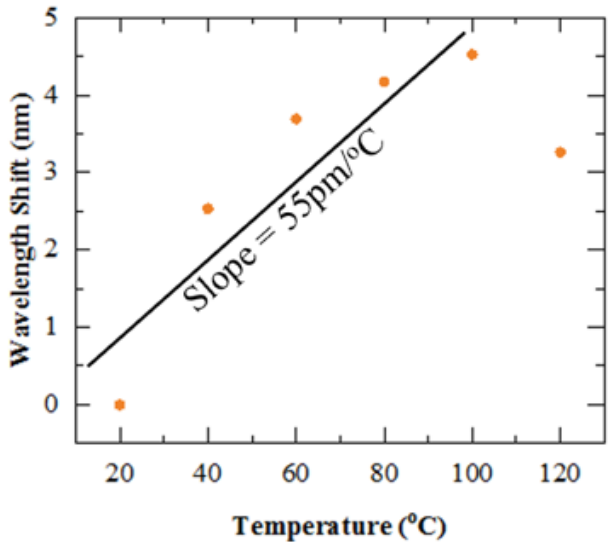

Figure 30. Temperature Vs Wavelength Shift for the Duplicate Single Cavity FPI Device

The initial sensitivity of the device is higher than before. The duplicate device with a 55 pm per degree Celsius versus the first device with a 34 pm per degree Celsius. This difference could be explained by the inherent variability in the fabrication process or by the small number of duplicate runs. The Nanoscribe 3-D two-photon polymerization process is not ideal for creating exact duplicates of a certain structure or device. The process is not completed in a clean room and is conducted by selectively exposing a drop of photosensitive IP-Dip polymer which is deposited simply by placing a drop on the tip of a fiber. The variability in the cleanliness of the area where work is conducted and the variability in the consistence of the IP-Dip drop applied may cause small differences in the resultant 3-D fabricated polymer structure. The other factor potentially leading to this difference in initial sensitivity is that only three duplicate experimental runs were accomplished and averaged together at each temperature range. There can be a significant amount of variation between runs as the heating source is not precisely controlled. A

larger number of runs for each experiment may produce results that more closely mimic each other.

The important take away from testing this duplicate single cavity FPI sensor is that it behaved the same way at higher temperatures. Originally it was expected to observe a linear shift across all testing temperatures, but at the higher temperatures (80^{o}C to 120^{o}C) the shift in reflection spectrum was significantly less. This phenomenon is only observed in the single cavity FPI device which is anchored to the fiber tip by the entire bottom of the 3-D fabricated structure. The cause of this change in shift due to temperature is believed to have something to do with the larger anchor area experienced by the single cavity FPI device which restricts the devices expansion.

Comparing Thermal Radiation Results to Theoretical Values

To make better sense of the results obtained a comparison was completed to the calculated theoretical values. Nanoscribe was contacted to requested data on their proprietary IP-Dip polymer used for these devices. Unfortunately they did not have any information about the coefficient of thermal expansion (CTE) of exposed IP-Dip so this value will need to be back calculated according to the experimental results. Nanoscribe did provide data on the refractive index of IP-Dip at different wavelengths and temperatures which is listed in Figure 31 below.

Temp (°C)	Refractive Index (n) of IP-Dip at given wavelengths (nm)						
	405	479.3	546.1	589.3	643.8	780	950
10	1.553	1.538	1.529	1.525	1.521	1.516	1.511
15	1.551	1.536	1.527	1.523	1.519	1.514	1.509
20	1.549	1.534	1.525	1.521	1.517	1.512	1.508
25	1.547	1.532	1.523	1.519	1.515	1.51	1.506
30	1.545	1.53	1.521	1.517	1.513	1.508	1.504
35	1.543	1.528	1.519	1.515	1.511	1.506	1.502
40	1.541	1.526	1.517	1.513	1.509	1.504	1.5
45	1.539	1.524	1.515	1.511	1.507	1.502	1.498
50	1.537	1.522	1.513	1.509	1.505	1.5	1.496
55	1.535	1.52	1.511	1.507	1.504	1.498	1.494
60	1.532	1.518	1.509	1.505	1.502	1.496	1.492
65	1.53	1.516	1.507	1.503	1.5	1.494	1.49
70	1.528	1.514	1.505	1.501	1.498	1.492	1.488
75	1.526	1.512	1.503	1.499	1.496	1.49	1.486
80	1.524	1.51	1.501	1.497	1.494	1.488	1.484

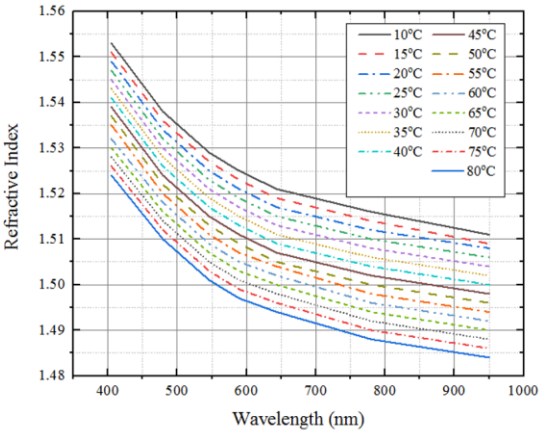

Figure 31. IP-Dip Refractive Index Data According to Temperature and Wavelength

Since the experimentation is completed with light at a wavelength of 1460 nm to 1640 nm this data needed to be extrapolated to those wavelengths. A two term power series was used to fit this data and extrapolate to the necessary wavelengths. Figure 32 shows this extrapolation.

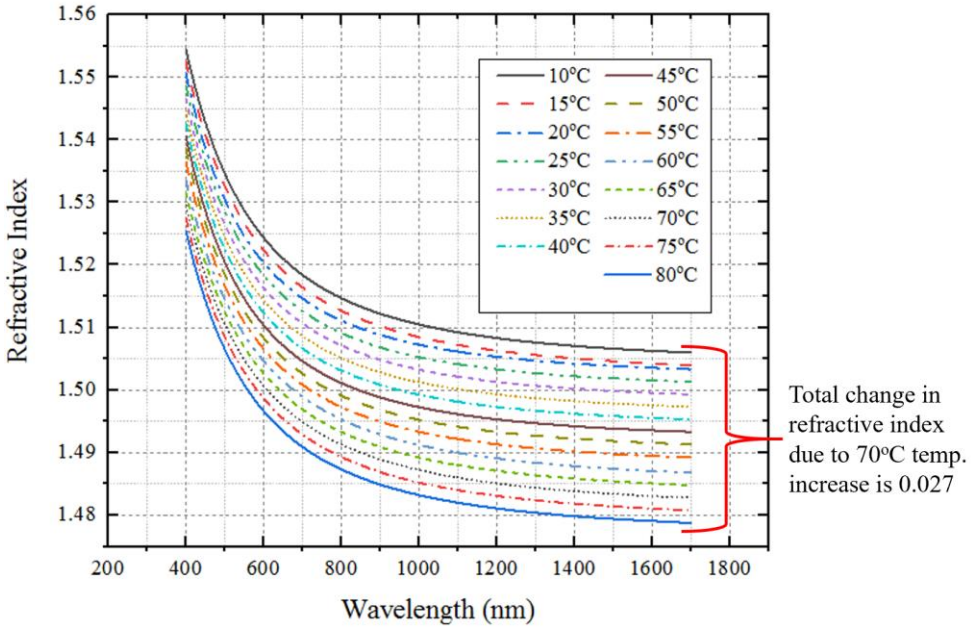

Figure 32. Extrapolated IP-Dip Refractive Index Data According to Temperature and Wavelength

As depicted in Figure 32, there is a significant change in the refractive index as temperatures increase. All experiments testing the fiber tip temperature sensor started at room temperature which is about 20°C. From 20°C to 80°C the refractive index of the IP-Dip polymer drops from 1.503 to 1.479 which is a difference of 0.024. It's estimated that the overall change to refractive index from 20°C to 120°C to be 0.04. Using equation (4) and the refractive index information supplied by Nanoscribe the CTE was calculated in Figure 33. The wavelengths chosen are from a peak of Figure 27 (A) that shows a clear shift. The CTE of exposed IP-Dip came out to be $2.935 \times 10^{-4}\ K^{-1}$.

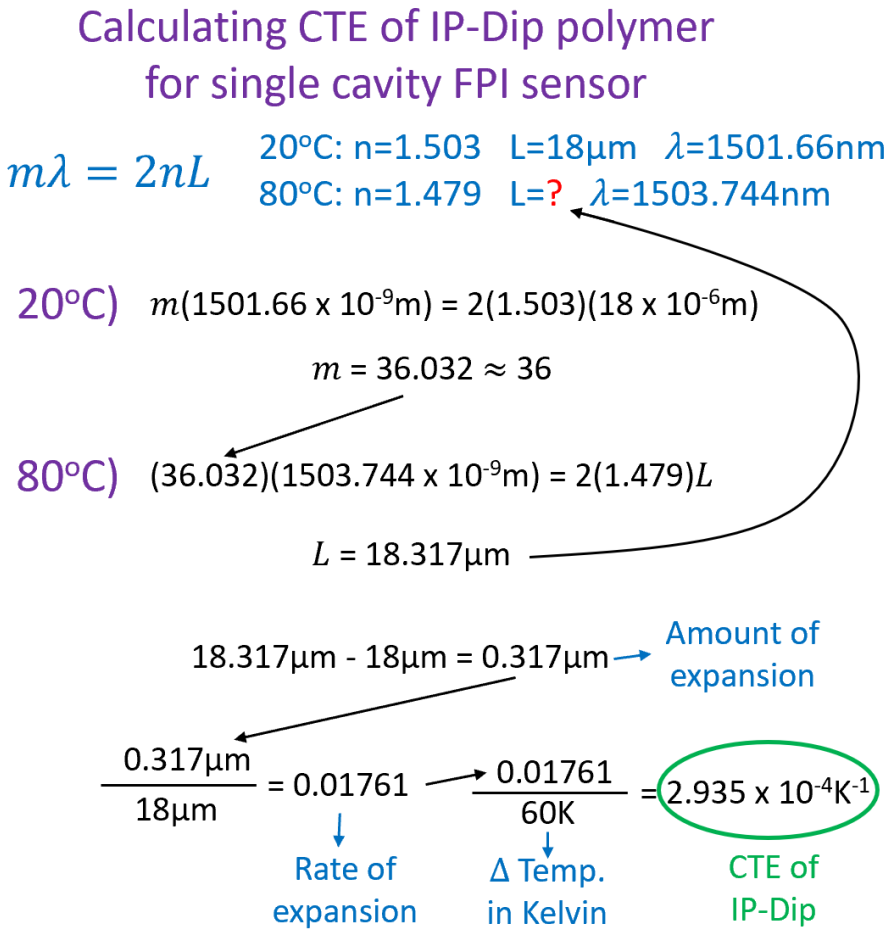

Figure 33. CTE Calculation of IP-Dip Polymer

The shift in the reflection spectrum due to temperature has been observed and analyzed. Now a comparison between room temperature results for the single and double cavity FPI fiber tip devices will be conducted. Figure 34 shows the unfiltered reflection spectrum from each device.

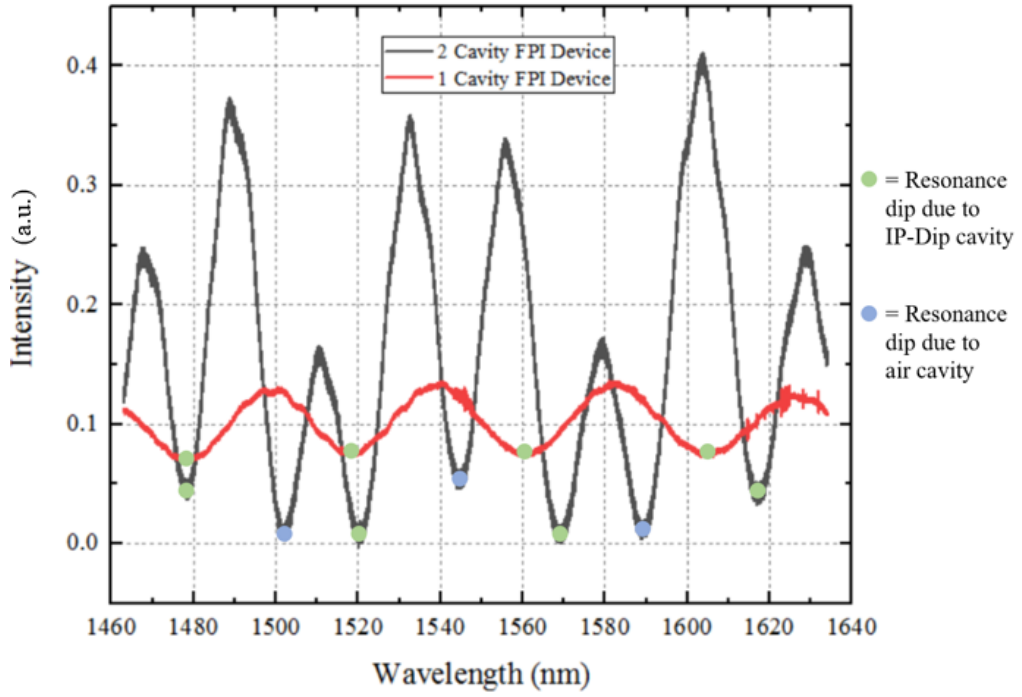

Figure 34. Reflection Spectrum of the Single and Double Cavity FPI Fiber Tip Devices at Room Temperature

As previously mentioned, the cavity of the single cavity FPI device is made of IP-Dip polymer. The double cavity FPI device is a suspended polymer structure meaning the first cavity is open to its environment and the second cavity is made of the IP-Dip polymer. All of the temperature sensor experiments were conducted in air meaning the first cavity of the double cavity FPI device is made of air.

The single cavity FPI device will have FSR's based only on the single IP-Dip cavity. Similarly, the double cavity will have FSR's associated with both cavities, one for air and one fore IP-Dip. The resonant dips of the double cavity FPI device that align closely to the dips of the single cavity FPI device are the dips due to the IP-Dip cavity. To review, the FSR is the distance between adjacent resonant intensity dips which are marked by the blue and green dots in Figure 34. The calculated theoretical values for these FSR's are shown in Figure 35.

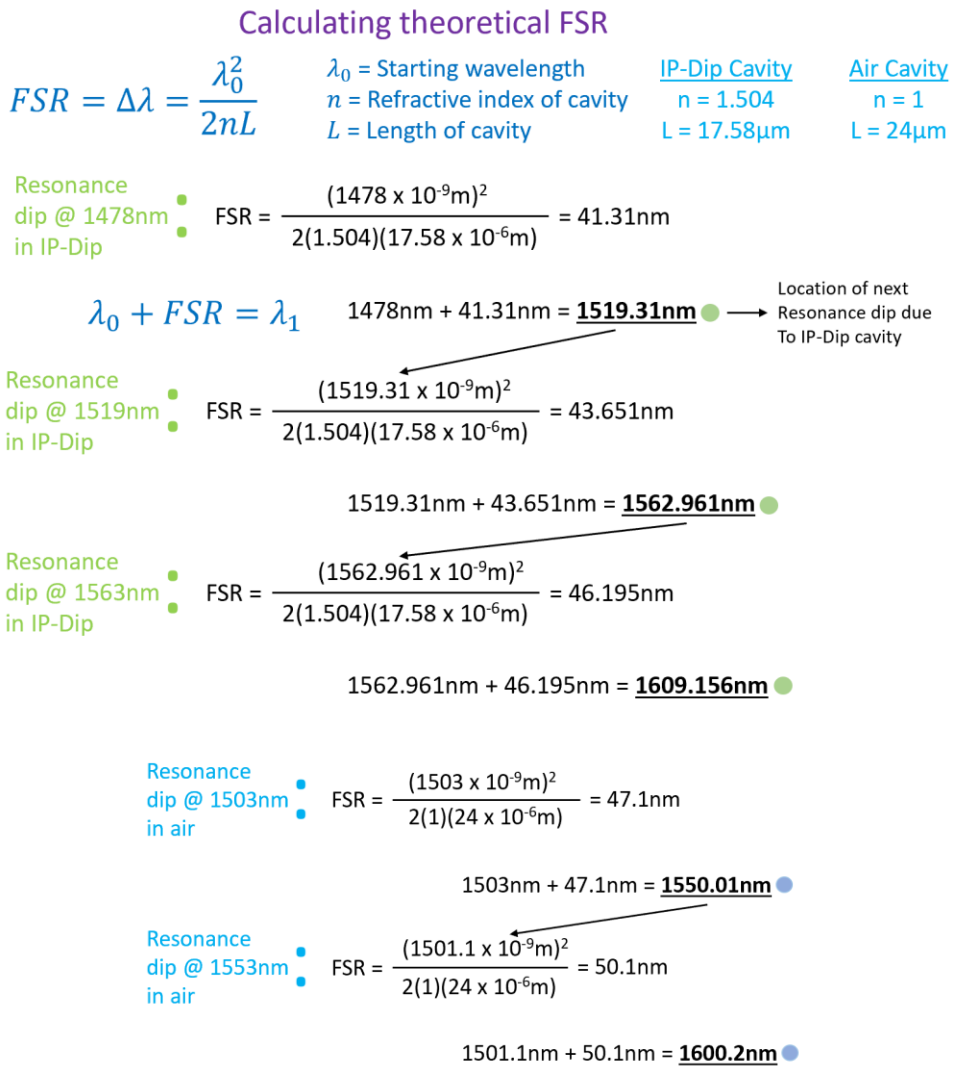

Figure 35. Theoretical FSR Calculations for Double Cavity FPI Sensor

Comparing these theoretical wavelengths to Figure 34 they are close to the actual measured values. In the calculations, the wavelengths are marked by green and blue dots which match up to the same dots in Figure 34. Theoretically the resonant dips of the single cavity FPI device and the resonant dips due to the IP-Dip cavity of the double cavity FPI device should be aligned perfectly. The actual results obtained do not show this which is due to the fabrication process of the fiber tip sensors, slight changes in environmental conditions, and/or difference in cavity surfaces. To insure the 3-D microfabricated polymer structure adheres to the tip of the fiber the focal point of the laser exposing the IP-Dip polymer, must start inside the actual fiber tip. As the laser focal point raises it is guaranteed to cross the plane in which the polymer structure and fiber tip face meet. Because of this slight overlap it is hard to create two devices of the same exact thickness. A variation in thickness, or cavity length, will alter the FSR which explains the difference between the resonant dips due to IP-Dip between the single and double cavity FPI device. Also, a slight change in humidity can alter the refractive index of air which would impact the reflection spectrum. Lastly, The first surface of the single cavity FPI sensor is a fiber core to IP-Dip surface as illustrated in Figure 15. The first surface of the double cavity FPI sensor's IP-Dip cavity is air to IP-Dip which is different and will affect the reflection spectrum.

VOC Sensing Results

Preliminary experiment on VOC detection was performed to justify the multifunctional capability of the sensors. Both the single and double cavity FPI fiber tip

sensors were exposed to evaporated IPA. It is expected that the reflection spectrum for both sensors will shift to the right as the resonant dip wavelengths will increase due to an increase in refractive index caused by the surrounding IPA. The double cavity FPI sensor should be much more sensitive as there is a total of three reflective surfaces and one entire cavity that is affected by the exposure to IPA. Figure 36 shows the reflection spectrum of the single cavity FPI sensor in air and exposed to 100% IPA.

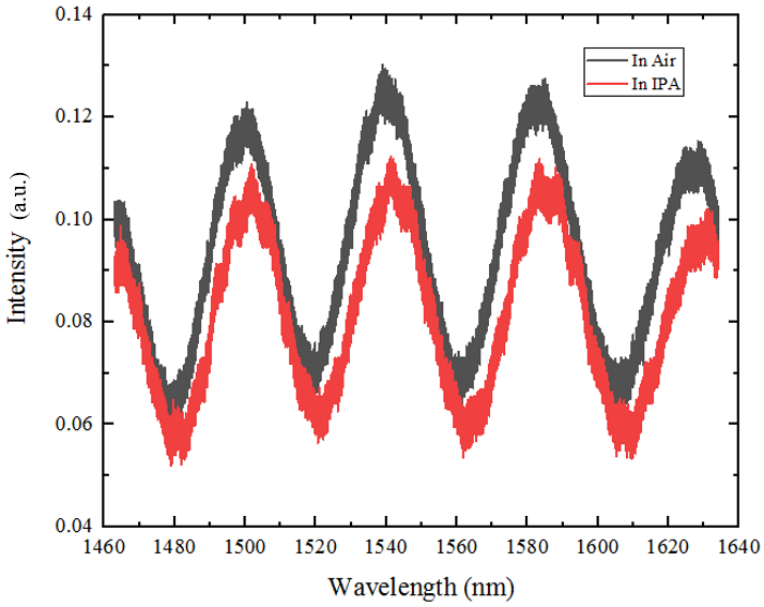

Figure 36. Reflection Spectrum of Single Cavity FPI Sensor Exposed to VOC

Exposing the single cavity FPI sensor to a VOC only changes one surface of the entire sensor, which is the interface between the top surface of the IP-Dip polymer structure and the atmosphere. Changing the refractive index on either side of this interface will have an impact of the reflected light according to Snell's law. This explains the slight shift in the reflection spectrum displayed in Figure 36. The refractive index of IPA is a known value which is approximately 1.3776. This compared to the refractive index of air, which is approximately one, gives this sensor a sensitivity of 7.945 nm per

refractive index unit (RIU). This is calculated by observing the shift in wavelength before and after exposure to IPA which is a shift of 3 nm. That divided by the change in refractive index from air to IPA which is 0.3776 yields the sensitivity of 7.945 nm/RIU. This calculation does assume that the sensor is immersed in 100% IPA vapors which may not be true. If this is not true then the actual sensitivity will be lower. The reflection spectrum of the double cavity FPI device in air and exposed to 100% IPA is displayed in Figure 37.

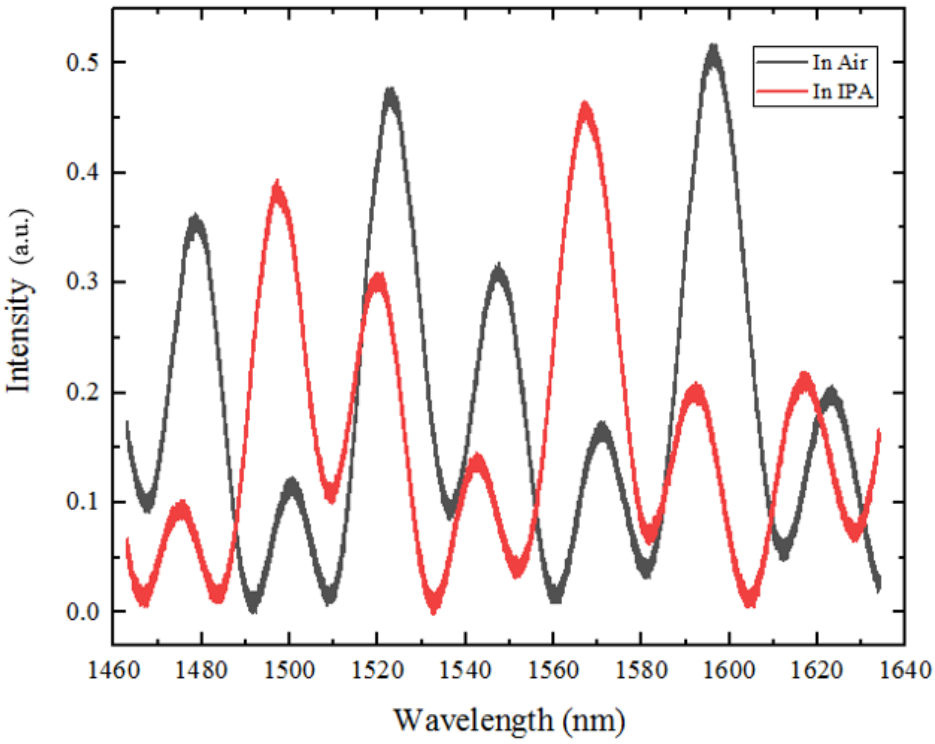

Figure 37. Reflection Spectrum of Double Cavity FPI Sensor Exposed to VOC

Theoretically the double cavity FPI sensor is going to be much more sensitive to VOC's than the single cavity sensor. This is shown in the apparent shift in reflection spectrum shown in Figure 37. It looks like the reflection spectrum has a large shift to the left when exposed to IPA, however this is not the case. The reflection spectrum is

periodic meaning it repeats itself which makes the spectral shift hard to see. Using equation (4) at a resonant dip, for this example this will be the dip in the reflection spectrum in Figure 37 at 1,491.488 nm wavelength. Using the refractive index of air and the cavity length of the air gap under the sensor, solve for the order of the resonant dip m which turns out to be approximately 32. Using the same order and cavity length, plug in the known refractive index of IPA which is 1.3776 and calculate the new wavelength at which the resonant dip occurs. This new resonant dip theoretically occurs around 2,054.65 nm wavelength which is a shift of 563.162 nm. This shift is larger than the span of the wavelength sweep completed in the experiment. The laser used in this experiment was the limiting factor for the wavelength sweep. Because of this the exact shift cannot be observed from the data obtained. However, the double cavity FPI sensor does have a theoretical sensitivity of 1491.425 nm per RIU.

Confocal Surfaced Sensor and Reflectivity Results

It is desirable to determine the resolution, or minimum detectable change, of these sensors. To do this accurately a better temperature application and control system must be developed and the quality factor of the sensors themselves needs to be improved. The reflection spectrum of the sensors above have broad resonant dips which make it difficult to see very small shifts due to change in temperature or refractive index. Improving the quality factor will decrease the full width half max (FWHM) which is a measurement of the width of the resonance dip at half of the maximum value. This will result in steeper, more precise resonant dips that will show smaller shifts more clearly.

Improving the quality factor of the temperature sensors was not completed in this thesis, but some ground work was accomplished leading to how the quality factor can be improved. Two separate methods were investigated, one was designing confocal reflective surfaces into the 3-D fabricated IP-Dip structure itself. Theoretically this would reflect more light back into the core of the fiber resulting in a higher extinction ratio. The second method investigated is simply increasing the reflectivity of the 3-D fabricated structure surfaces by depositing a reflective thin film. This thin reflective film will theoretically increase the finesse of the sensor which will increase the quality factor.

A new devices design was created on a fiber tip which is displayed in Figure 16. The same experimental set up as before was utilized to obtain a reflection spectrum at room temperature. These results are displayed in Figure 38.

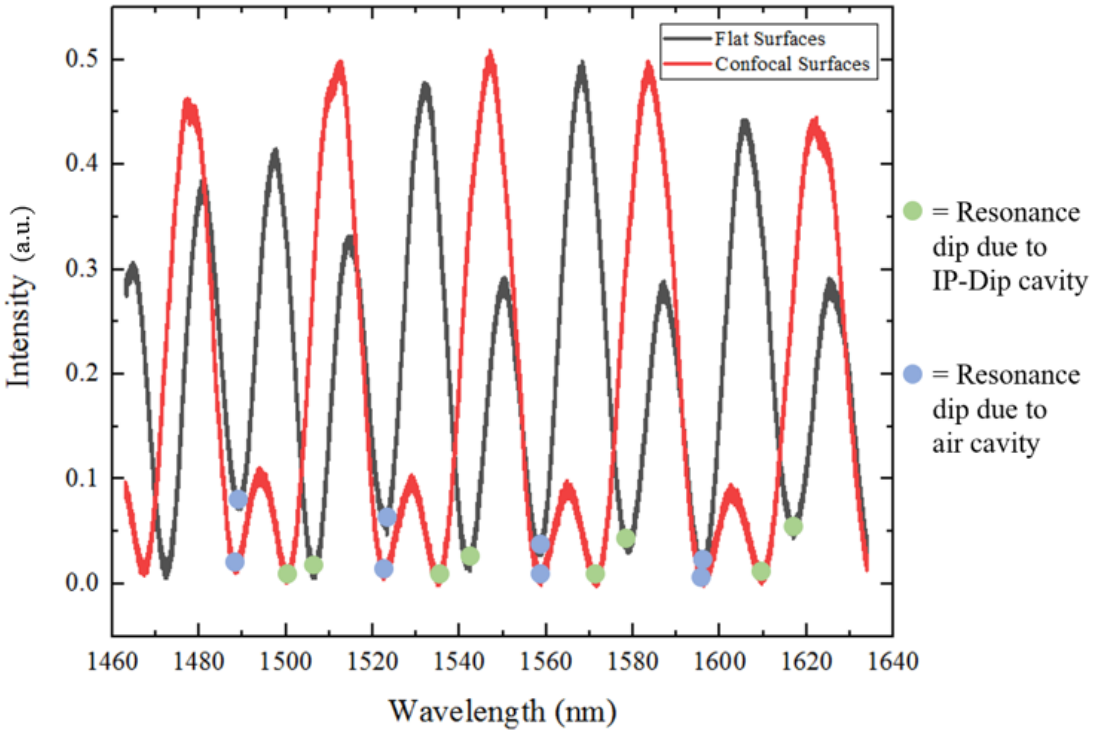

Figure 38. Reflection Spectrum of Flat and Confocal Surface Double Cavity FPI Fiber Tip Devices at Room Temperature

Comparing the flat and confocal surfaced sensors to one another it is observed that the confocal device reflected more light (higher intensity) back to the detector for the first cavity encountered, which is the air cavity. The average light intensity reached of the reflections within the first cavity is 314.966 mV (45.83 μW) and 494.674 mV (71.98 μW) for the flat and confocal devices respectively. The extinction ratio of the confocal device is much greater at 606.56 compared to that of the flat surface device with an extinction ratio of 99.465.

There is also significantly less light reflected from the second, IP-Dip polymer cavity. The average light intensity reached of the reflections within the second cavity is 456.7375 mV (66.46 μW) and 101.025 mV (14.7 μW) for the flat and confocal devices respectively. This is not all that surprising as each surface of the confocal device is specifically designed to reflect light. Light transmitted through the first confocal surface has a smaller chance to get reflected back to the core of the fiber. Lastly, the FWHM of the two devices are very similar. The FWHM of the flat surfaced device is 10.676 nm which is smaller than that of the confocal surfaced device at 12.134 nm. This confocal device design does not increase the quality factor of the sensor, but it does increase the extinction ratio.

It is important to note that the dimensions of the confocal surfaced two cavity FPI structure needed to be altered to accommodate the entire curved surface. Because of this a different flat surfaced two cavity FPI structure with the same dimensions was made for comparison purposes. The flat surfaced two cavity FPI sensor that yielded the reflection spectrum in Figure 38 is a different flat surfaced two cavity FPI sensor than the one

displayed in Figure 15 (B). The air cavity is 35 micrometers (instead of 22.5) and the IP-Dip polymer cavity is 20 micrometers long (instead of 17.58).

The last attempt to increase the quality factor is to apply a thin reflective layer to the fiber tip device. No fiber tip sensors were coated in this thesis but thin reflective layers of silicon nitride (SiN) was used to coat both sides of a one milimeter thick glass slide which was then tested to see if reflectivity was improved. Figure 39 shows the different thicknesses of the SiN and the reflection spectrum associated with each one.

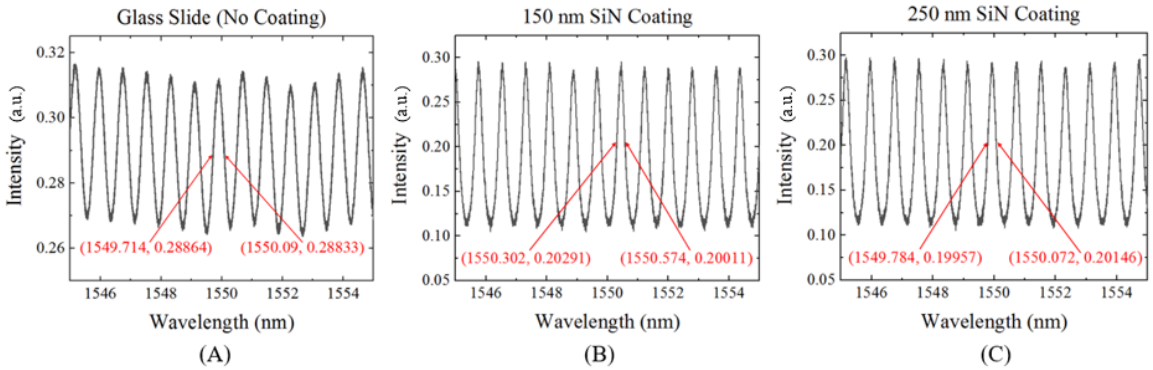

Figure 39. Transmission Spectrum of SiN Coated Glass Slides

All these transmission spectra look very similar, but the first big difference is in the extinction ratio. The glass slide with no coating (A) has a maximum of 312.083 mV at 0.465 mW and a minimum of 265.558 mV at 0.396 mW yielding an extinction ratio of 1.174. Both the SiN coated glass acted similarly with an improved extinction ratio. The 150 nm SiN coated slide (B) had a maximum of 295.53 mV at 0.441 mW and a minimum of 105.22 mV at 0.157 mW yielding an extinction ratio of 2.809. The 250 nm SiN coated slide (C) had a maximum of 291.98 mV at 0.435 mW and a minimum of 108.25 mV at .161 mW yielding an extinction ratio of 2.702. The SiN coating improved the extinction ratio by roughly 135%.

The FWHM was also improved by the SiN coating. The non-coated glass slide has a FWHM of 0.376 nm. This is larger than that of the two SiN coated slides which have a FWHM of 0.272 nm for the 150 nm coating, and 0.288 nm for the 250 nm coating. The SiN coating resulted in an approximate 25% decrease to the FWHM measurement. With an increased extinction ratio and decreased width, a SiN coating can certainly improve the quality factor of an optical fiber tip sensor.

Summary

The hypothesis for thermal radiation sensing was that the thermo-elastic effect would dominate, and the wavelengths of resonant dips would increase resulting in a linear spectral shift to the right. This was partially correct, as the thermo-elastic effect did dominate over the thermo-optic effect and a spectral shift to the right was observed, however this shift was not linear for all of the sensors. The double cavity FPI sensor operated as expected but the single cavity FPI sensor shifted much less due to temperature between 80^{o}C and 120^{o}C. The reason for this is not known for certain but it is believed to have something to do with the large anchor area resulting in a thermal expansion restriction. The highest sensitivity achieved by these optical fiber tip temperature sensors is 50 pm/^{o}C which is an improvement over the related work which achieved a sensitivity 43 pm/^{o}C [24].

VOC sensing for both the single and double cavity FPI sensors was accomplished and a spectral shift for both sensors was observed. The single cavity sensor was limited in sensitivity only yielding a 6.472nm/RIU shift which is significantly less than the largest sensitivity discovered during the literature review of 1394nm/RIU [11]. The double

cavity FPI sensor did show a much larger spectral shift, however the experimental wavelength sweep conducted was not large enough to cover the theoretical shift the sensor should experience. The theoretical sensitivity of the double cavity FPI sensor is 1491 nm/RIU which is an improvement over what has been seen in the literature review.

Lastly, it was shown that a confocal surfaced sensor design did not improve the quality factor of the overall sensor, but it did improve the extinction ratio. There is promising data showing improvement in reflectivity with thin reflective SiN coatings. The two different thicknesses of SiN that were tested (150 and 250 nm) showed very similar results improving the extinction ratio by approximately 135% and decreasing the FWHM by approximately 25%. This is compelling evidence that a thin conformal coating of SiN can improve the quality factor of the fiber optic sensors tested in this thesis.

V. Conclusions and Recommendations

Conclusions of Research

This research shows evidence that a multi-functional microscopic optical fiber tip sensor can be successfully fabricated. A single sensor was utilized to measure temperature change and refractive index change due to the presence of gas. Theoretically this sensor can detect any gas or liquid that has a different refractive index.

Significance of Research

Three main concepts were proven with the research conducted in this thesis. The first is that a linear shift of the reflection spectrum associated with the double cavity FPI sensor is observed as temperature increases. The linear shift is uniform over the entire spectrum. The second concept was showing the negligible shift in the reflection spectrum of the single cavity FPI sensor when exposed to IPA. This is because the only cavity in this sensor is the IP-Dip polymer cavity which is not significantly changed when exposed to IPA. The final concept proven is that the reflection spectrum of the double cavity FPI sensor is shifted a significantly when exposed to IPA. This is because the double cavity FPI sensor has a cavity open to the atmosphere which is significantly changed with the presence of IPA. All three of these concepts put together show the functionality of the double cavity FPI sensor as a temperature immune self-referencing refractive index sensor. This is better illustrated in Figure 40.

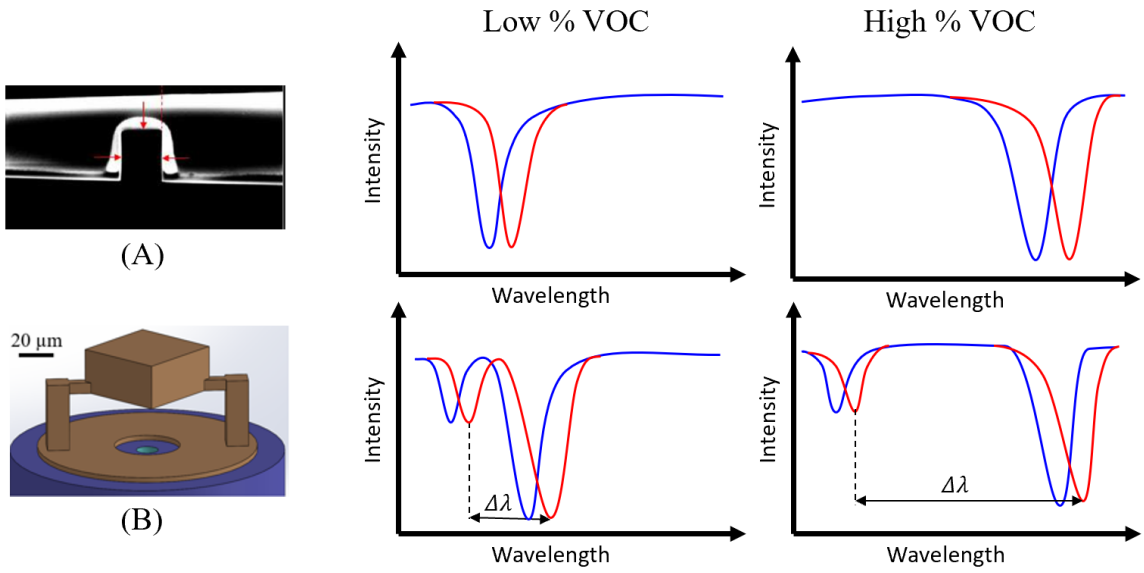

Figure 40. Temperature Immune Self Referencing Sensor

The sensor shown in part (A) is a single cavity FPI fiber optic sensor fabricated by etching a micro-notch into the fiber core [31]. This single cavity will have a wavelength resonant dip associated with it which is displayed in the adjacent reflection spectra. The wavelength the resonant dip occurs at will increase as the concentration of surrounding VOC is increased due to the increase in refractive index. According to the first main concept proven in this thesis, as the temperature increases (shown by the red line) the wavelength the resonant dip occurs at will also slightly increase. A single cavity FPI sensor does not have the ability to distinguish if a small shift in the reflection spectrum is due to an increase in temperature or a slight increase in VOC concentration.

Figure 40 (B) is the double cavity FPI fiber tip sensor fabricated and tested throughout this thesis. There is a wavelength resonant dip associated with each cavity (the IP-Dip polymer and air cavity). Both cavities will show a linear shift in reflection spectrum due to increased temperature as shown by the red line, but only the cavity open

to the atmosphere will have a significant spectral shift when exposed to higher concentrations of a VOC. This has been shown by the second and third concept proven in this research. This behavior yields a temperature immune self-referencing sensor because the double cavity FPI sensor can measure change in refractive index by observing the change in wavelength between the two resonant dips. This change in wavelength remains constant no matter what temperature the sensor is exposed to.

Another significant point of this research is the fabrication process used to create the optical fiber tip sensors. Sensors like this have been fabricated before [34], but the process to do so is extremely lengthy and comes with many limitations. Having the ability to 3-D micromachine the sensor on the tip of an optical fiber grants the freedom to design the sensor for any specific need or purpose. The structure can hold nearly any shape of any size down to a resolution of 150 nm. There is also evidence [23] that exposing the 3-D polymer structure at different light intensities will result in slightly different property materials (such as CTE). This is yet another method of flexibility in the fabrication process. This sensor fabrication process can be utilized to design any sensor for any application involving material refractive index properties.

Recommendations for Future Research

The research conducted in this thesis can be carried on in many different directions. The biggest impact that future research could have on this research topic would be to improve the quality factor of the fiber tip sensors. Preliminary research for this was already conducted, which investigated confocal sensor surfaces and dielectric reflective coatings. This could be takin further and successfully implemented onto an

actual sensor. Improving the quality factor would allow for the resolution of the sensors to be significantly improved.

Direct experimentation could be conducted to better prove the functionality of the temperature immune self-referencing sensor. This concept was pieced together by several experiments, but could be further demonstrated by conducting an experiment to measure different concentrations of a VOC at different temperatures.

Specifically for the fiber tip temperature sensor, higher temperatures could be tested for both the single and double cavity FPI sensors. Testing to higher temperatures may require different equipment, but could give insight on the single cavity FPI sensor reacting differently in the temperature range of 80^{o}C to 120^{o}C. Finding the maximum temperature sensible would also yield valuable information to the functionality of these fiber tip sensors.

During the literature review there was a close look at Bragg grating sensors and how well they perform. There were no Bragg grating sensors fabricated in this thesis research. Utilizing the same 3-D fabrication process, a Bragg grating sensor could be 3-D fabricated onto the tip of an optical fiber to illuminate all unwanted resonant wavelength dips. This sensor could then be put through the same experiments to obtain new results to be compared to what was obtained in this thesis.

Another potential follow on research topic is that these fiber tip sensors could be used to test several other different gases and liquids with different refractive indices. This could be done through simple experimentation and add value to the sensor in demonstrating the full capability of what the senor can detect. Lastly, research could be conducted on how to better make this technology suitable for real world application. The

sensors currently are fairly brittle (the structure on the tip will break if it comes into physical contact with anything), and are overly sensitive to environmental conditions such as humidity or dust. Development of a packaging system to protect the fiber tip sensors, but still allow for some sort of exposure for detection could be hugely beneficial.

Appendix A: Full Designs and Dimensions of Each Fiber Tip Device

The figures below show all of the dimensions of the fiber tip devices fabricated in this thesis research. These devices were designed in Solidworks 2016 x64 and all dimensions are in millimeters. The Nanoscribe software (DeScribe 2.4.4) automatically converts millimeters to micrometers for any input STL design file. So these devices are designed in millimeters, but once fabricated are actually in micrometers.

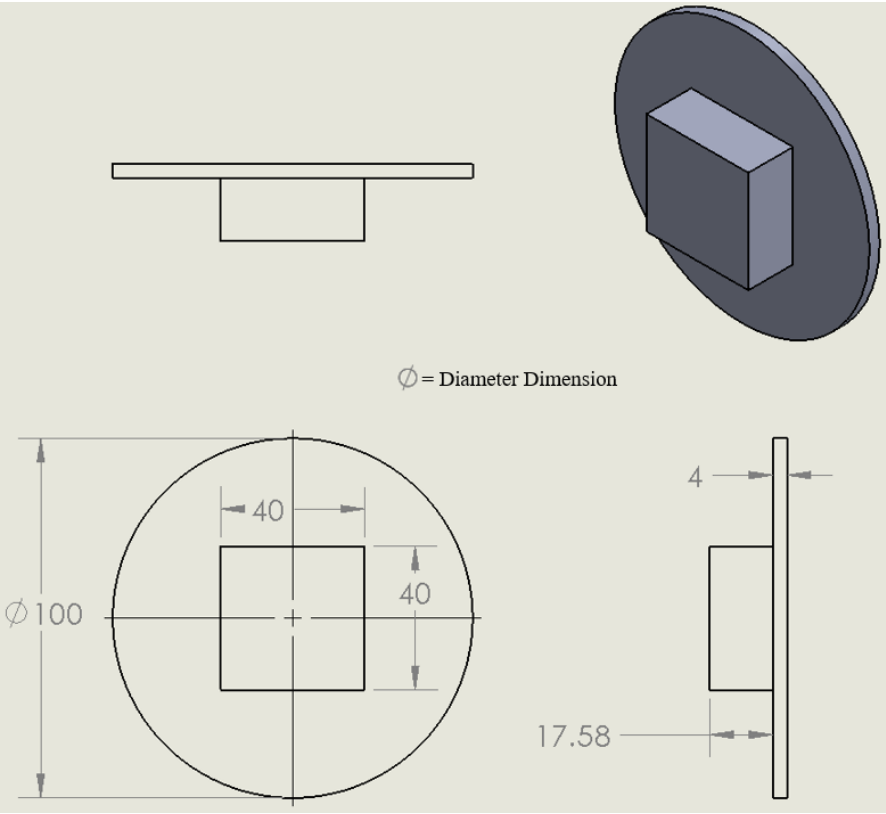

Figure 41. Drawing of Flat Surfaced Single Cavity FPI Sensor

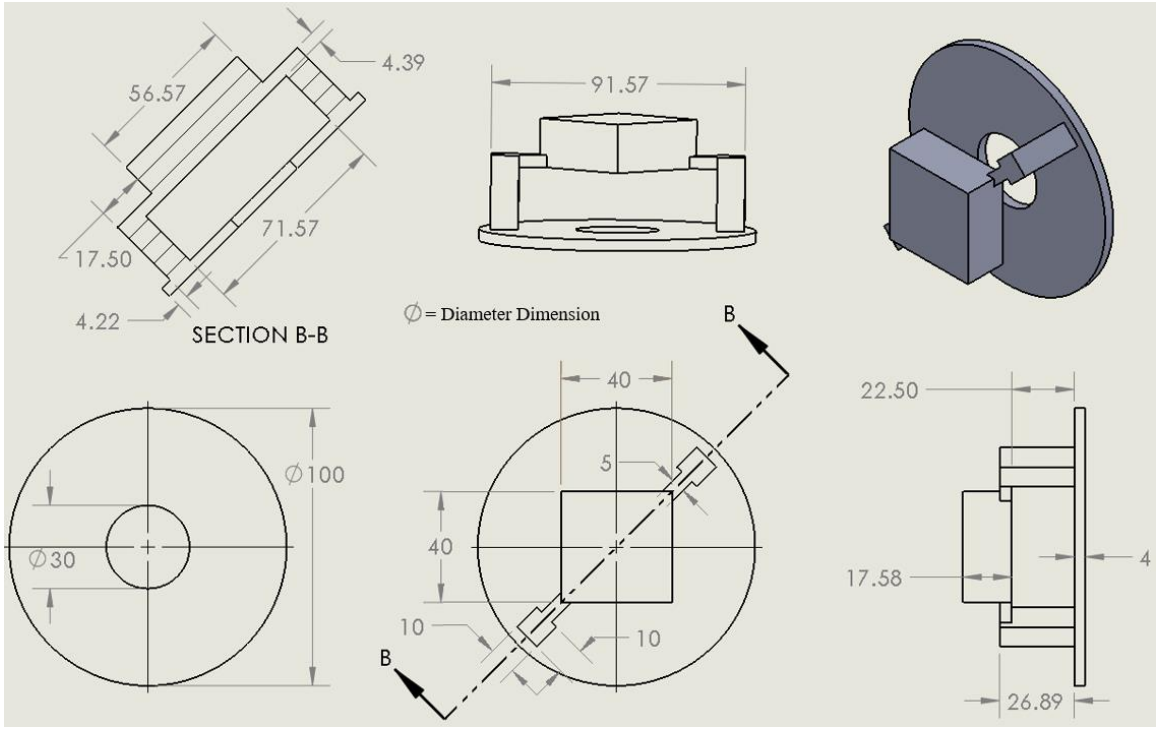

Figure 42. Drawing of Flat Surfaced Double Cavity FPI Sensor

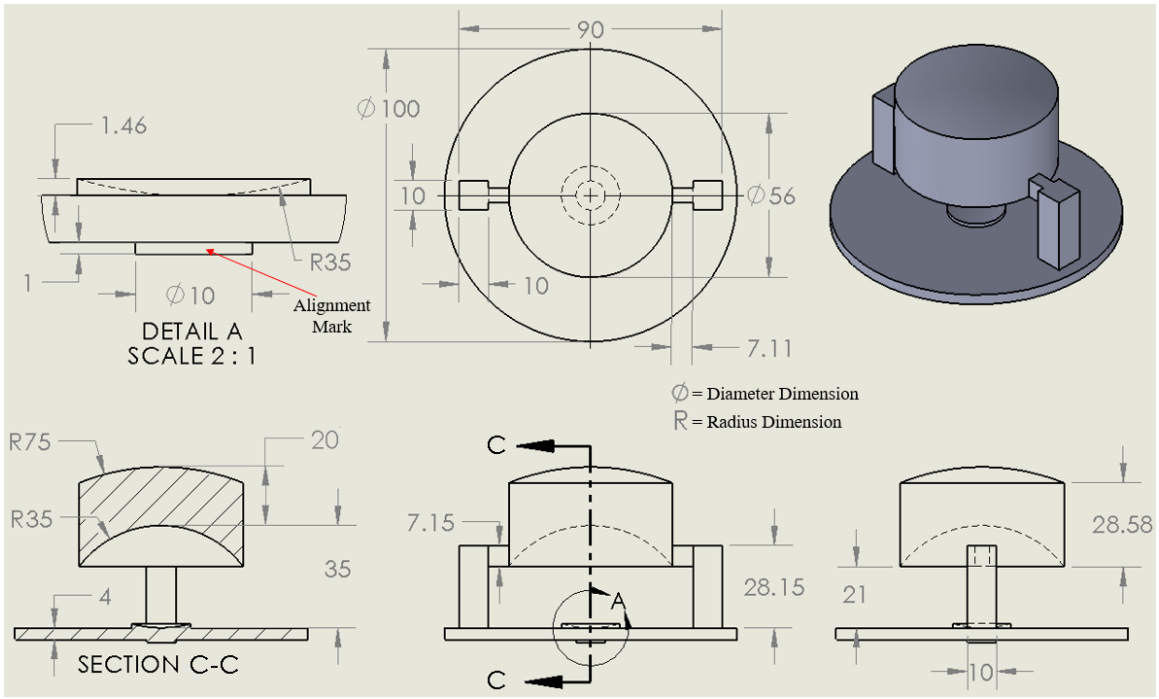

Figure 43. Drawing of Confocal Surfaced Double Cavity FPI Sensor

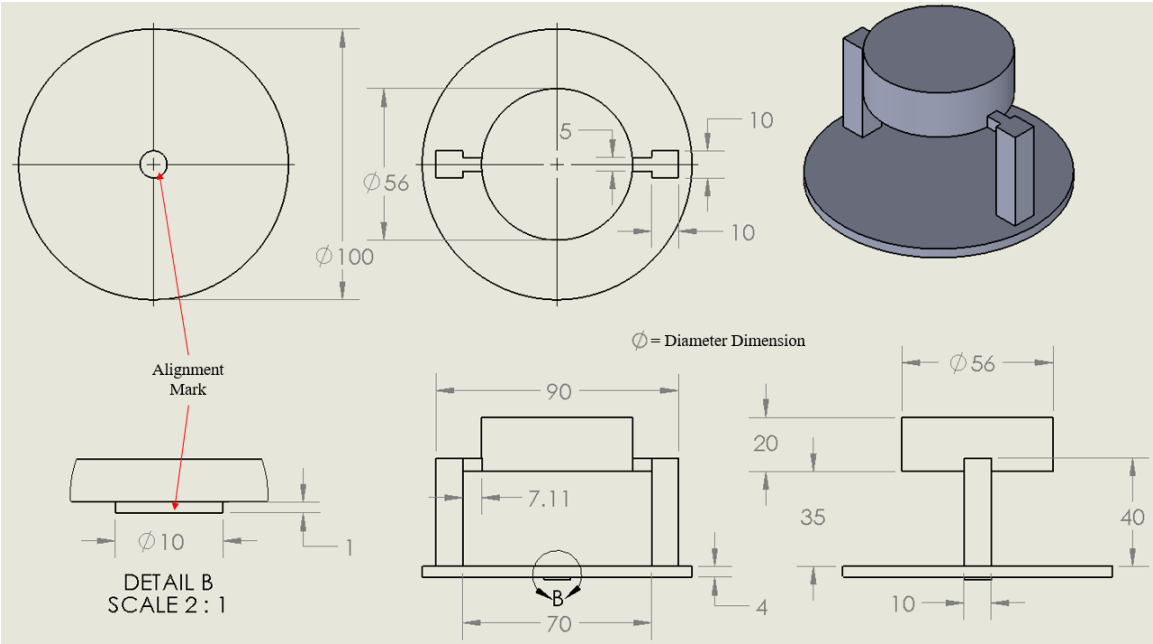

Figure 44. Drawing of Flat Surfaced Double Cavity FPI Sensor (for Comparison with Confocal Surfaced Sensor)

The important things to note is that the hole in the base of Figure 42 is there to prevent any obstruction of light emitting out of the fiber core. This is not done for the confocal surfaced sensor because a curved surface over the fiber core was desired. It is also important to note that there is an alignment mark in Figure 43 and Figure 44 which is used to manually align the 3-D fabrication with the core of the fiber. This alignment mark does not actually show up on the device as the focal point of the Nanoscribe fabrication process is inside the fiber when this is being constructed. Visually watching the laser attempt to fabricate the alignment mark, the laser can be aligned to the core of the fiber.

The design of the confocal surfaced structure required slightly different cavity lengths due to the shape of the surfaces. The air and IP-Dip cavity for the flat surfaced double cavity FPI sensor is 22.5 µm and 17.58 µm respectively. This is smaller than that of the confocal surfaced double cavity FPI sensor which had an air cavity of 35 µm and

IP-Dip cavity of 20 µm. Because of this another flat surfaced double cavity FPI sensor was created with the same cavity lengths as the confocal surfaced sensor which is displayed in Figure 44. This sensor was created strictly for comparison with the confocal surfaced double cavity FPI sensor.

Appendix B: How to Properly Prepare Optical Fiber for Sensor Fabrication

The equipment needed to do this are kimwipes, isopropanol (IPA), cleaver, fiber strippers, and a proper fiber storage container. A kimwipe is a professional delicate wipe made by Kimtech. First step is to cut an appropriate length for your fiber. Experimentation later will require mounting and splicing of this fiber meaning there will need to be enough room on the fiber to do so, even if a few splice attempts fail. It is recommended to have at least two feet of fiber to work with. Cutting the fiber to the desired length can be done by curling it into a loop and pulling tight to break the fiber at the desired location or fiber strippers can be used.

Once the desired fiber sample is cut a single tip will need to be cleaned and cleaved to provide a perfectly flat surface for sensor fabrication. First strip the sheathing off of the fiber tip exposing it. The length of the exposed fiber is dependent on the type of cleaver used (should be 2 to 3 cm long for the cleaver used in this research). For a proper cleave the fiber sheathing should not be struck by the diamond blade, meaning there should be enough exposed fiber on the tip to be sure the diamond blade strikes the exposed fiber cladding. It is also important to make sure there is enough exposed fiber to clamp down on the opposite side of the diamond blade which will ensure the fiber is held tightly at both ends while the diamond blade cleaves. Some fibers with high temperature resistant sheathing are hard to cleanly strip. In this case you can use an open flame to burn off any remaining sheathing. Figure 45 below shows a fiber properly positioned in the cleaver.

Figure 45. Sheathed Optical Fiber Positioned in the Cleaver

As shown, there is approximately two to three centimeters of exposed fiber cladding at the tip of the fiber. Once the fiber tip is exposed it must be cleaned. To do this put a few drops of IPA onto a kimwipe. While wearing gloves pinch the fiber with the wet spot of the kimwipe below the exposed tip of the fiber. While gently pinching the fiber slide the kimwipe in one fluid motion off of the tip of the fiber which will clean the exposed tip. This process can be repeated a few times to ensure a properly cleaned tip. Now that the fiber tip is exposed and cleaned it is ready to be cleaved. Cleaving a fiber tip results in a perfectly flat fiber tip surface which is needed for the 3-D fabrication process.

These instructions are specific to the cleaver used in this thesis which is a Fujikura CT-30 fiber optic cleaver. Before placing the fiber in the cleaver press the diamond blade towards the center of the cleaver while the cleaver is open. A click should take place and the blade should be locked in the back position. Place the fiber into the cleaver as shown in Figure 45. Use the magnetic strap to clamp down the fiber in the

proper position. Once the fiber is secured simple close the cleaver. This will unlock the spring-loaded diamond blade which will then cleave the exposed part of the fiber tip. Once the diamond blade has been released open the cleaver and carefully take out the fiber allowing nothing to touch the tip. Once the fiber is cleaved it is important that nothing touches the newly cleaved tip because damage can easily occur.

After cleaving the fiber, it is important to inspect it to confirm the cleave was accomplished successfully. This is simply done using a microscope (recommended 20x objective). Place the fiber in a device that holds the tip suspended in air and is perpendicular to the microscopes field of view. Two glass slides can be used to sandwich the fiber with the cleaved tip sticking out approximately five millimeters from the glass slide edges. Figure 46 below shows a properly cleaved tip as well as a damaged tip. Once the tip is properly cleaved it is ready for 3-D fabrication. If fabrication is not taking place yet, then it is important to store the fiber correctly to ensure no damage or degradation takes place. Whichever container is used be sure that the exposed fiber tip is held suspended in air preventing contact with any other surface. It is also recommended to keep it in an air tight container to prevent the fiber sample from getting dirty or affected from atmospheric humidity.

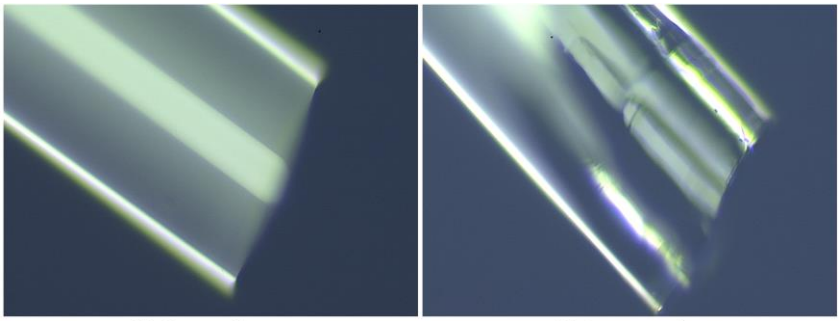

Figure 46. Cleaved Optical Fiber

Appendix C: Nanoscribe Tutorial

Some adaptive changes needed to be made to the Nanoscribe for it to have the ability to create a structure onto a fiber tip. The Nanoscribe is designed to produce micro structures onto thin flat substrates such as a glass slide or silicon wafer. This is due to the sample mounting design of the Nanoscribe. Figure 47 below shows one type of sample holder for the Nanoscribe.

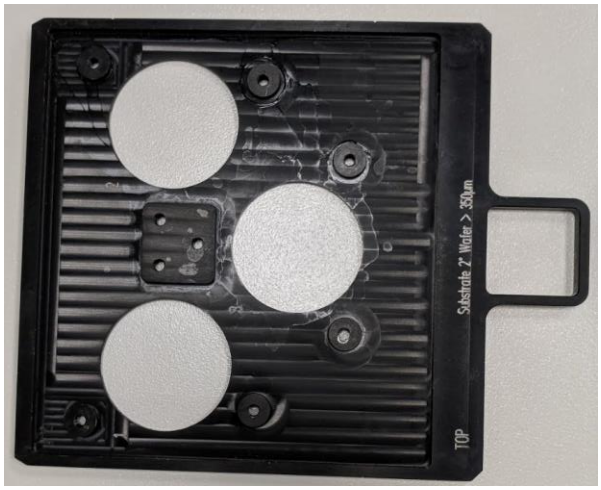

Figure 47. Nanoscribe Sample Holder

This specific holder is designed for small silicon wafers. To accommodate a fiber sample, a holder was designed, and 3-D printed out of Ultem 9085 resin to fit into the top of the Nanoscribe and mount to the specific sample displayed in Figure 47. The design of the printed fiber chuck holder is displayed in Figure 48 and covered in greater detail in Appendix D. This fiber holder was printed by the AFIT 3-D printing lab and was designed to hold a fiber chuck. The design utilizes a set screw that tightens to hold a fiber chuck which is holding the fiber in place. The set screw hole was tapped after printing to

accommodate the set screw that was used. The mounting screw holes did not need tapping as screws from the Nanoscribe sample holder was used which screw into the threads on the sample holder. Figure 49 shows the fiber chuck holder mounted to the Nanoscribe sample holder.

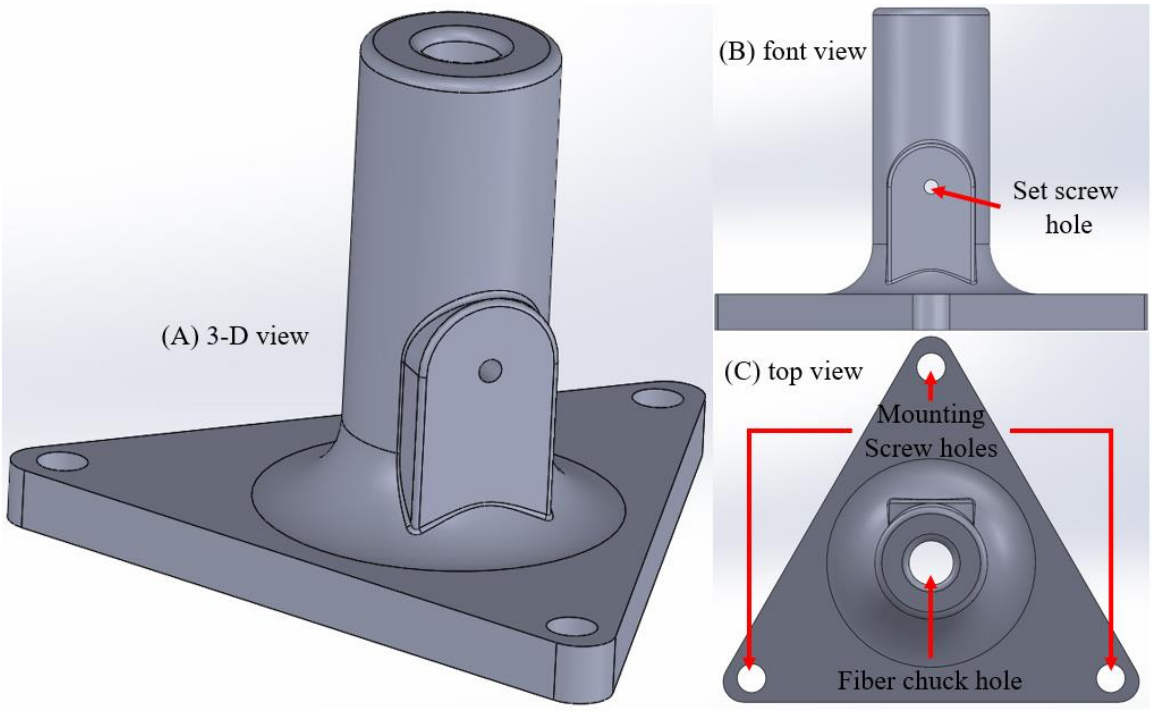

Figure 48. 3-D Printed Optical Fiber Chuck Holder

Figure 49. Fiber Chuck Holder Mounted to Sample Holder

There are several different fiber chucks that will work for this purpose, but it is recommended to use an all metal chuck as the development process for the IP-Dip can decompose certain polymer structures. Figure 50 shows an image of the fiber chuck utilized for this thesis. The purpose of using a fiber chuck is to gain more precision when holding the fiber in place.

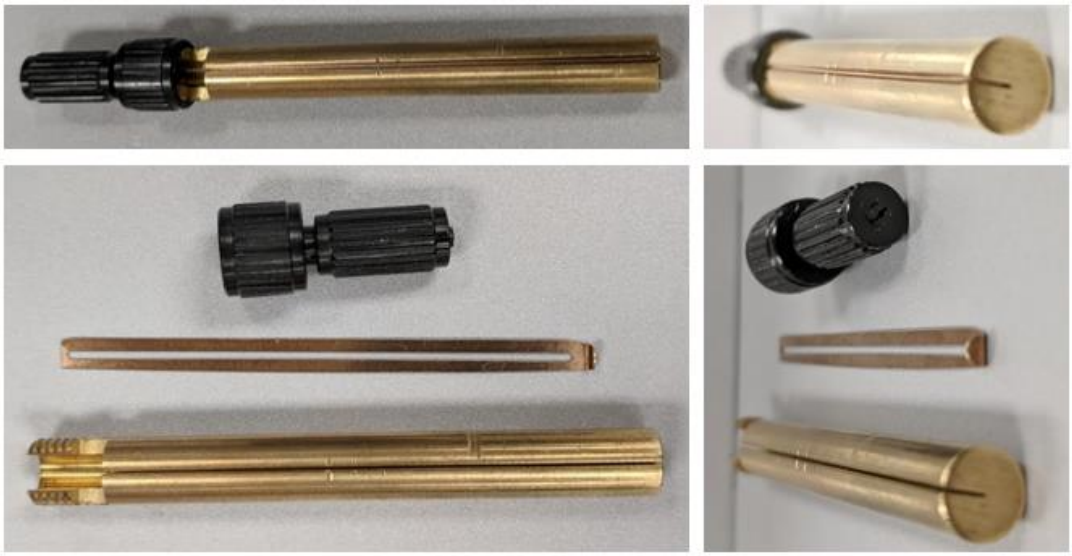

Figure 50. Fiber Chuck used for 3-D Microfabrication of Polymer Structures

When preparing and operating the Nanoscribe be sure to wear proper eye protection and be in a room with proper lighting. The IP-Dip is a UV light sensitive material, so it is required to be in a non-UV lit room when working with the material. Be sure the proper lens is clean and mounted to the Nanoscribe. A Zeiss Plan-Apochromat 63x/14 oil DIC lens was used for this thesis.

Now mount the fiber inside the fiber chuck with the fiber tip of interest extended roughly one millimeter or less past the end of the fiber chuck. Then mount the fiber

chuck into the fiber chuck holder. Be sure to do this carefully and not damage the fresh cleave on the tip of the fiber. If a side mount fiber chuck (displayed in Figure 50) is properly used the fiber tip will not be damaged, however if a pull through fiber chuck is used be sure to slide the back end of the fiber through or cleave the fiber after it has already been slid through the chuck to prevent any damage to the cleaved tip. Once the fiber is fully mounted in the chuck and fiber chuck holder it is time to deposit the IP-Dip. Deposit roughly one to three drops of IP-Dip so that the entire fiber tip and chuck end is covered. Then flip the entire fiber chuck holder over and mount it to the Nanoscribe. The IP-Dip resin has enough viscosity to keep it in place for several minutes. To mount the fiber chuck holder to the sample holder in Figure 49 while inside the Nanoscribe, the light on top needs to be removed as shown in Figure 51.

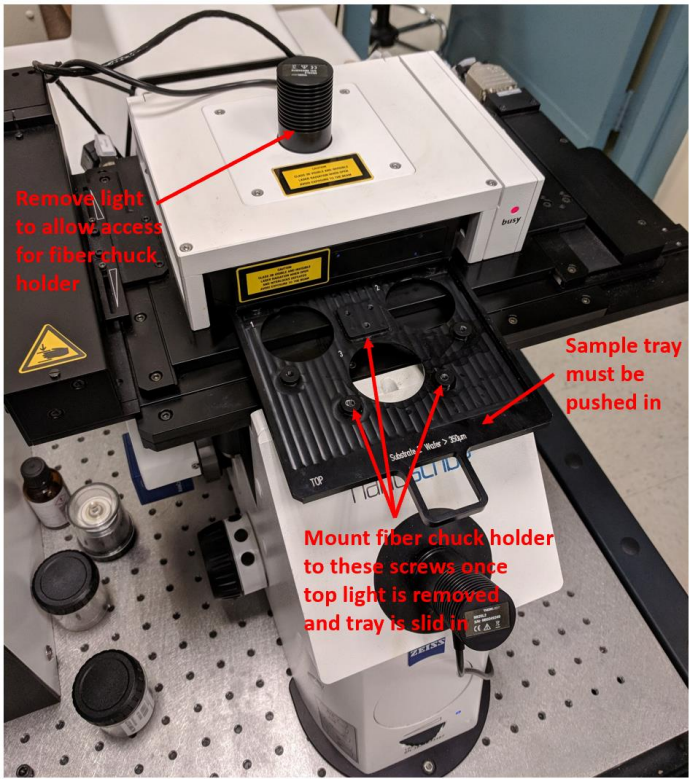

Figure 51. Mounting Fiber to the Nanoscribe

Using the NanoWrite 1.8.6 (software used to operate the Nanoscribe), load the structure that will be 3-D fabricated onto the fiber. The design of this structure can be done multiple ways, however Solidworks 2016 was utilized for this research. DeScribe 2.4.4 is the software that can input any design in the format of a .STL file and will automatically convert from millimeters to micrometers. Once an STL design file is stored on the Nanoscribe computer simple double click it to open DeScribe. A rendering of the design will appear similar to Figure 52.

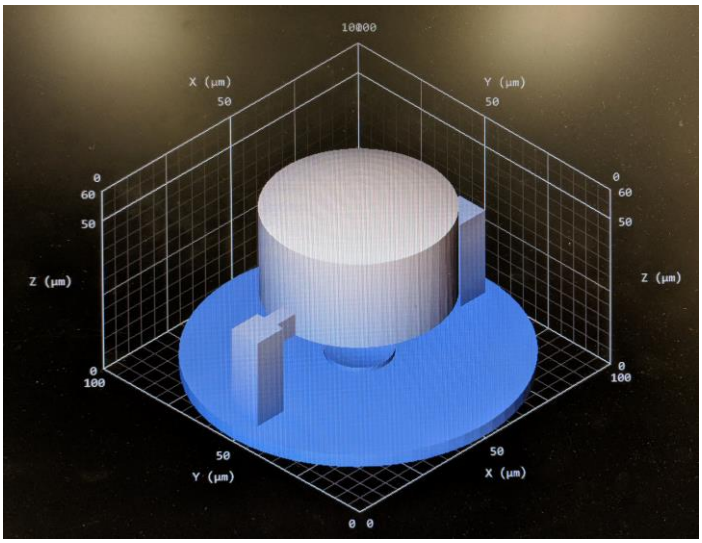

Figure 52. Nanoscribe DeScribe STL File Rendering

If the rendered image does not look correct be sure to open DeScribe and select the correct rendering mode. The rendering mode used for Figure 52 above is voxel lines. Figure 53 below shows the DeScribe menu for changing the rendering mode.

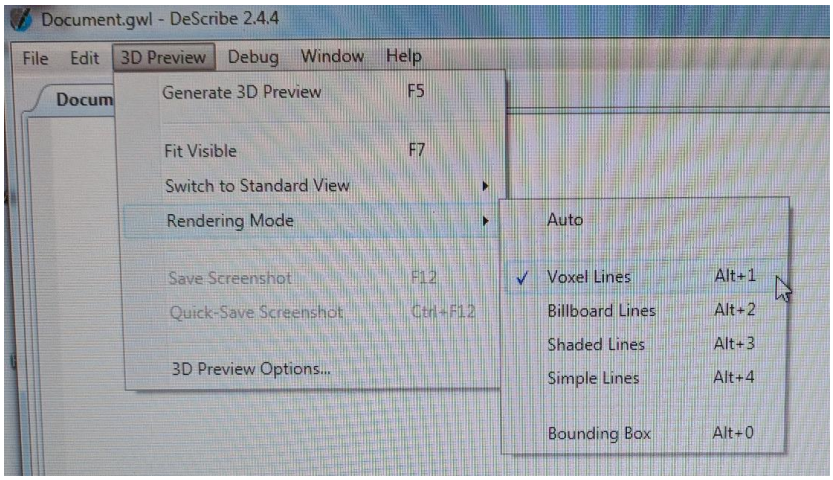

Figure 53. DeScribe Image Rendering Menu

While still in DeScribe, all fabrication parameters need to be chosen. These parameters include device orientation, vertical slicing, horizontal hatching, scan mode, and output file name. Figure 54 shows the parameters utilized in this thesis research.

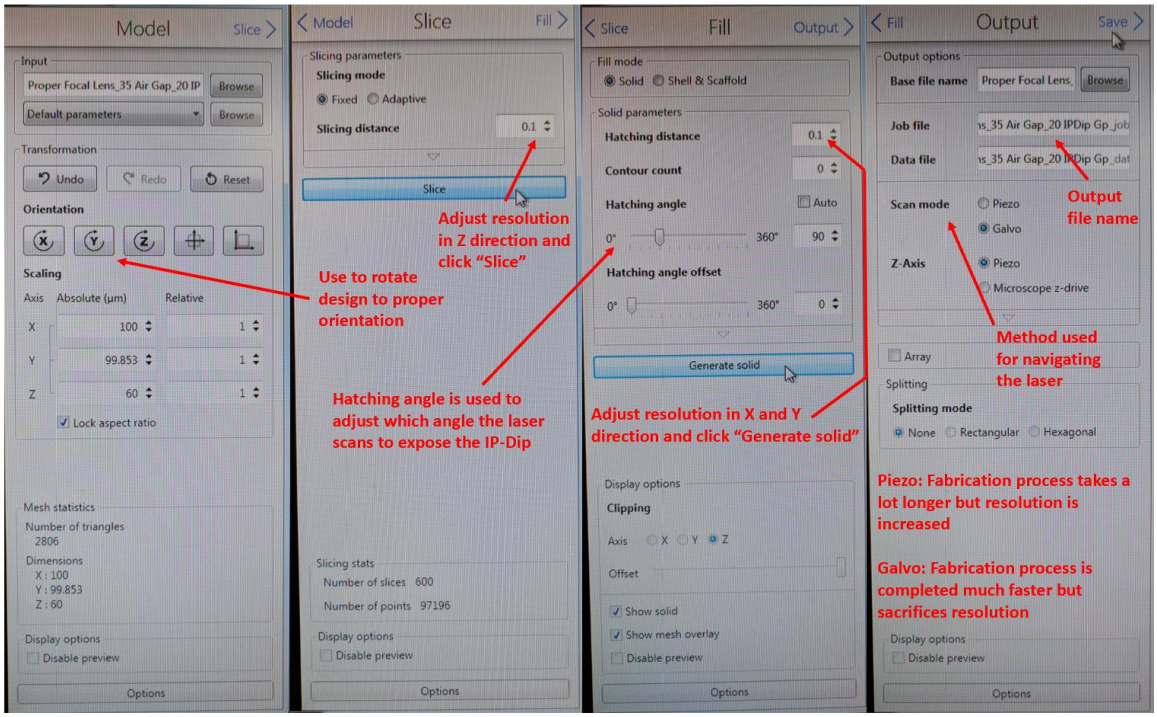

Figure 54. Nanoscribe Fabrication Parameters Used

Set the slicing and hatching distance to 0.1 for the highest device resolution. Set the Nanoscribe operating mode to galvometer which utilizes multiple mirrors at variable angles to guide the lasers performing the 3-D fabrication. There is also a piezoelectric and servo operating mode for different circumstances. The piezoelectric operating mode is a much slower, finer detail process utilized for extremely small (100's of nanometers), precise feature sizes. The servo operating mode is just the opposite which is used for much larger structures and can write at a much faster speed by sacrificing accuracy.

Once the device parameters are set and saved a .job file is generated. This file is what is used by NanoWrite to guide the Nanoscribe fabrication. It is recommended to open the newly generated .job file to make some adjustments. Adjust the laser power as necessary for the specific structure. It is recommended that a few test runs be completed ahead of time to determine the best laser power for the given conditions. A laser power of 42% was used for this research. The move stage and find interface commands also need to be deleted as the optical fiber surface will need to be manually found. Figure 55 shows these edits made.

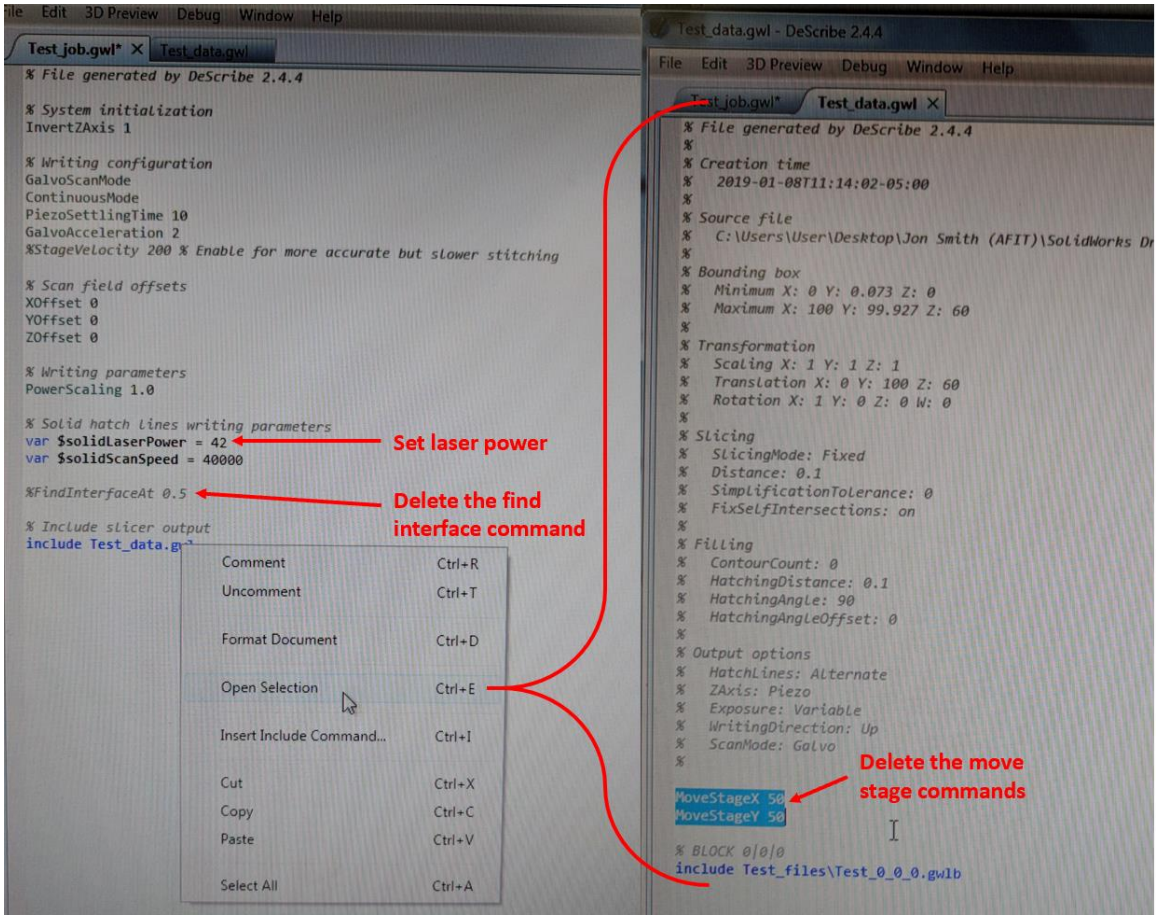

Figure 55. Editing Nanoscribe .job File for Fiber Fabrication

Once all the settings are properly set then input the job into NanoWrite. To do this first turn on the Nanoscribe and imaging microscope. The power switches are shown in Figure 56. Then double click the NanoWrite desktop icon to open the software. A window will pop up requesting to calibrate the stage; click “Calibrate.” Once the stage is calibrated a window will pop up asking which sample holder is loaded. Figure 57 below shows the sample holder used in this research and which location to choose.

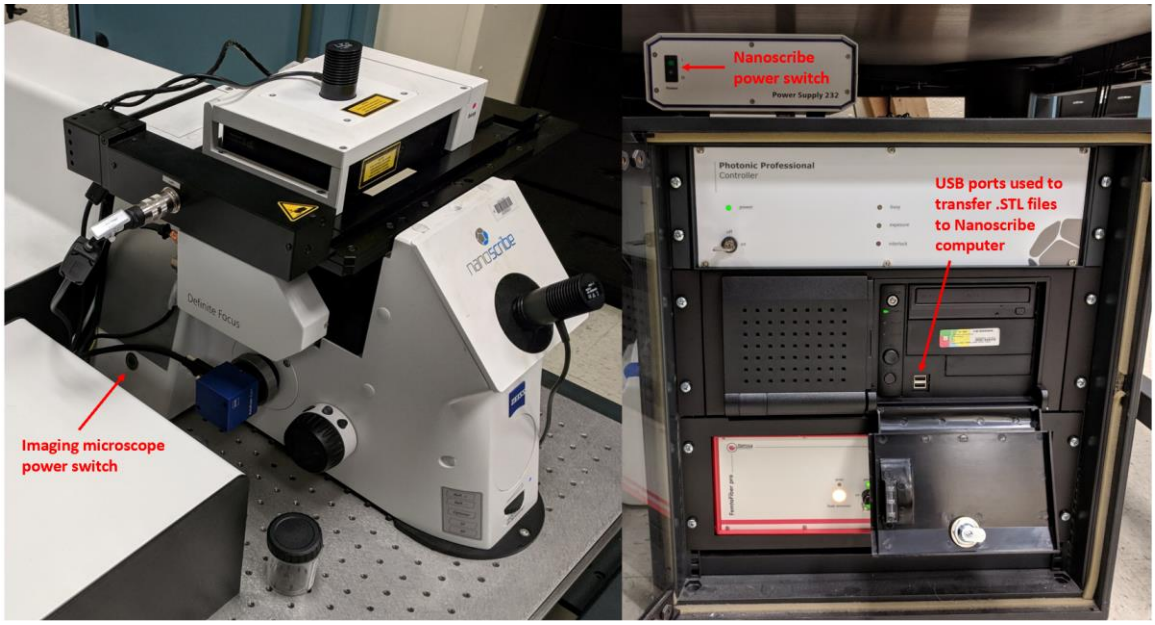

Figure 56. Nanoscribe Power Switch Locations

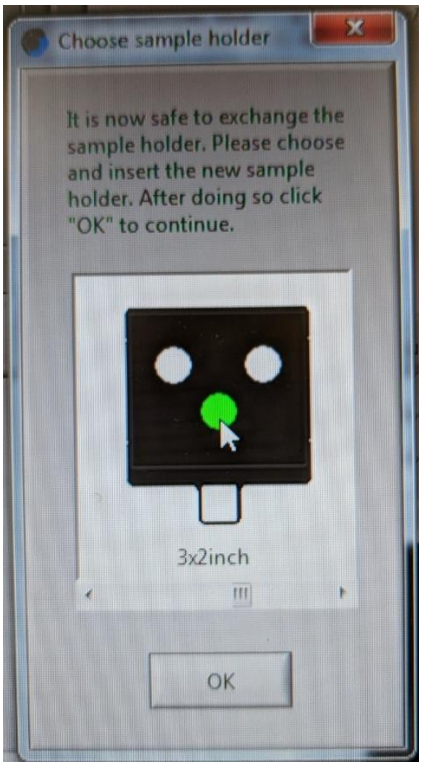

Figure 57. Nanoscribe Sample Holder Selection

Now that NanoWrite is open and calibrated the .job file created earlier can be imported. Simply click the “Load Job” button on the left side of the screen and select the desired .job file.

Next, the substrate, or surface to fabricate on, must be found. The Nanoscribe has a function that can do this automatically, but unfortunately that only works with familiar substrate such as Indium-Tin-Oxide (ITO) glass slides or silicon wafers. The tip of the fiber needs to be manually found by moving the fiber closer to the lens until the face of the fiber chuck comes into focus. To accomplish this the stage needs to be moved and the imaging microscope settings need to be adjusted. Through trial and error, it has been found that manually moving the stage to a Y value of 6600 micrometers nearly centers the stage on the optical fiber. Figure 58 below shows the imaging microscope settings.

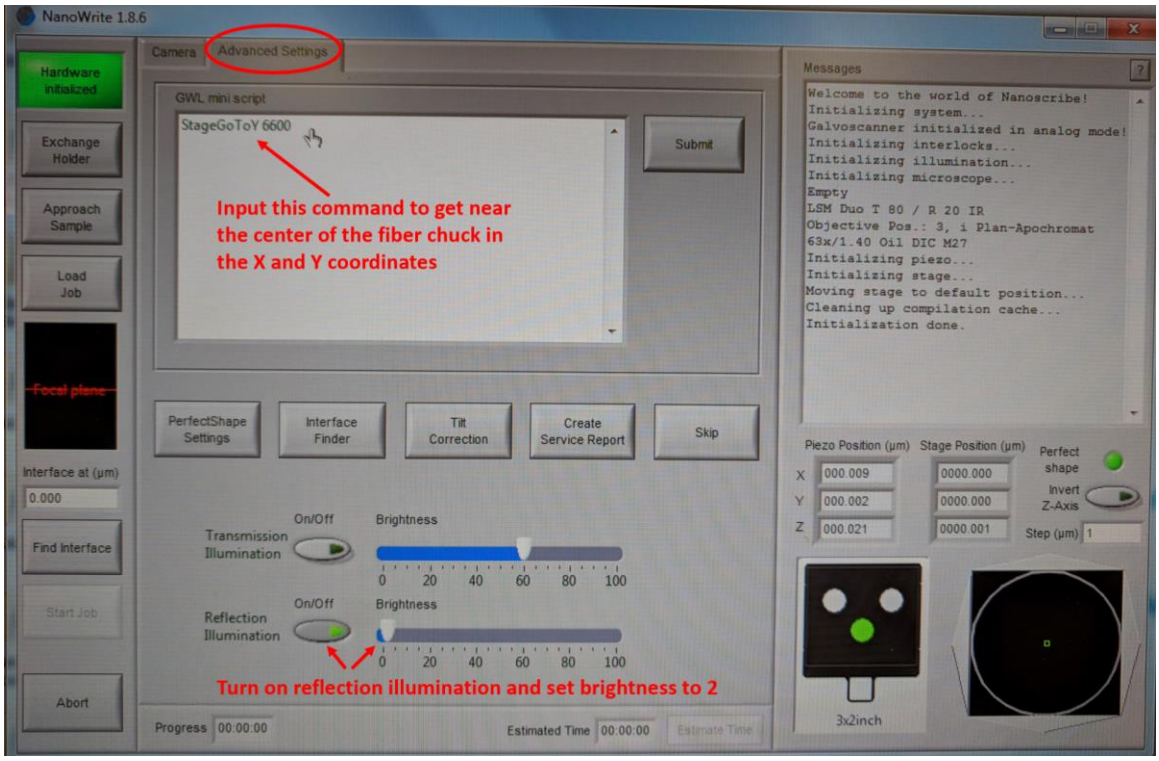

Figure 58. Nanoscribe Imaging Microscope & Stage Settings

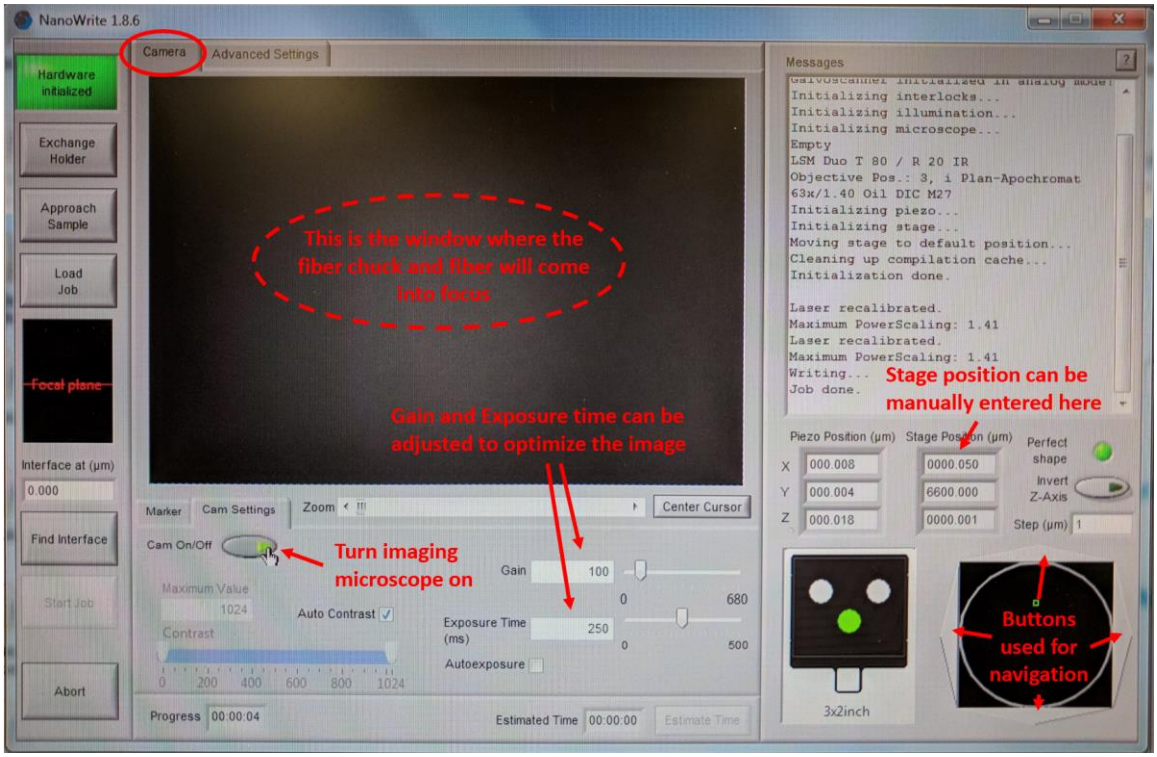

Figure 59. Nanoscribe Operating Interface

Use the imaging microscope window displayed in Figure 59 to locate the surface of the fiber chuck. As the lens gets closer to the fiber chuck the image will get much brighter. If it becomes too bright simple adjust the gain and exposure time to dim the image. Once the fiber chuck surface is found use the navigational buttons to locate the fiber tip. Utilize any defining features of the fiber chuck to help locate the fiber. In this research a side loading fiber chuck was used so the slot in which the fiber fit into was first located, and then the fiber was located from there. To make the fiber easier to find a red LED light can be utilized to shin through the back end of the fiber which will illuminate the core of the fiber making it easier to find. 3-D fabrication can begin once the core (x and y coordinates) and surface of the fiber tip (z coordinate) are located. To ensure that the 3-D fabricated structure adheres to the surface of the fiber tip it is

important to start the fabrication process slightly below the fiber face (inside the glass fiber). As the structure is created it will ensure that contact is made with the fiber face. Through many trials the best results have come when starting the fabrication process about five microns below the fiber surface. This means once the optical fiber is found and the fiber tip is in focus, move the stage five microns closer to the fiber before starting the fabrication process. Once the desired fabrication location is found simply click the “Start Job” button on the left side of the screen. Depending on the size of the structure being made, fabrication can take anywhere from two to twenty minutes.

Once the device is hardened inside the IP-Dip resin it needs to be developed to wash away all the unexposed IP-Dip. To develop the 3-D fabricated structure first soak the device in a beaker filled with propylene glycol monomethyl ether acetate for twenty minutes. Then transfer the device to another beaker with IPA and soak for another twenty minutes. Finally let the device air dry for approximately ten to twenty minutes. Once the device is fully developed it can then be inspected under a microscope to ensure the device was fabricated successfully and adhered to the fiber tip. If fabrication was initiated in the wrong location (too far away from the fiber tip surface) then the 3-D fabricated device would not properly adhere to the fiber surface which will result in the entire structure washing away during the development phase.

Appendix D: Design Dimensions of Nanoscribe Fiber Chuck Holder

The design created in Solidworks 2016 x64 edition for the fiber chuck holder used to mount to the Nanoscribe for fiber tip printing is shown below in Figure 60.

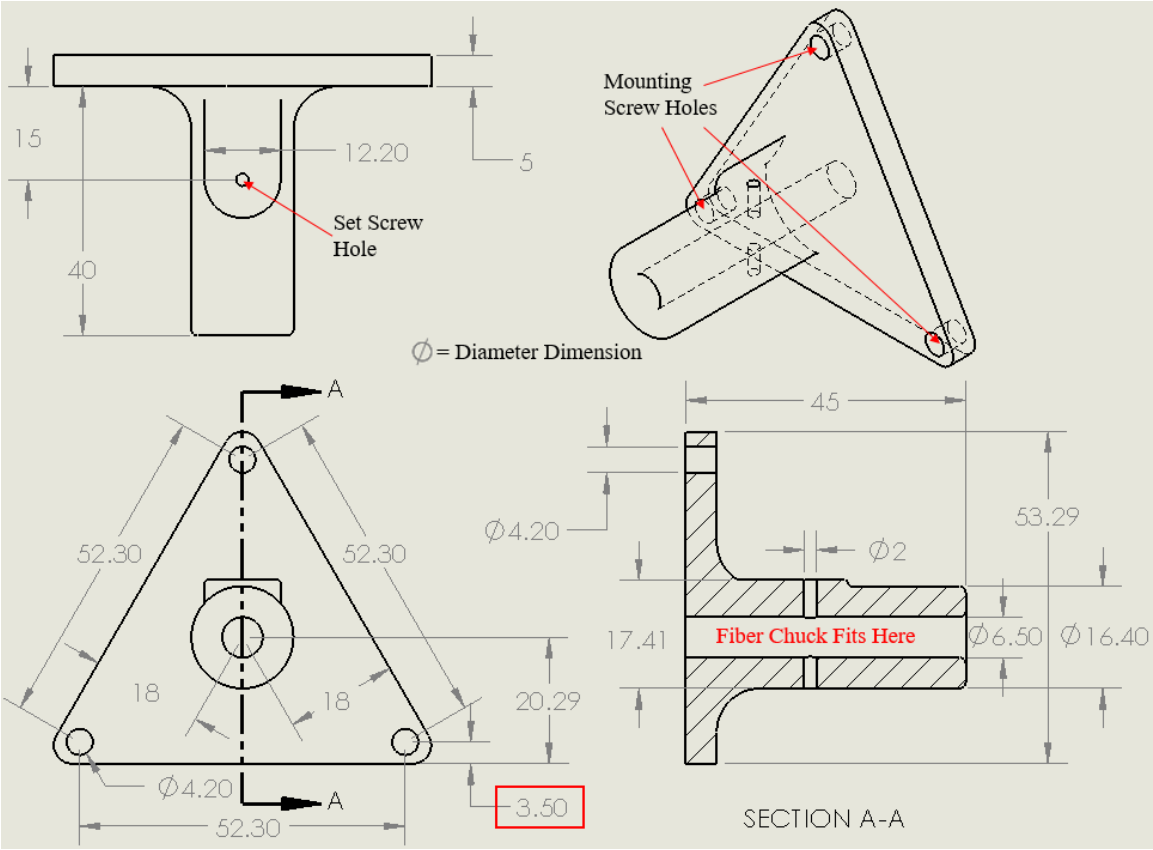

Figure 60. Nanoscribe Fiber Chuck Holder

All dimensions are in millimeters. The set screw hole is tapped after fabrication matching the threads to which ever set screw is used. The mounting screw holes remain untapped as the Nanoscribe mounting screws simply slide through them and thread into the sample holder. The diameter of the hole fitting the fiber chuck must be adjusted to the fiber chuck that will be used. Be sure to design in a small amount of tolerance for the

chuck to fit. The spacing between the mounting screw holes is significantly important and should not be changed. There is also very little clearance between the mounting screws and the wall of the Nanoscribe so the dimension noted in the red square is significant as well, because if it is made any larger the fiber chuck holder will not fit inside the Nanoscribe.

Appendix E: Matlab Code Utilized for Data Analysis

The data obtained directly from the digital oscilloscope after an experimental run is a text file with two columns of data separated by a comma. The first column is the x axis which is wavelength and the second column is the y axis which is intensity. A trigger signal is also recorded in tandem to mark the beginning of each wavelength sweep recorded. The Matlab code below was used to separate the data into two column vectors and clip the data so that everything before the sweep started and after the sweep ended was deleted. Matlab 2017a was used for all analysis performed in this thesis research.

```
clear all; close all; clc;

%-------------------------------------------------------------
%Get data file
data = 'Fiber Device 7 at 20C after heat_1463nm sweep to 1634 nm_2nm
per sec_10pm step_1mW_RoomTemp 21C_Run2_25Oct18_DSO9254A_1'

d = csvread(data);   %Save data in file as a matrix

%Split matrix into columb vectors
d_1 = d(:,1);    %Sweep step
d_2 = d(:,2);    %Intensity

%Get trigger to data file
trigger = 'Fiber Device 7 at 20C after heat_1463nm sweep to 1634 nm_2nm
per sec_10pm step_1mW_RoomTemp 21C_Run2_25Oct18_DSO9254A_3'

t = csvread(trigger);

%Split matrix into columb vectors
t_1 = t(:,1);    %Sweep step
t_2 = t(:,2);    %Intensity

%----------Cycle through the trigger data to find start point----------
cycle = length(t_2);
clip1 = 1;
clip2 = 1;

for i = 1:cycle
```

```
    int1 = t_2(i);

    if i < cycle
        int2 = t_2(i+1);
    end

    if i < cycle-1
        int3 = t_2(i+2);
    end

    %if there is a large change in Intensity (trigger signal)
    %then save that spot as "clip1" for begining clip
    if abs(int1-int2) >= 0.08
        clip1 = i+1;
    elseif abs(int1-int3) >= 0.08
        clip1 = i+1;
    end
end

%add length of sweep to clip1 to get "clip2" for end clip
clip2 = clip1+85500;
%-------------------------------------------------------------------

%Where the clips are located
%(Just use these to check the clips if you want to)
Intensity_at_clip1 = t_2(clip1);
time_at_clip1 = t_1(clip1);
Intensity_at_clip2 = t_2(clip2);
time_at_clip2 = t_1(clip2);

%This is the Intensity daty properly clipped
clipped_Intensity = d_2(clip1:clip2);

fig = figure(1);
subplot(3,1,1)
plot(d_1, d_2)
xlabel('time (sec)')
ylabel('Intensity (mV)')
hold on
subplot(3,1,2)
plot(t_1, t_2)
subplot(3,1,3)
plot(d_1(clip1:clip2),clipped_Intensity)
%Increase figure window size
pos = get(fig,'position');
set(fig,'position',[pos(1:2)/4 pos(3:4)*2])

%----------This increases the decimals of my data cursor----------
datacursormode on;
dcm_obj = datacursormode(gcf);
set(dcm_obj,'DisplayStyle','datatip','UpdateFcn',@DataClipCallback);
%Need to have "DataClipCallback.m" saved in the same file path
```

The variable titled “Clipped_Intensity” is the raw intensity data gathered during the wavelength sweep. When looking at the graphs Matlab produces a higher precision is desired when using the data curser. To get that the bottom section of code was completed and “DataClipCallback” was used. The code in DataClipCallback is displayed below.

```
function output_txt = myfunction(obj,event_obj)
% Display the position of the data cursor
% obj          Currently not used (empty)
% event_obj    Handle to event object
% output_txt   Data cursor text string (string or cell array of
strings).

pos = get(event_obj,'Position');
output_txt = {['X: ',num2str(pos(1),9)],...
    ['Y: ',num2str(pos(2),9)]};

% If there is a Z-coordinate in the position, display it as well
if length(pos) > 2
    output_txt{end+1} = ['Z: ',num2str(pos(3),4)];
end
```

Once this data is clipped it must be filtered to remove the noise (especially for data runs at higher temperatures). The codes used for filtering this data is displayed below.

```
clear all; close all; clc
%Testing import data file


X = 'Wavelength sweep data_1463nm to 1634nm.txt'
wave = csvread(X);
%-----------------------------------20 Degrees C-----------------
%Get data file
file20 = 'Fiber Device 5 at 20C after heat_Brick no air
gap_Run1_19Dec18_37C_clipped intensity.txt'

t20 = csvread(file20);   %Save data in file as a matrix

s20 = smoothdata(t20);
```

```
%subplot(4,1,1)
%plot(L20, t20_2)
plot(wave, s20)
xlabel('Wavelength (nm)')
ylabel('Intensity (mV)')
hold on


%-------------------------------------40 Degrees C-----------------
%Get data file
file40 = 'Fiber Device 5 at 40C_Brick no air gap_Run1_19Dec18_38C-
42C_clipped intensity.txt'

t40 = csvread(file40);   %Save data in file as a matrix

s40 = smoothdata(t40);

%subplot(4,1,1)
%plot(L40, t40_2)
plot(wave, s40)
%xlabel('Wavelength (nm)')
%ylabel('Intensity (mV)')
%hold on


%-------------------------------------60 Degrees C-----------------
%Get data file
file60 = 'Fiber Device 5 at 60C_Brick no air gap_Run1_19Dec18_58C-
62C_clipped intensity.txt'

t60 = csvread(file60);   %Save data in file as a matrix

s60 = smoothdata(t60);

%subplot(4,1,2)
%plot(L60, t60_2)
plot(wave, s60)
%xlabel('Wavelength (nm)')
%ylabel('Intensity (mV)')
%hold on


%-------------------------------------80 Degrees C-----------------
%Get data file
file80 = 'Fiber Device 5 at 80C_Brick no air gap_Run1_19Dec18_78C-
83C_clipped intensity.txt'

t80 = csvread(file80);   %Save data in file as a matrix

s80 = smoothdata(t80);
```

```
%subplot(4,1,3)
%plot(L80, t80_2)
plot(wave, s80)
%xlabel('Wavelength (nm)')
%ylabel('Intensity (mV)')
%hold on


%-------------------------------------100 Degrees C-----------------
%Get data file
file100 = 'Fiber Device 5 at 100C_Brick no air gap_Run1_19Dec18_98C-
101C_clipped intensity.txt'

t100 = csvread(file100);   %Save data in file as a matrix

s100 = smoothdata(t100);

%subplot(4,1,3)
%plot(L100, t100_2)
plot(wave, s100)
%xlabel('Wavelength (nm)')
%ylabel('Intensity (mV)')
%hold on


%-------------------------------------120 Degrees C-----------------
%Get data file
file120 = 'Fiber Device 5 at 120C_Brick no air gap_Run1_19Dec18_118C-
124C_clipped intensity.txt'

t120 = csvread(file120);   %Save data in file as a matrix

s120 = smoothdata(t120);

%subplot(4,1,4)
%plot(L120, t120_2)
plot(wave, s120)
%xlabel('Wavelength (nm)')
%ylabel('Intensity')
legend('20C','40C','60C','80C','100C','120C')

%----Curve Fitting Commands to use-------
%cftool(L120,t120_2);
%This opens the curve fit tool with the specific data
%Use "Fourier with 8 terms"

%fitted_Y_120 = feval(fittedmodel120,L120);
%This gives you the new y data values (use the same x values from
before)
```

The data titled “s20, s40… s120” is the filtered intensity data at that corresponding temperature. I designed this portion of code to filter six different data sets at once (one for each temperature range). Once all of the data is filtered I then used Microsoft excel (version 2013) to average the filtered intensity data together across all similar runs. Meaning all of my experiments conducted at 20oC for a certain fiber tip sensor was averaged together after being filtered. This is done to produce more consistent results. Once all of the data was filtered and averaged I used the below Matlab code to plot the data for initial analysis.

```
clear all; close all; clc;

%Get data file
fileX = 'Wavelength sweep data_1463nm to 1634nm'
x = csvread(fileX);

file20 = 'AVERAGED Overall Intensity_Fiber Device 1 at 20C after
heat_No Air Gap_6Nov18.txt'
t20 = csvread(file20);

file40 = 'AVERAGED Overall Intensity_Fiber Device 1 at 40C_No Air
Gap_6Nov18.txt'
t40 = csvread(file40);

file60 = 'AVERAGED Overall Intensity_Fiber Device 1 at 60C_No Air
Gap_6Nov18.txt'
t60 = csvread(file60);

file80 = 'AVERAGED Overall Intensity_Fiber Device 1 at 80C_No Air
Gap_6Nov18.txt'
t80 = csvread(file80);

file100 = 'AVERAGED Overall Intensity_Fiber Device 1 at 100C_No Air
Gap_6Nov18.txt'
t100 = csvread(file100);

file120 = 'AVERAGED Overall Intensity_Fiber Device 1 at 120C_No Air
Gap_6Nov18.txt'
t120 = csvread(file120);
```

```
plot(x, t20)
xlabel('Wavelength (nm)')
ylabel('Intensity (mV)')
hold on
plot(x, t40)
plot(x, t60)
plot(x, t80)
plot(x, t100)
plot(x, t120)
legend('20C','40C','60C','80C','100C','120C')

%----------This increases the decimals of my data cursor----------
datacursormode on;
dcm_obj = datacursormode(gcf);
set(dcm_obj,'DisplayStyle','datatip','UpdateFcn',@DataClipCallback);

%----Curve Fitting Commands to use-------
%cftool(x,t120);
%This opens the curve fit tool with the specific data
%Use "Fourier with 8 terms"

%fitted_Y_120 = feval(fittedmodel120,x);
%This gives you the new y data values (use the same x values from
before)
```

This would produce graphs sufficient for analysis, but the graphs and figures displayed in this thesis were completed using OriginPro 2018. The data clipped and filtered from Matlab was then imported into OriginPro to create publication quality figures that are clear and concise.

Bibliography

[1] “Basic Polarization Techniques and Devices.” *Meadowlark Optics Inc*. (2005).

[2] Bethune, Donald S., and James J. Wynne. "Peter Pitirimovich Sorokin: Laser pioneer dedicated to understanding, creating, and using light." *Proceedings of the National Academy of Sciences* 113, no. 1 (2016): 12-13.

[3] Bhatia, Vikram, and Ashish M. Vengsarkar. "Optical fiber long-period grating sensors." *Optics letters* 21, no. 9 (1996): 692-694.

[4] Biercuk, M. J., D. J. Monsma, C. M. Marcus, J. S. Becker, and R. G. Gordon. "Low-temperature atomic-layer-deposition lift-off method for microelectronic and nanoelectronic applications." *Applied Physics Letters* 83, no. 12 (2003): 2405-2407.

[5] Chandrahalim, Hengky, Qiushu Chen, Ali A. Said, Mark Dugan, and Xudong Fan. "Monolithic optofluidic ring resonator lasers created by femtosecond laser nanofabrication." *Lab on a Chip* 15, no. 10 (2015): 2335-2340.

[6] Chen, Li Han, Tao Li, Chi Chiu Chan, R. Menon, Papusamy Balamurali, Mutukumaraswamy Shaillender, Björn Neu et al. "Chitosan based fiber-optic Fabry–Perot humidity sensor." *Sensors and Actuators B: Chemical* 169 (2012): 167-172.

[7] Chen, Poki, Chun-Chi Chen, Chin-Chung Tsai, and Wen-Fu Lu. "A time-to-digital-converter-based CMOS smart temperature sensor." *IEEE Journal of Solid-State Circuits* 40, no. 8 (2005): 1642-1648.

[8] Chen, Qikai, Mesut Meterelliyoz, and Kaushik Roy. "A CMOS thermal sensor and its applications in temperature adaptive design." In *Proceedings of the 7th International Symposium on Quality Electronic Design*, pp. 243-248. IEEE Computer Society, 2006.

[9] Chintapatla, Shravan, and John F. Muth. "Electrothermal Wrinkling of Silicon Nitride Membrane Mirror in a Fabry-Perot Cavity." In *Lasers and Electro-Optics Society, 2007. LEOS 2007. The 20th Annual Meeting of the IEEE*, pp. 767-768. IEEE, 2007.

[10] Choi, Hae Young, Kwan Seob Park, Seong Jun Park, Un-Chul Paek, Byeong Ha Lee, and Eun Seo Choi. "Miniature fiber-optic high temperature sensor based on a hybrid structured Fabry–Perot interferometer." *Optics letters* 33, no. 21 (2008): 2455-2457.

[11] Chryssis, Athanasios N., Sang M. Lee, Sang B. Lee, Simarjeet S. Saini, and Mario Dagenais. "High sensitivity evanescent field fiber Bragg grating sensor." *IEEE Photonics Technology Letters* 17, no. 6 (2005): 1253-1255.

[12] Elosua, Cesar, Ignacio Matias, Candido Bariain, and Francisco Arregui. "Volatile organic compound optical fiber sensors: A review." *Sensors* 6, no. 11 (2006): 1440-1465.

[13] Feng, Jing, Ming Ding, Jun-Long Kou, Fei Xu, and Yan-Qing Lu. "An optical fiber tip micrograting thermometer." *IEEE Photonics Journal* 3, no. 5 (2011): 810-814.

[14] Garcia, Jose A., David Monzón-Hernández, Oswaldo Cuevas, Berenice Noriega-Luna, and Erika Bustos. "Optical fiber detector for monitoring volatile hydrocarbons during electrokinetic treatment of polluted soil." *Journal of Chemical Technology & Biotechnology* 91, no. 8 (2016): 2162-2169.

[15] Genberg, Victor, Keith Doyle, and Gregory Michels. "Optical interface for MSC. Nastran." In *MSC 2004 VPD Conference*. 2004.

[16] George, Steven M. "Atomic layer deposition: an overview." *Chemical reviews* 110, no. 1 (2009): 111-131.

[17] Grobnic, Dan, Stephen J. Mihailov, Huimin Ding, and Christopher W. Smelser. "Bragg grating evanescent field sensor made in biconical tapered fiber with femtosecond IR radiation." *IEEE photonics technology letters* 18, no. 1 (2006): 160-162.

[18] Hagleitner, C., D. Lange, N. Kerness, A. Kummer, W. H. Song, Andreas Hierlemann, O. Brand, and H. Baltes. "CMOS single-chip multisensor gas detection system." In *Micro Electro Mechanical Systems, 2002. The Fifteenth IEEE International Conference on*, pp. 244-247. IEEE, 2002.

[19] Hagleitner, Christoph, Dirk Lange, Andreas Hierlemann, Oliver Brand, and Henry Baltes. "CMOS single-chip gas detection system comprising capacitive, calorimetric and mass-sensitive microsensors." *IEEE Journal of Solid-State Circuits* 37, no. 12 (2002): 1867-1878.

[20] Han, Jaeheon. "Fabry–Perot cavity chemical sensors by silicon micromachining techniques." *Applied physics letters* 74, no. 3 (1999): 445-447.

[21] Hecht, Eugene. "Optics 4th edition." *Optics, 4th Edition, Addison Wesley Longman Inc, 1998* (1998).

[22] Hill, Kenneth O., and Gerald Meltz. "Fiber Bragg grating technology fundamentals and overview." *Journal of lightwave technology* 15, no. 8 (1997): 1263-1276.

[23] Hutt, D. L., K. J. Snell, and P. A. Bélanger. "Alexander Graham Bell's Photophone." *Optics and Photonics News* 4, no. 6 (1993): 20-25.

[24] Hu, T. Y., Y. Wang, C. R. Liao, and D. N. Wang. "Miniaturized fiber in-line Mach–Zehnder interferometer based on inner air cavity for high-temperature sensing." *Optics letters* 37, no. 24 (2012): 5082-5084.

[25] Iadicicco, Agostino, A. Cusano, A. Cutolo, R. Bernini, and M. Giordano. "Thinned fiber Bragg gratings as high sensitivity refractive index sensor." *IEEE Photonics Technology Letters* 16, no. 4 (2004): 1149-1151.

[26] Jung, Jaehoon, Hui Nam, Byoungho Lee, Jae Oh Byun, and Nam Seong Kim. "Fiber Bragg grating temperature sensor with controllable sensitivity." *Applied optics* 38, no. 13 (1999): 2752-2754.

[27] Kapron, F. P., Donald B. Keck, and Robert D. Maurer. "Radiation losses in glass optical waveguides." *Applied Physics Letters* 17, no. 10 (1970): 423-425.

[28] Kersey, A. D., and T. A. Berkoff. "Fiber-optic Bragg-grating differential-temperature sensor." *IEEE Photonics technology letters* 4, no. 10 (1992): 1183-1185.

[29] Kim, Young-Jae, Un-Chul Paek, and Byeong Ha Lee. "Measurement of refractive-index variation with temperature by use of long-period fiber gratings." *Optics letters* 27, no. 15 (2002): 1297-1299.

[30] Knight, Jonathan C. "Photonic crystal fibres." *nature* 424, no. 6950 (2003): 847.

[31] Kou, Jun-long, Jing Feng, Liang Ye, Fei Xu, and Yan-qing Lu. "Miniaturized fiber taper reflective interferometer for high temperature measurement." *Optics Express* 18, no. 13 (2010): 14245-14250.

[32] Liao, Changrui R., D. N. Wang, Min Wang, and Minghong Yang. "Fiber in-line Michelson interferometer tip sensor fabricated by femtosecond laser." *IEEE Photonics Technology Letters* 24, no. 22 (2012): 2060-2063.

[33] Liao, C. R., T. Y. Hu, and D. N. Wang. "Optical fiber Fabry-Perot interferometer cavity fabricated by femtosecond laser micromachining and fusion splicing for refractive index sensing." *Optics express* 20, no. 20 (2012): 22813-22818.

[34] Lee, Byeong Ha, Young Ho Kim, Kwan Seob Park, Joo Beom Eom, Myoung Jin Kim, Byung Sup Rho, and Hae Young Choi. "Interferometric fiber optic sensors." *sensors* 12, no. 3 (2012): 2467-2486.

[35] Lee, C. E., Henry F. Taylor, A. M. Markus, and E. Udd. "Optical-fiber Fabry–Perot embedded sensor." *Optics letters* 14, no. 21 (1989): 1225-1227.

[36] Lee, Chung E., and Henry F. Taylor. "Fiber-optic Fabry-Perot temperature sensor

using a low-coherence light source." *Journal of lightwave technology* 9, no. 1 (1991): 129-134.

[37] Li, H. H. "Refractive index of silicon and germanium and its wavelength and temperature derivatives." *Journal of Physical and Chemical Reference Data* 9, no. 3 (1980): 561-658.

[38] Lu, Guang, and Joseph T. Hupp. "Metal− organic frameworks as sensors: a ZIF-8 based Fabry− Pérot device as a selective sensor for chemical vapors and gases." *Journal of the American Chemical Society* 132, no. 23 (2010): 7832-7833.

[39] Mahamood, Rasheedat Modupe. "Laser Basics and Laser Material Interactions." In *Laser Metal Deposition Process of Metals, Alloys, and Composite Materials*, pp. 11-35. Springer, Cham, 2018.

[40] Ma, Jun, Jian Ju, Long Jin, Wei Jin, and Dongning Wang. "Fiber-tip micro-cavity for temperature and transverse load sensing." *Optics express* 19, no. 13 (2011): 12418-12426.

[41] Ma, Xiaodong, Haibin Huo, Wenhui Wang, Ye Tian, Nan Wu, Charles Guthy, Mengyan Shen, and Xingwei Wang. "Surface-enhanced Raman scattering sensor on an optical fiber probe fabricated with a femtosecond laser." *Sensors* 10, no. 12 (2010): 11064-11071.

[42] Meltz, Gerald, William W. Morey, and James R. Dunphy. "Fiber Bragg grating chemical sensor." In *Chemical, Biochemical, and Environmental Fiber Sensors III*, vol. 1587, pp. 350-362. International Society for Optics and Photonics, 1992.

[43] Morey, William W., James R. Dunphy, and Gerald Meltz. "Multiplexing fiber Bragg grating sensors." *Fiber & Integrated Optics* 10, no. 4 (1991): 351-360.

[44] Nanoscribe GmbH. http://www.nanoscribe.de/en/technology/ Accessed 11 January 2019

[45] Nogi, Masaya, Keishin Handa, Antonio Norio Nakagaito, and Hiroyuki Yano. "Optically transparent bionanofiber composites with low sensitivity to refractive index of the polymer matrix." *Applied Physics Letters* 87, no. 24 (2005): 243110.

[46] Patrick, H. J., G. M. Williams, A. D. Kersey, J. R. Pedrazzani, and A. M. Vengsarkar. "Hybrid fiber Bragg grating/long period fiber grating sensor for strain/temperature discrimination." *IEEE Photonics Technology Letters* 8, no. 9 (1996): 1223-1225.

[47] Peng, Jiankun, Yapeng Qu, Weijia Wang, Tengpeng Sun, and Minghong Yang. "Thin-film-based optical fiber Fabry–Perot interferometer used for humidity

sensing." *Applied optics* 57, no. 12 (2018): 2967-2972.

[48] Porro, Samuele, Alladin Jasmin, Katarzyna Bejtka, Daniele Conti, Denis Perrone, Salvatore Guastella, Candido F. Pirri, Alessandro Chiolerio, and Carlo Ricciardi. "Low-temperature atomic layer deposition of TiO2 thin layers for the processing of memristive devices." *Journal of Vacuum Science & Technology A: Vacuum, Surfaces, and Films* 34, no. 1 (2016): 01A147.

[49] Qu, Jingyuan, Muamer Kadic, Andreas Naber, and Martin Wegener. "Micro-structured two-component 3D metamaterials with negative thermal-expansion coefficient from positive constituents." *Scientific reports* 7 (2017): 40643.

[50] Rakić, Aleksandar D., Aleksandra B. Djurišić, Jovan M. Elazar, and Marian L. Majewski. "Optical properties of metallic films for vertical-cavity optoelectronic devices." *Applied optics* 37, no. 22 (1998): 5271-5283.

[51] Ran, Zeng Ling, Yun Jiang Rao, Wei Jun Liu, X. Liao, and Kin Seng Chiang. "Laser-micromachined Fabry-Perot optical fiber tip sensor for high-resolution temperature-independent measurement of refractive index." *Optics express* 16, no. 3 (2008): 2252-2263.

[52] Rao, Yun-Jiang, David J. Webb, David A. Jackson, Lin Zhang, and Ian Bennion. "In-fiber Bragg-grating temperature sensor system for medical applications." *Journal of Lightwave Technology* 15, no. 5 (1997): 779-785.

[53] Rao, Yun-Jiang, Ming Deng, De-Wen Duan, Xiao-Chen Yang, Tao Zhu, and Guang-Hua Cheng. "Micro Fabry-Perot interferometers in silica fibers machined by femtosecond laser." *Optics express* 15, no. 21 (2007): 14123-14128.

[54] Rao, Yun-Jiang. "Recent progress in applications of in-fibre Bragg grating sensors." *Optics and lasers in Engineering* 31, no. 4 (1999): 297-324.

[55] Rao, Yun-Jiang. "Recent progress in fiber-optic extrinsic Fabry–Perot interferometric sensors." *Optical Fiber Technology* 12, no. 3 (2006): 227-237.

[56] Said, A. A., M. Dugan, S. de Man, and D. Iannuzzi. "Carving fiber-top cantilevers with femtosecond laser micromachining." *Journal of Micromechanics and Microengineering* 18, no. 3 (2008): 035005.

[57] Sang, Xinzhu, Chongxiu Yu, T. Mayteevarunyoo, Kuiru Wang, Qi Zhang, and Pak L. Chu. "Temperature-insensitive chemical sensor based on a fiber Bragg grating." *Sensors and Actuators B: Chemical* 120, no. 2 (2007): 754-757.

[58] Schiebener, P., Johannes Straub, J. M. H. Levelt Sengers, and J. S. Gallagher. "Refractive index of water and steam as function of wavelength, temperature and

density." *Journal of physical and chemical reference data* 19, no. 3 (1990): 677-717.

[59] Sutapun, Boonsong, Massood Tabib-Azar, and Alex Kazemi. "Pd-coated elastooptic fiber optic Bragg grating sensors for multiplexed hydrogen sensing." *Sensors and Actuators B: Chemical* 60, no. 1 (1999): 27-34.

[60] Székely, Vladimir, Cs Márta, Zsolt Kohari, and Márta Rencz. "CMOS sensors for on-line thermal monitoring of VLSI circuits." *IEEE Transactions on Very Large Scale Integration (VLSI) Systems* 5, no. 3 (1997): 270-276.

[61] Tian, Ming, Ping Lu, Li Chen, Deming Liu, and Minghong Yang. "Micro multicavity Fabry–Pérot interferometers sensor in SMFs machined by femtosecond laser." *IEEE Photonics Technology Letters* 25, no. 16 (2013): 1609-1612.

[62] Tian, Ming, Ping Lu, Li Chen, Deming Liu, Minghong Yang, and Jiangshan Zhang. "Femtosecond laser fabricated in-line micro multicavity fiber FP interferometers sensor." *Optics Communications* 316 (2014): 80-85.

[63] Tierney, Sven, Sondre Volden, and Bjørn Torger Stokke. "Glucose sensors based on a responsive gel incorporated as a Fabry-Perot cavity on a fiber-optic readout platform." *Biosensors and Bioelectronics* 24, no. 7 (2009): 2034-2039.

[64] Tsai, Woo-Hu, and Chun-Jung Lin. "A novel structure for the intrinsic Fabry-Perot fiber-optic temperature sensor." *Journal of Lightwave Technology* 19, no. 5 (2001): 682-686.

[65] Udd, Eric, and William B. Spillman Jr, eds. *Fiber optic sensors: an introduction for engineers and scientists*. John Wiley & Sons, 2011.

[66] Vancura, C., M. Ruegg, Y. Li, D. Lange, C. Hagleitner, O. Brand, A. Hierlemann, and H. Baltes. "Magnetically actuated CMOS resonant cantilever gas sensor for volatile organic compounds." In *TRANSDUCERS, Solid-State Sensors, Actuators and Microsystems, 12th International Conference on, 2003*, vol. 2, pp. 1355-1358. IEEE, 2003.

[67] Vaughan, M. *The Fabry-Perot interferometer: history, theory, practice and applications*. Routledge, 2017.

[68] Villatoro, Joel, Mark P. Kreuzer, Rajan Jha, Vladimir P. Minkovich, Vittoria Finazzi, Gonçal Badenes, and Valerio Pruneri. "Photonic crystal fiber interferometer for chemical vapor detection with high sensitivity." *Optics Express* 17, no. 3 (2009): 1447-1453.

[69] Wan, Lei, Hengky Chandrahalim, Cong Chen, Qiushu Chen, Ting Mei, Yuji Oki, Naoya Nishimura, L. Jay Guo, and Xudong Fan. "On-chip, high-sensitivity

temperature sensors based on dye-doped solid-state polymer microring lasers." *Applied Physics Letters* 111, no. 6 (2017): 061109.

[70] Wan, Xiaoke, and Henry F. Taylor. "Intrinsic fiber Fabry–Perot temperature sensor with fiber Bragg grating mirrors." *Optics letters* 27, no. 16 (2002): 1388-1390.

[71] Watanabe, Toshio, Naoki Ooba, Yasuhiro Hida, and Makoto Hikita. "Influence of humidity on refractive index of polymers for optical waveguide and its temperature dependence." *Applied Physics Letters* 72, no. 13 (1998): 1533-1535.

[72] Wei, Tao, Yukun Han, Yanjun Li, Hai-Lung Tsai, and Hai Xiao. "Temperature-insensitive miniaturized fiber inline Fabry-Perot interferometer for highly sensitive refractive index measurement." *Optics Express* 16, no. 8 (2008): 5764-5769.

[73] Wolfbeis, Otto S. "Fiber-optic chemical sensors and biosensors." *Analytical chemistry* 80, no. 12 (2008): 4269-4283.

[74] Yao, Mian, Xia Ouyang, Jushuai Wu, A. Zhang, Hwa-Yaw Tam, and P. Wai. "Optical Fiber-Tip Sensors Based on In-Situ μ-Printed Polymer Suspended-Microbeams." *Sensors* 18, no. 6 (2018): 1825.

[75] Yeo, T. L., T. Sun, K. T. V. Grattan, D. Parry, R. Lade, and B. D. Powell. "Characterisation of a polymer-coated fibre Bragg grating sensor for relative humidity sensing." *Sensors and Actuators B: Chemical* 110, no. 1 (2005): 148-156.

[76] Yoshino, Toshihiko, Kiyoshi Kurosawa, Katsuji Itoh, and Teruzi Ose. "Fiber-optic Fabry-Perot interferometer and its sensor applications." *IEEE Journal of quantum electronics* 18, no. 10 (1982): 1624-1633.

[77] Zhang, Bowei, and Mojtaba Kahrizi. "High-temperature resistance fiber Bragg grating temperature sensor fabrication." *IEEE Sensors Journal* 7, no. 4 (2007): 586-591.

[78] Zhang, Yinan, Lei Yuan, Xinwei Lan, Amardeep Kaur, Jie Huang, and Hai Xiao. "High-temperature fiber-optic Fabry–Perot interferometric pressure sensor fabricated by femtosecond laser." *Optics letters* 38, no. 22 (2013): 4609-4612.

[79] Zhang, Zhiyi, Ping Zhao, Peng Lin, and Fengguo Sun. "Thermo-optic coefficients of polymers for optical waveguide applications." *Polymer* 47, no. 14 (2006): 4893-4896.

REPORT DOCUMENTATION PAGE

Form Approved
OMB No. 0704-0188

PLEASE DO NOT RETURN YOUR FORM TO THE ABOVE ADDRESS.

1. REPORT DATE *(DD-MM-YYYY)*	2. REPORT TYPE	3. DATES COVERED *(From - To)*
21-03-2019	Master's Thesis	August 2017 - March 2019

4. TITLE AND SUBTITLE

3-D Multifunctional Sensors Fabricated on Fiber Tips Using a Two-Photon Polymerization Process

5a. CONTRACT NUMBER

5b. GRANT NUMBER

5c. PROGRAM ELEMENT NUMBER

6. AUTHOR(S)

Smith, Jonathan W, Captain, USAF

5d. PROJECT NUMBER

18G358G, 19G174

5e. TASK NUMBER

5f. WORK UNIT NUMBER

7. PERFORMING ORGANIZATION NAME(S) AND ADDRESS(ES)

Air Force Institute of Technology
Graduate School of Engineering and Management (AFIT/EN)
2950 Hobson Way
Wright-Patterson AFB OH 45433-7765

8. PERFORMING ORGANIZATION REPORT NUMBER

AFIT-ENG-MS-19-M-056

9. SPONSORING/MONITORING AGENCY NAME(S) AND ADDRESS(ES)

Intentionally Left Blank

10. SPONSOR/MONITOR'S ACRONYM(S)

11. SPONSOR/MONITOR'S REPORT NUMBER(S)

12. DISTRIBUTION/AVAILABILITY STATEMENT

Depending on the distribution, find the correct statement from the AFIT Style Guide. Please ensure to use the entire distribution statement.

13. SUPPLEMENTARY NOTES

Request to delay distribution for one year to allow patent pending paperwork to be completed. The title of the patent is Design of temperature fluctuation immune, self-referencing Fabry–Pérot cavity sensors.

14. ABSTRACT

This thesis conducts research involving designing, fabricating, and testing optical fiber tip refractive index sensors. The fabrication process used for these sensors is a two-photon polymerization process utilizing a photo sensitive polymer. Unlike planar lithography, this fabrication process allows the creation of arbitrary shapes with a great degree of freedom. There is a total of three different designed fiber tip sensors that are all fabricated and tested. One is a flat surfaced single cavity Fabry-Pérot interferometer (FPI) device, another is a flat surfaced double cavity FPI device, and the last is a confocal surfaced double cavity FPI device. These sensors are tested for both thermal radiation and volatile organic compounds (VOC) sensing. Thermal radiation sensing involves exposing the device to temperatures ranging from room temperature up to 120oC. As the temperature increases the fiber tip structure expands which changes its reflection spectrum. Each device was also exposed to isopropanol in gaseous form which results in a refractive index change. This change is also observed in the reflection spectrum. Lastly, research was conducted on thin dielectric reflective coatings for the purpose of increasing the reflectivity of the device surfaces resulting in a higher quality factor.

15. SUBJECT TERMS

Fabry-Perot Interferometer, 3-D Fabrication, Optical Fiber Tip Sensor

16. SECURITY CLASSIFICATION OF:			17. LIMITATION OF ABSTRACT	18. NUMBER OF PAGES	19a. NAME OF RESPONSIBLE PERSON
a. REPORT	b. ABSTRACT	c. THIS PAGE			Dr. Hengky Chandrahalim, AFIT/ENG
U	U	U	UU	127	19b. TELEPHONE NUMBER *(Include area code)* (312) 785-3636 x4483 hengky.chandrahalim@afit.